Control of Separated Flows

Prof. Philippe Lavoie

UNIVERSITY OF TORONTO

Institute for Aerospace Studies
UNIVERSITY OF TORONTO
Centre for Research in Sustainable Aviation

Summer School on Sustainable Aviation
Active Flow Control
Toronto, 16 & 17 May 2016

Outline

A. What is a separated flow and why does it separate?

B. Examples of separated flows on an airplane, and what it does to performance

C. Control of separation on streamlined bodies

D. Flow State Estimation - Enabler for Closed-loop Control

E. Summary and Closing Remarks

Flow Separation

- The streamlines of a flow tends to follow surfaces, due to the Coanda effect.
- If the curvature is “too large”, the flow will “separate” from the surface, creating a separated shear layer.
- More precisely, the adverse pressure gradient, against which the fluid must work, produces a local flow reversal and thus separation of the shear layer.

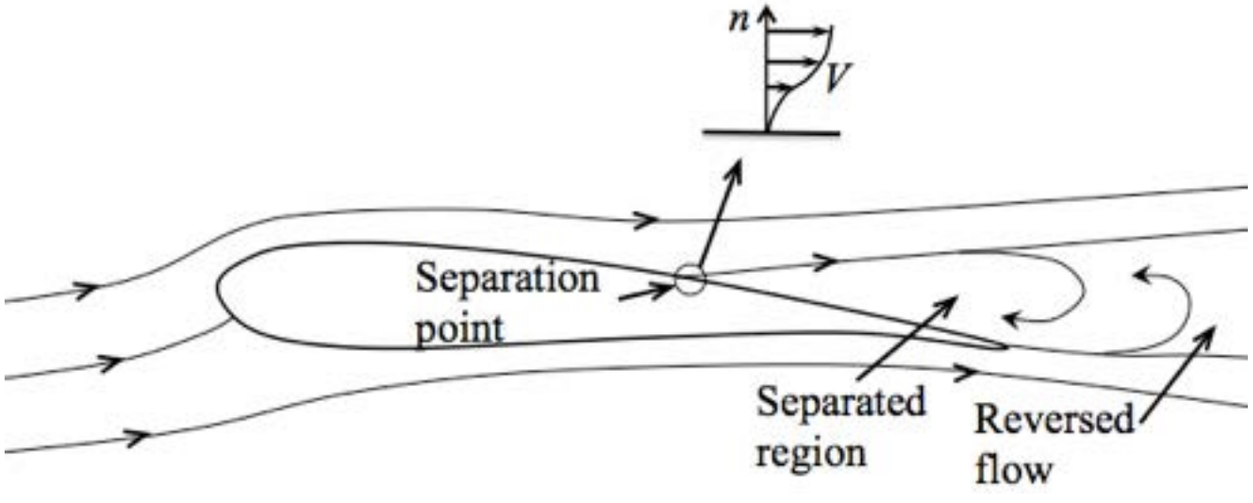

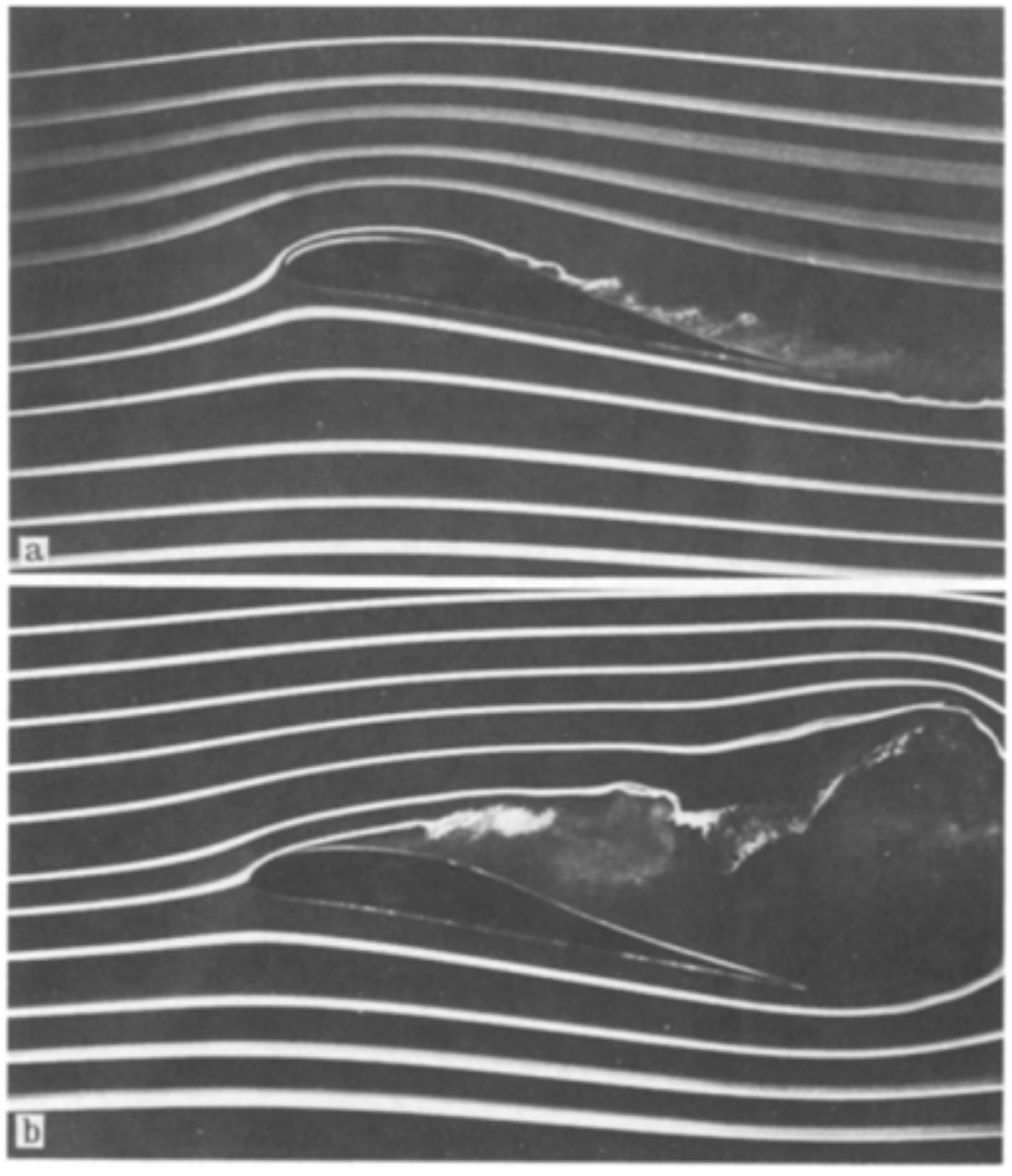

Mueller et al. (1983)

Physics Behind Flow Separation

Consider the x-momentum equation for a boundary layer:

$$\rho u \frac{\partial u}{\partial x} + \rho v \frac{\partial u}{\partial y} = -\frac{\mathrm{d}p_e}{\mathrm{d}x} + \frac{\partial}{\partial y}\left(\mu \frac{\partial u}{\partial y}\right)$$

Assuming constant viscosity, the equation at the wall becomes,

$$\frac{\mathrm{d}p_e}{\mathrm{d}x} = \mu \frac{\partial^2 u}{\partial y^2}$$

Thus, a positive (adverse) pressure gradient wants to induce a positive curvature to the velocity profile.

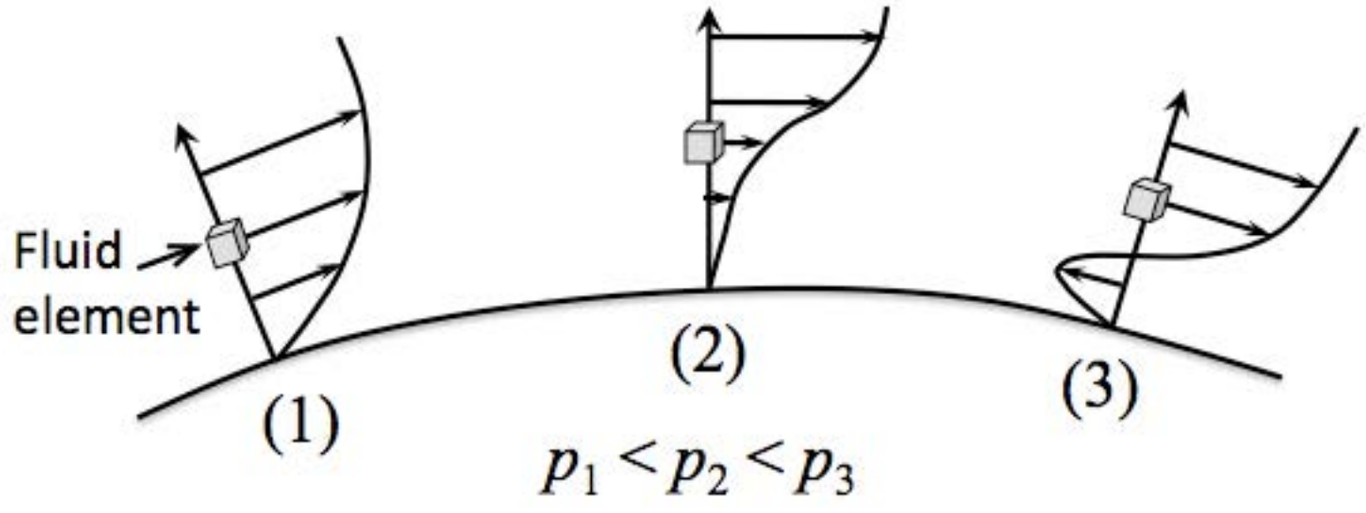

Flow Separation in Aviation

www.airplane-pictures.net

Feero et al. (2015)

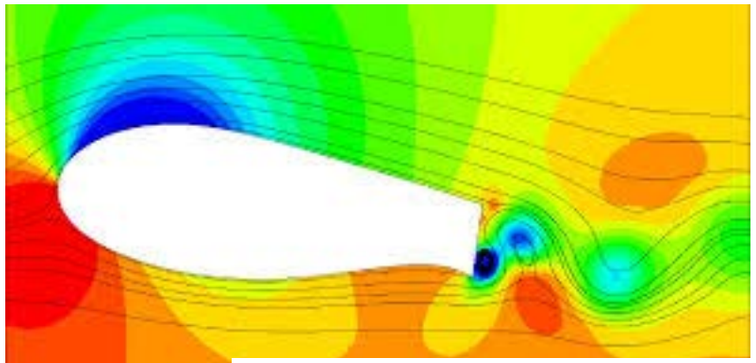

Baker & van Dam (2008)

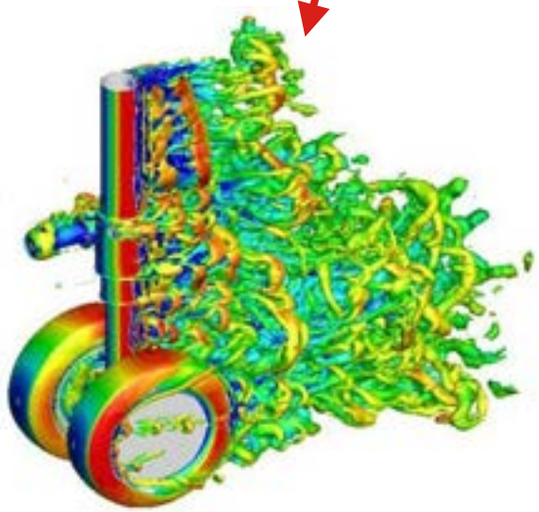

www.southampton.ac.uk

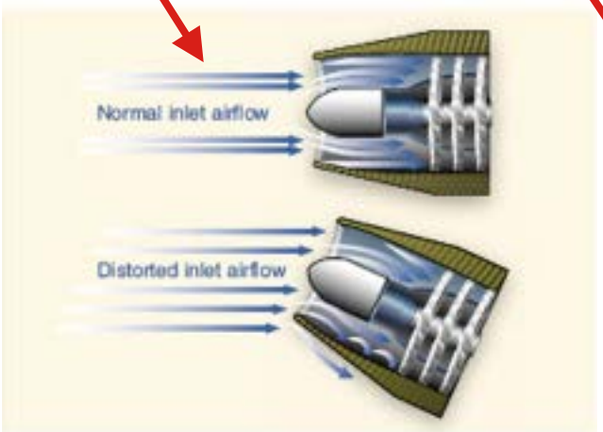

www.flightlearnings.com

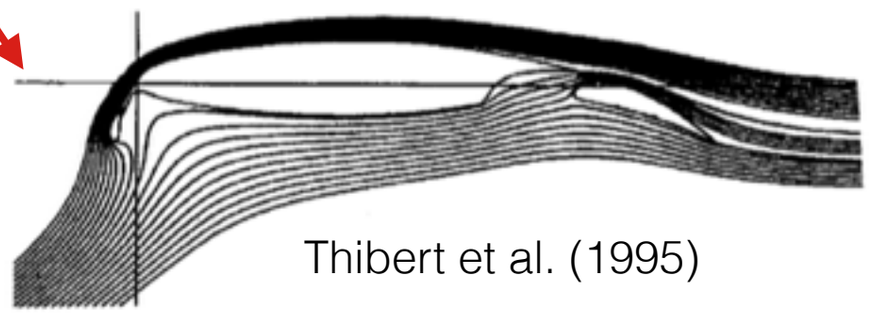

Thibert et al. (1995)

Why Control Separation?

If an aircraft is well designed, flow separation should not be an issue, except for extreme situations (e.g., one-engine out, large wind gust) or when loss of lift and increase drag is needed (e.g., spoilers, landing gear).

Why should aviation care then?

A. Many boundaries of the flight envelop set by flow separation.

B. Separation control as an enabler technology:

- Decrease the size of vertical stabilizer (reduces weight and drag)
- Gapless high-lift (less weight and noise)
- Decrease number of stages in the compressor (less weight)
- Reduce unsteady aerodynamic loads on landing gear and wing (less weight and noise - maybe drag also)

Technology Enabler (Example 1)

Take-off and landing speed controlled by $C_{L\max}$, which is limited by flow separation

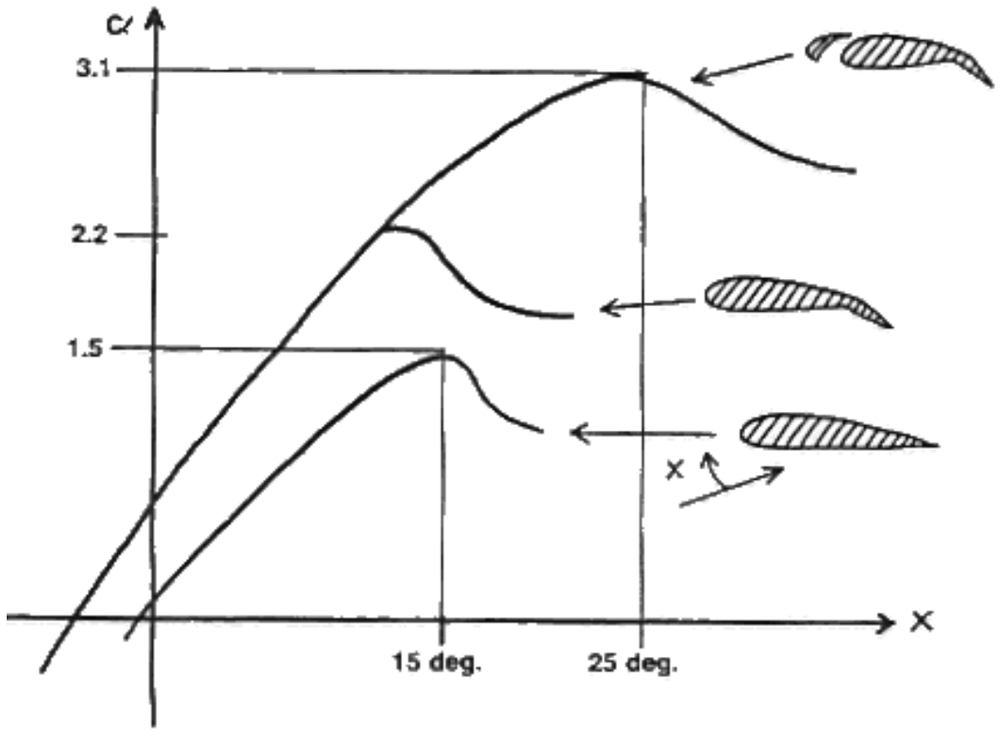

Figure 1

Slotted Fowler flaps of a Boeing 747.

Gap between slap and flap bleeds air from pressure side to energies the boundary layer.

- Very heavy and complex systems

Could separation control replace that heavy system?

Control on Streamlined Bodies

A key element of separation on streamlined bodies is that the point of separation can move or change based on conditions.

Fundamentally, since separation is cause by the loss of energy near the boundary due to an adverse pressure gradients, there are two possible strategies:

1. Re-energise the boundary layer
    i. Laminar separation: induce transition to turbulence
    ii. Turbulent separation: increase turbulence and mixing
2. Virtual aerodynamic shaping

First Example of Separation Control

Prandtl, in developing his boundary layer theory, devised some of the first systematic flow control experiments using constant suction.

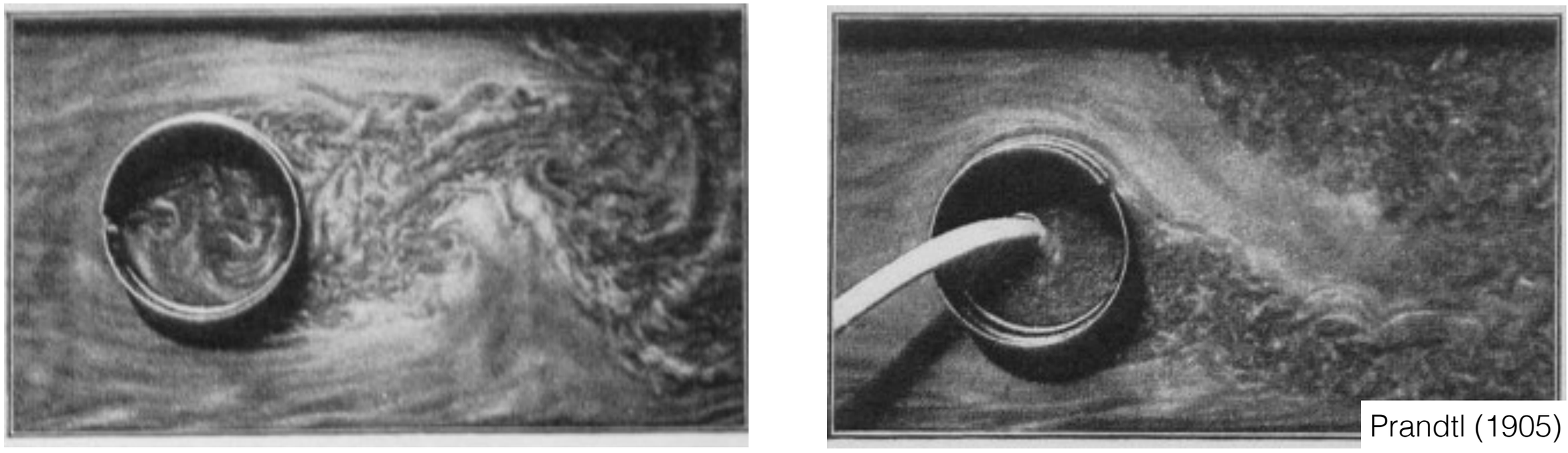

Prandtl (1905)

By removing low momentum fluid in the boundary layer, separation point moved further back.

This method not usually used due to weight and energy requirements.

- Some exceptions, primarily in military applications

A Smarter Way?

A key element of modern active flow control methodology is to use unsteady forcing, typically exciting an existing instability in the flow.

For instance consider a simple free-shear-layer:

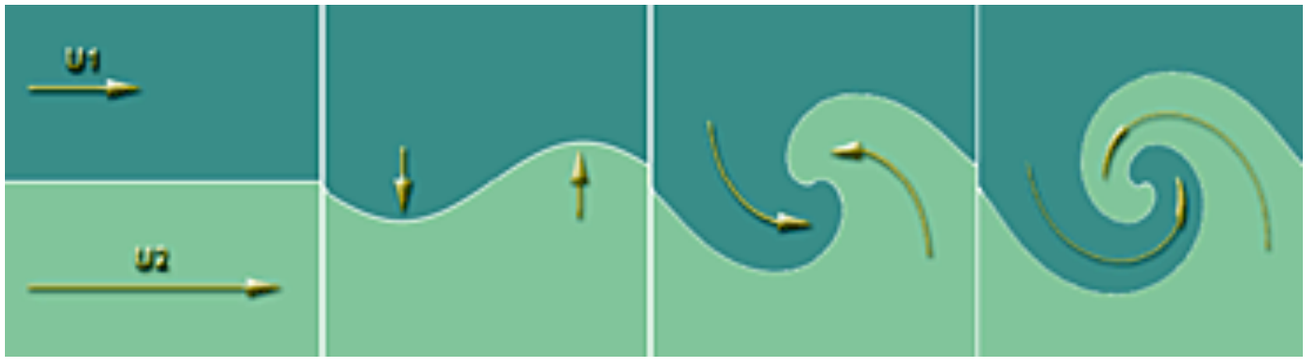

Kelvin-Helmholtz inability leads to a roll-up of the shear layer.

Reduced (normalised) frequency:

$$f^+ = \frac{f\ell}{U}$$

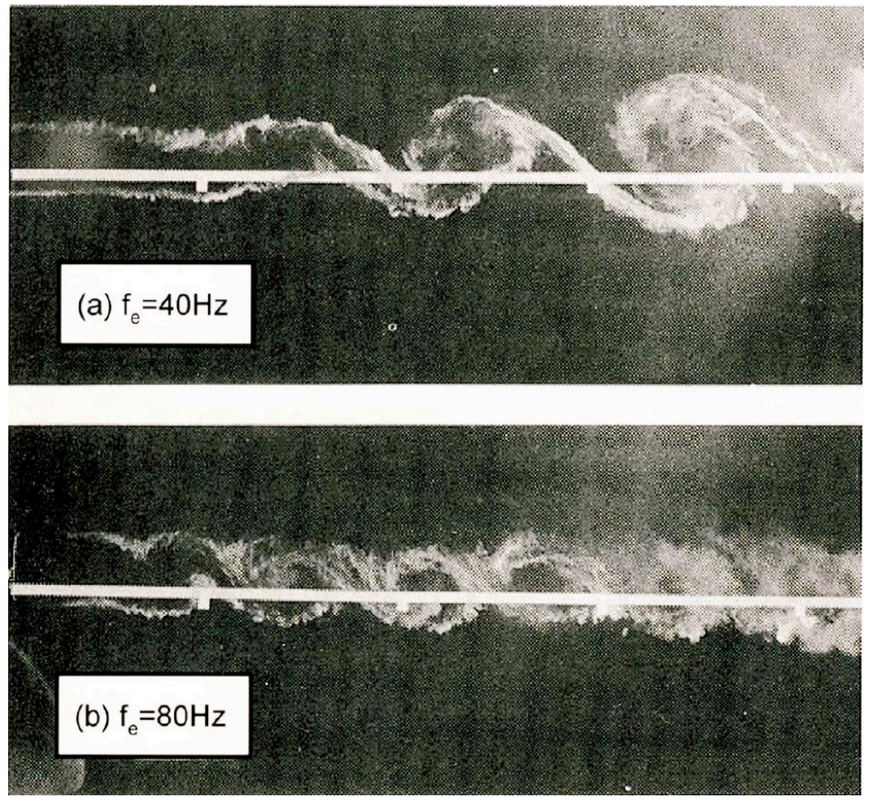

Greenblatt & Wygnanski (2000)

Instabilities on an Airfoil

Multiple instabilities and flow structures for an airfoil.

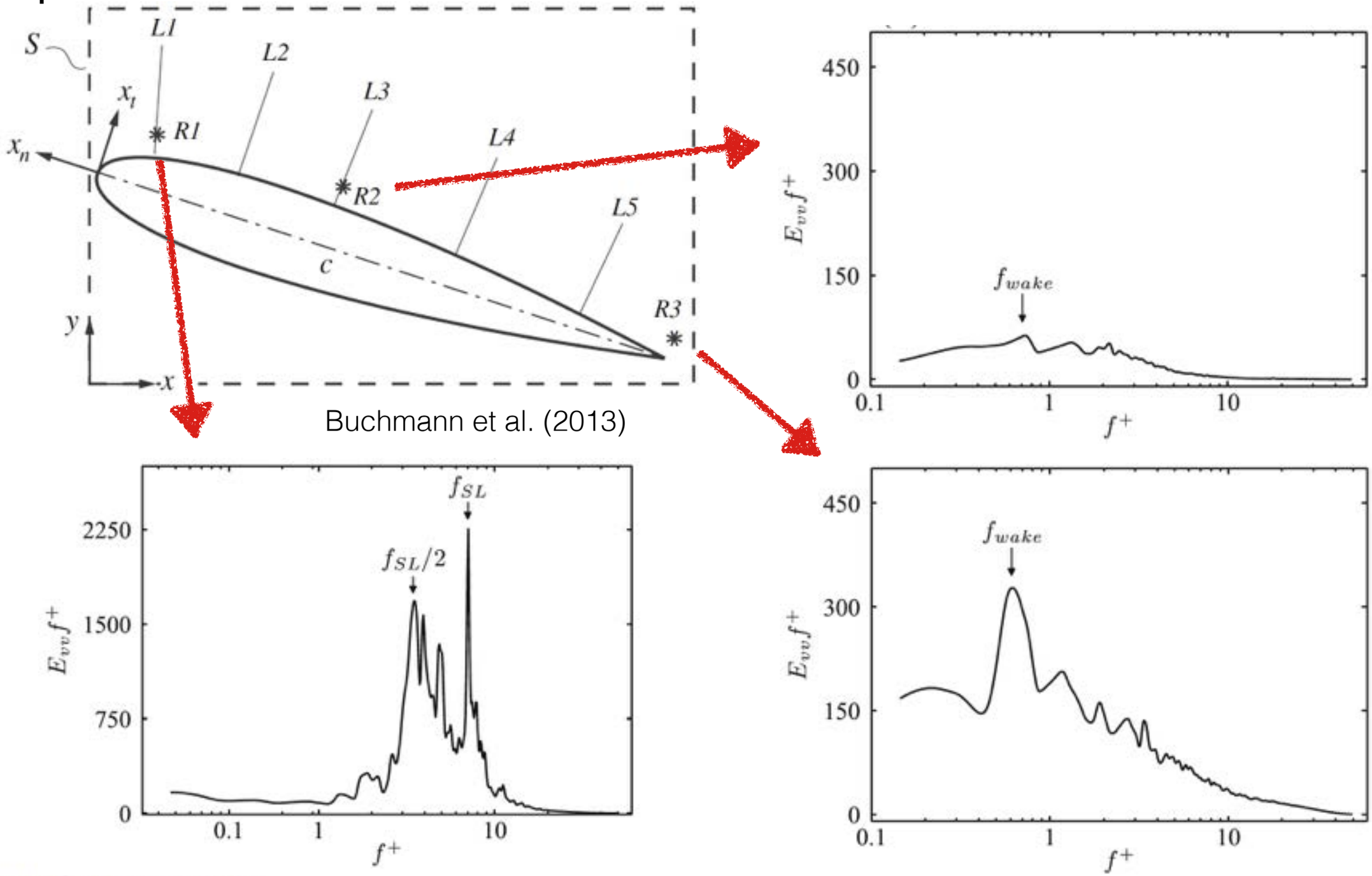

Instabilities on an Airfoil

Multiple instabilities and flow structures for an airfoil.

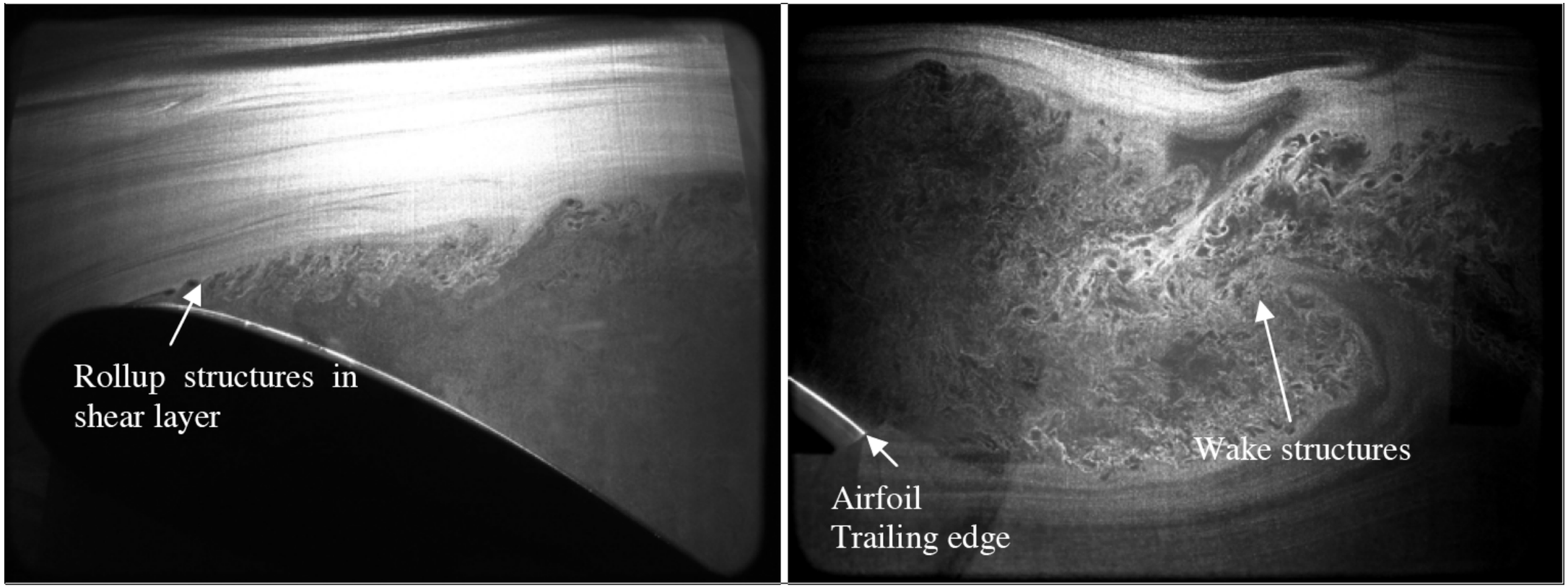

Tian, Cattafesta & Mittal (2006)

Two are of interest today:

- Shear-layer instability - high frequency, $f^+ = \dfrac{fc}{U_\infty} = \mathcal{O}(10)$

- Wake instability (von Karman vortices) - low frequency, $f^+ = \mathcal{O}(1)$

Separation Control Actuators

There are many types of actuators used for separation control. Will focus here on applications that use two types:

Synthetic jets:
- no fluid source
- high frequency
- moderate velocity
- moving parts

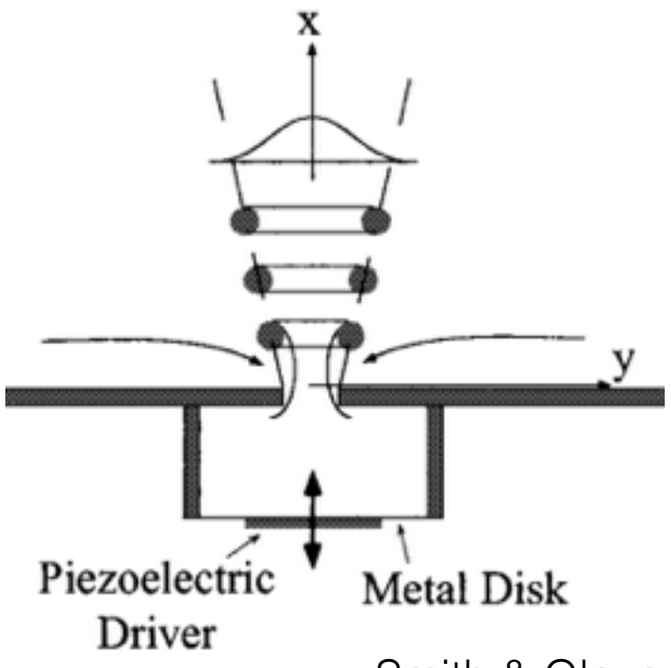

Smith & Glezer (1998)

Fluidic oscillators (or sweeping jets):
- high speed
- no moving parts
- fixed velocity-frequency relation
- external source of fluid

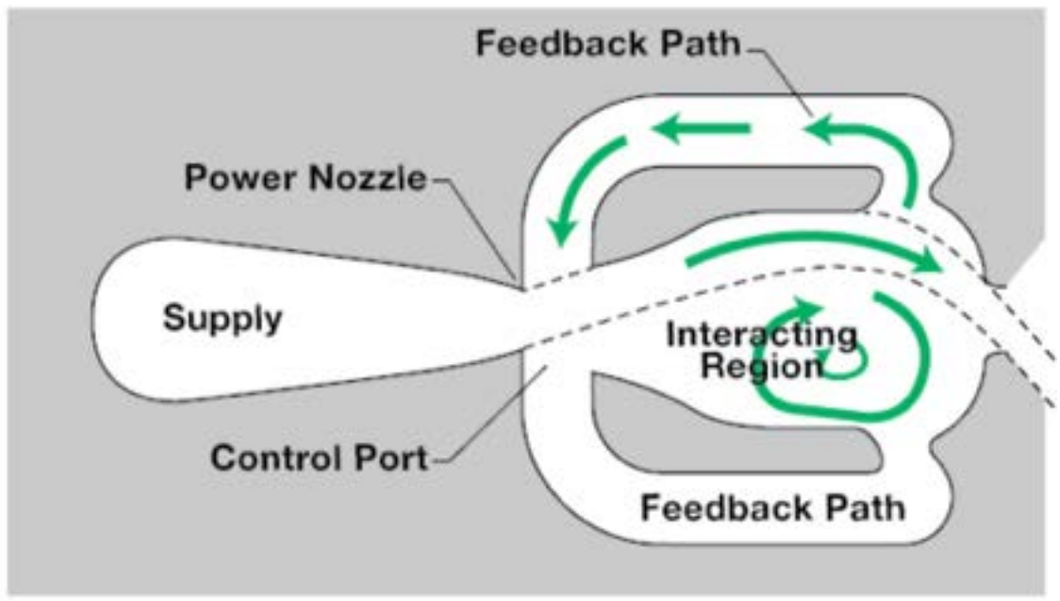

Raman & Raghu (2004)

Normalised Forcing Amplitude

The forcing amplitude can be expressed either as a momentum or velocity ratio.

Momentum coefficient

$$C_\mu = \frac{\text{momentum from actuator}}{\text{momentum of flow}} = \frac{1/2\rho_j U_j A_j}{1/2\rho_\infty U_\infty^2 A}$$

Velocity ratio

$$V_r = \frac{U_j}{U_\infty}$$

Often not possible to separate which of these is the governing/dominant coefficient to consider. Historically, momentum coefficient is used, but more interest in the effect of velocity ratio in recent years.

Performance of Separation Control

A few things to expect with control:

- No change at low angles of attack
- Increase in stall angle
- Increase in $C_{L\max}$

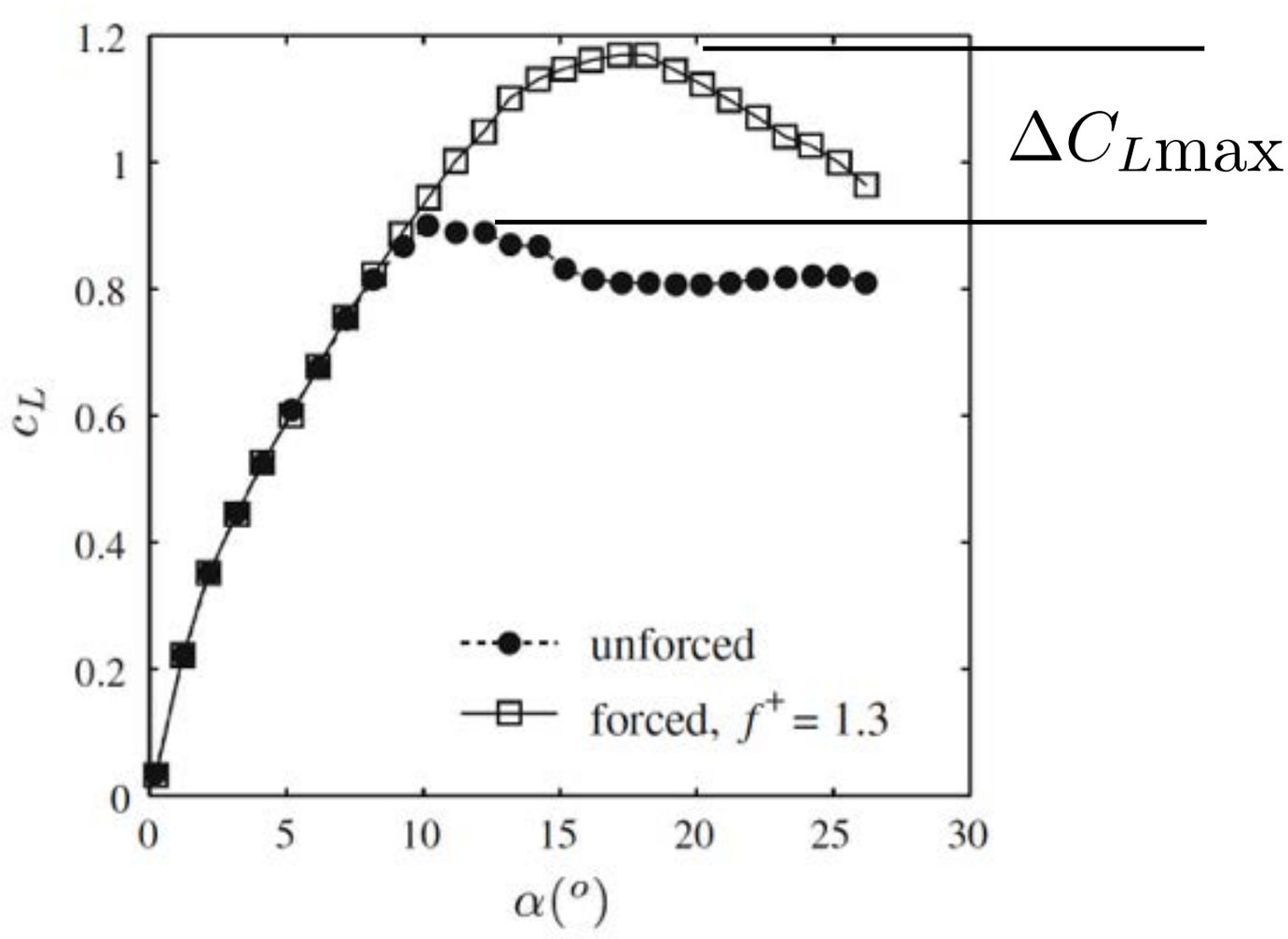

Fig. 1 Lift coefficient c_L of a NACA-0015 airfoil; (*filled circle*) no forcing and (*open square*) ZNMF forcing at the leading edge, $f^+ = 1.3$, $c_\mu = 0.0014$. Figure adapted from Tuck and Soria (2008)

Low Frequency Control

Vibrating ribbon at the leading edge, excitation at low frequency $f^+ = 2.6$.

Truncated NACA 0015 at Re = 40,000

Flow is reattached. Formation of large coherent structures convecting over the airfoil surface.

Reattachment due to increase momentum transfer near the surface due to the forcing and resulting coherent structures.

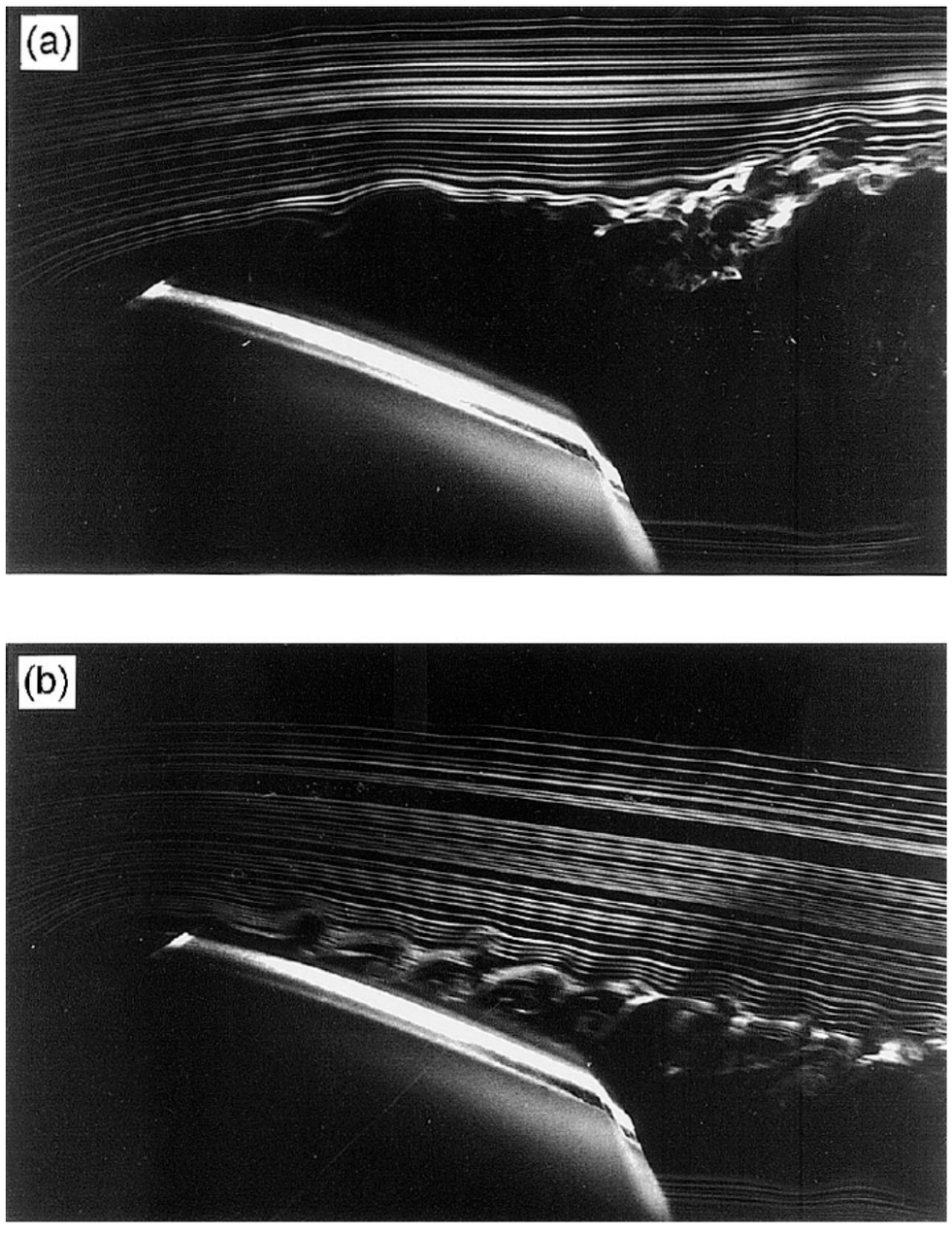

Greenblatt & Wygnanski (2000)

Effect of Momentum Coefficient

A minimum forcing amplitude is required to reattach the flow.

Beyond threshold, performance remain more or less constant.

Over actuation can lead to small loss of performance.

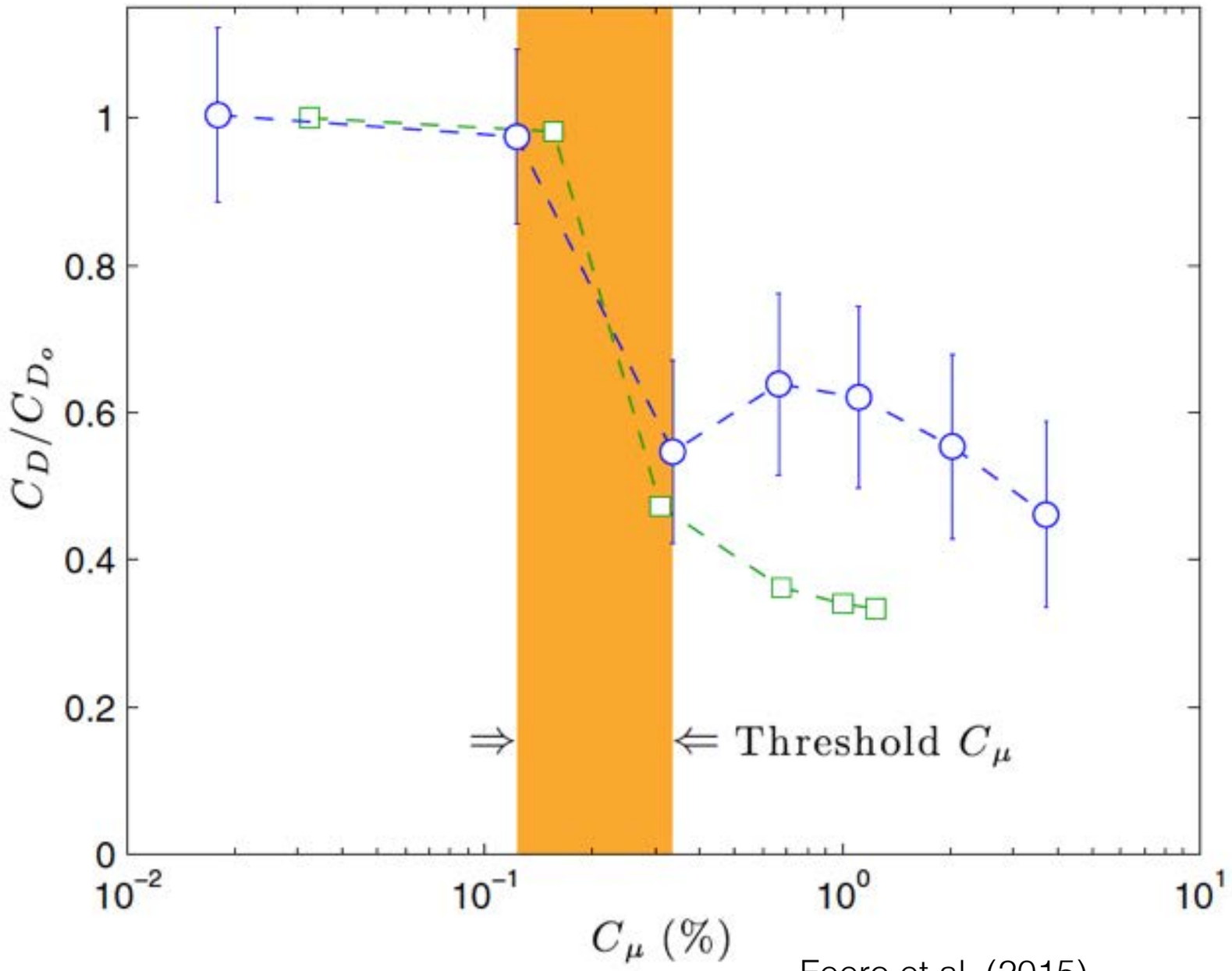

Feero et al. (2015)

Low Frequency Control

Effect of actuation frequency:

- “narrow-band” efficient - locks onto the receptivity of separated shear layer
- sensitivity reduces with Re

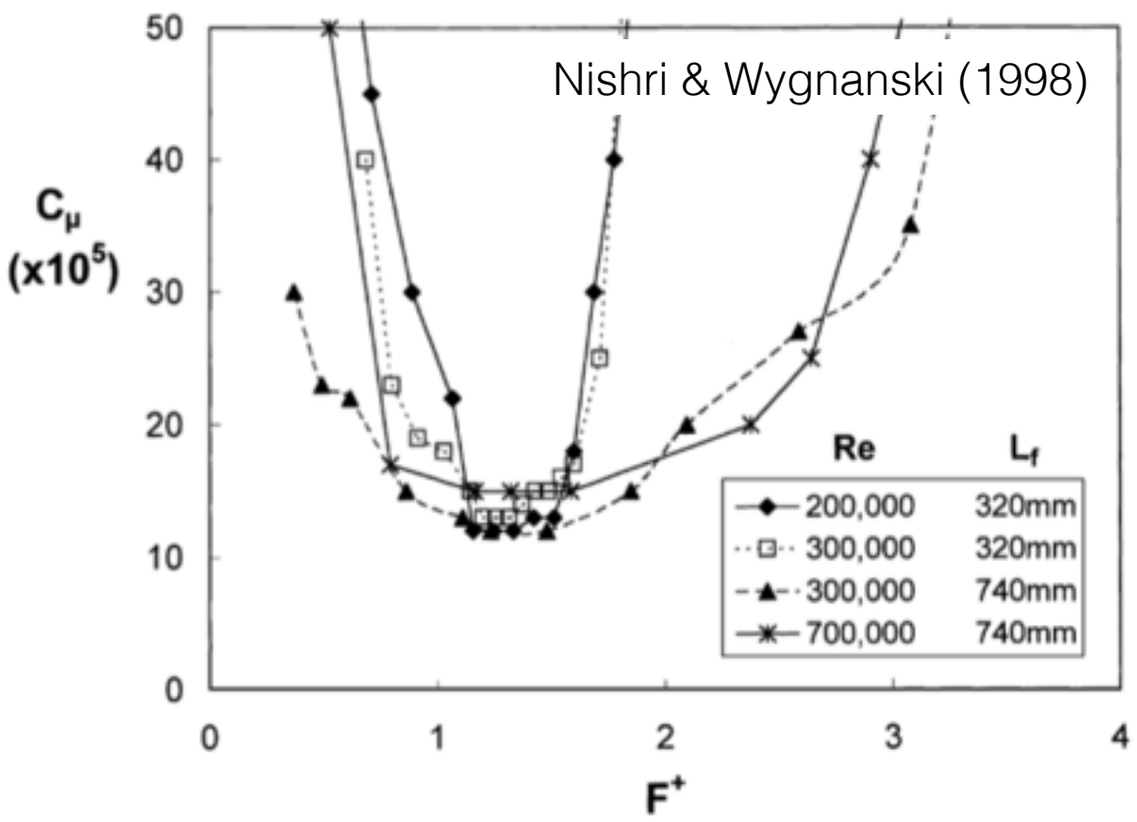

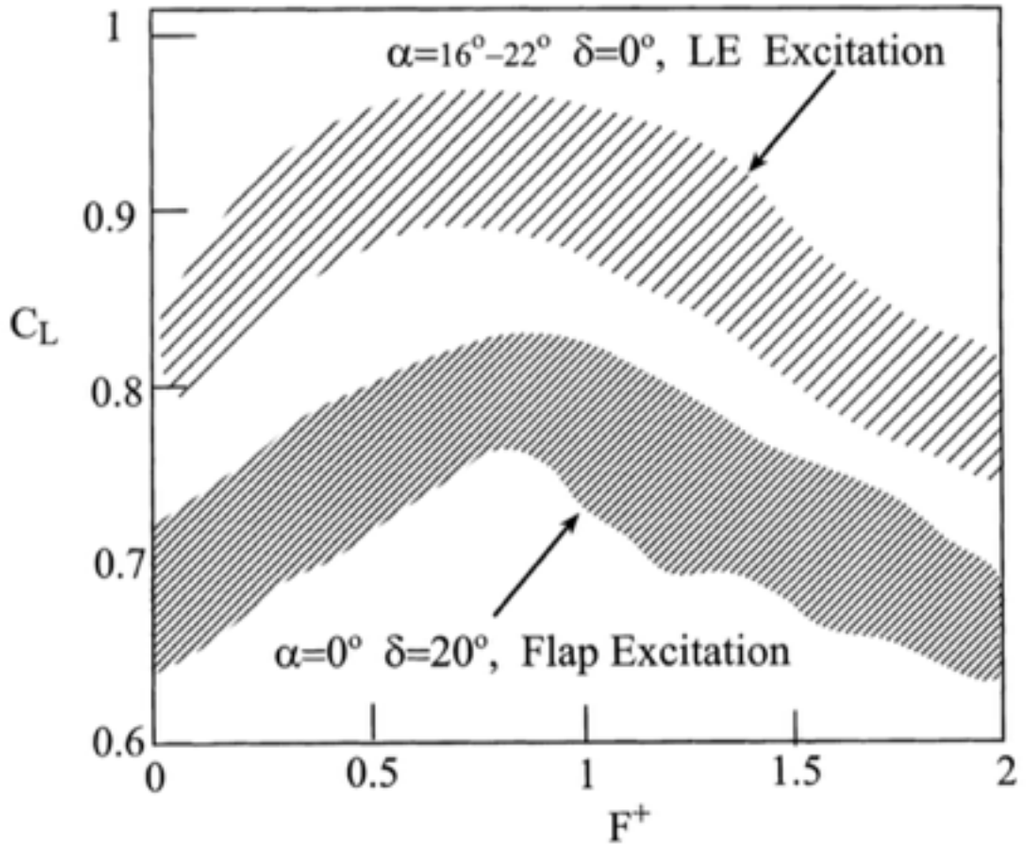

Greenblatt & Wygnanski (2000)

Effect of Forcing location

Shear layer most receptive at the point of separation

- Forcing upstream will dissipate
- Forcing downstream needs to over-power the separated region to be effective

Unfortunately, some lack of systematic evidence of control effectiveness with forcing location.

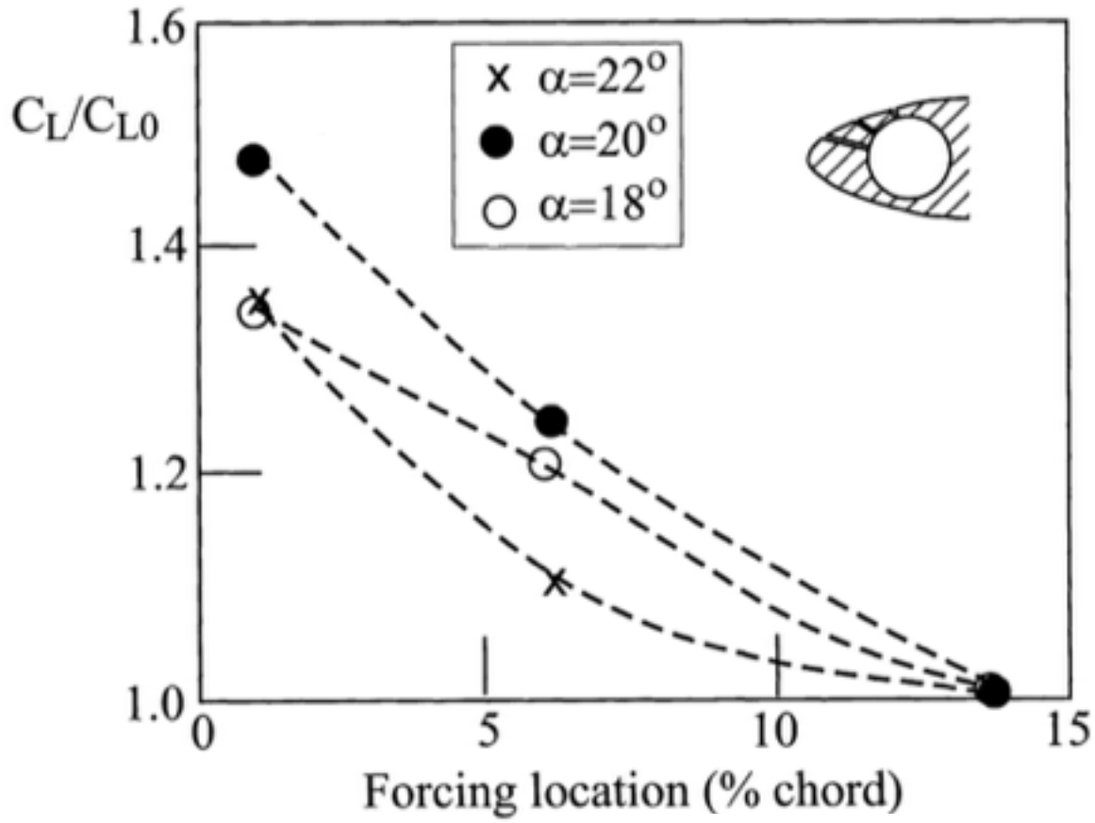

Hsiao et al. (1994)

NACA 63_3-018 with leading edge stall

Caveat: forcing angle not constant

Unsteadiness of the Control

NACA 0015 at Re = 10^4
and 18° angle of attack.
Synthetic jet at the LE

$$f^+ = 1.3 \;\; \& \;\; C_\mu = 1.4\%$$

Phase-averaged vorticity

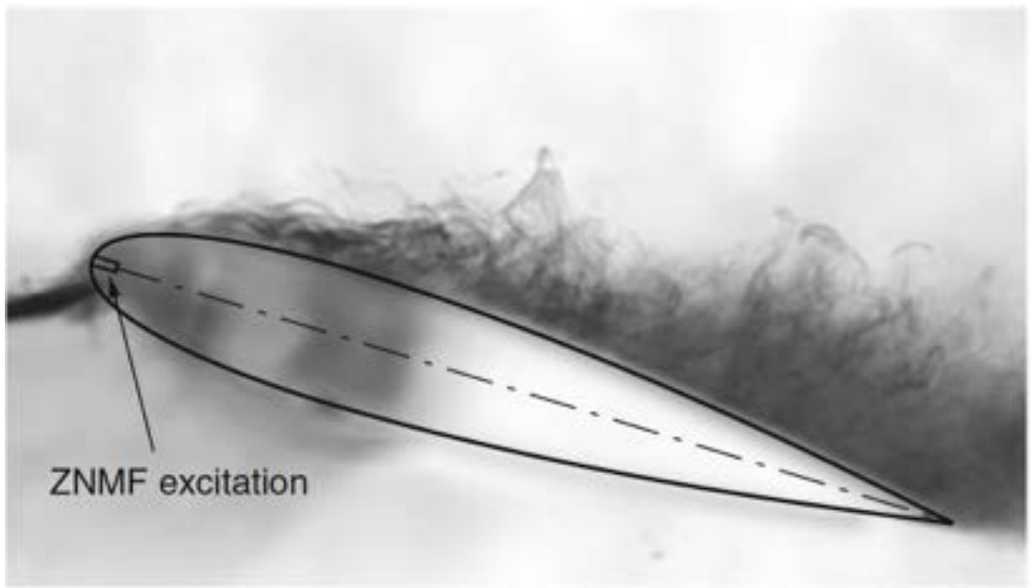

Buchmann et al. (2013)

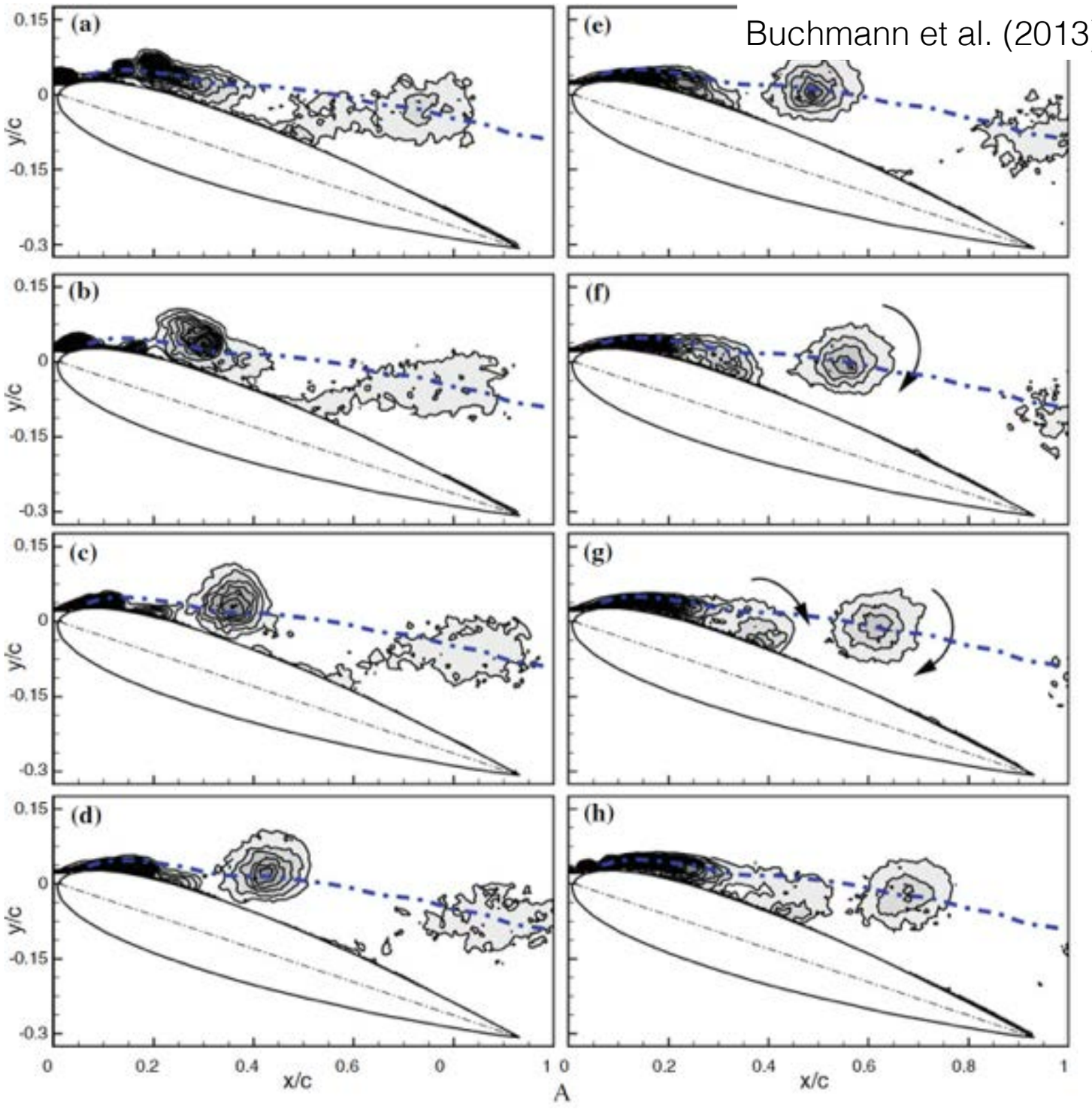

High Frequency Forcing

Work by Glezer and co-workers using high frequency excitation found interesting results on an unconventional airfoil.

- Streamlined cylinder made to readily change location of excitation.

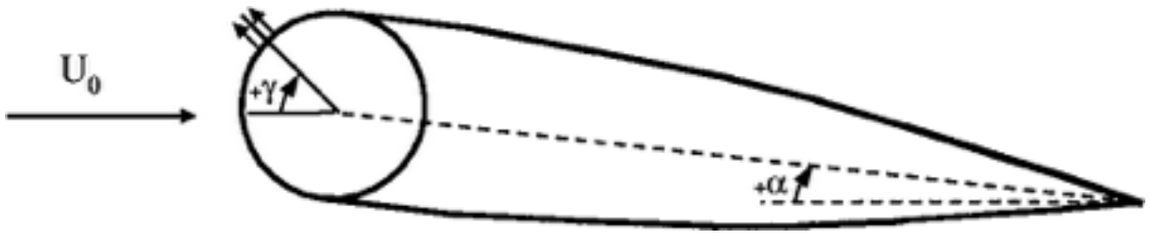

$$Re_c = 3.1 \times 10^5$$

$$C_\mu = 3.5 \times 10^{-3}$$

High frequency excitation, uncoupled from the natural frequency of the separated shear layer.

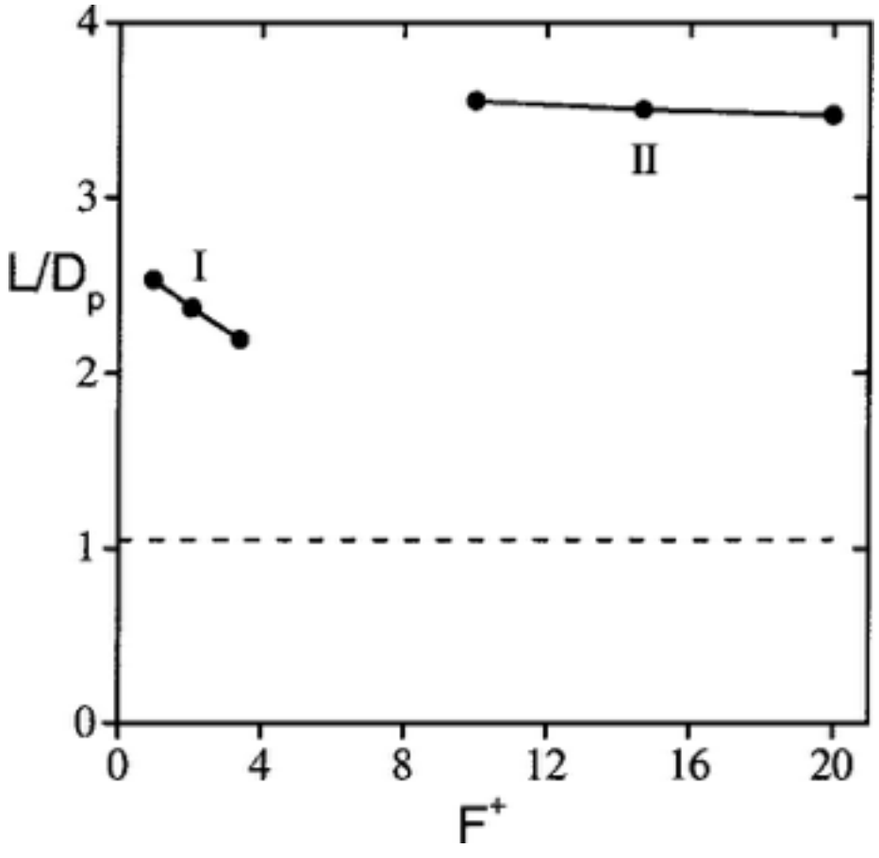

Amitay et al. (2001)

Virtual Aerodynamic Shaping

At high frequency, the forcing can appear quasi-steady to the flow if the highest times scale of the flow is much smaller than that of the forcing.

$$Re_d = 40,000$$

Notice the small deviation of the streamlines in Fig. 7(b)

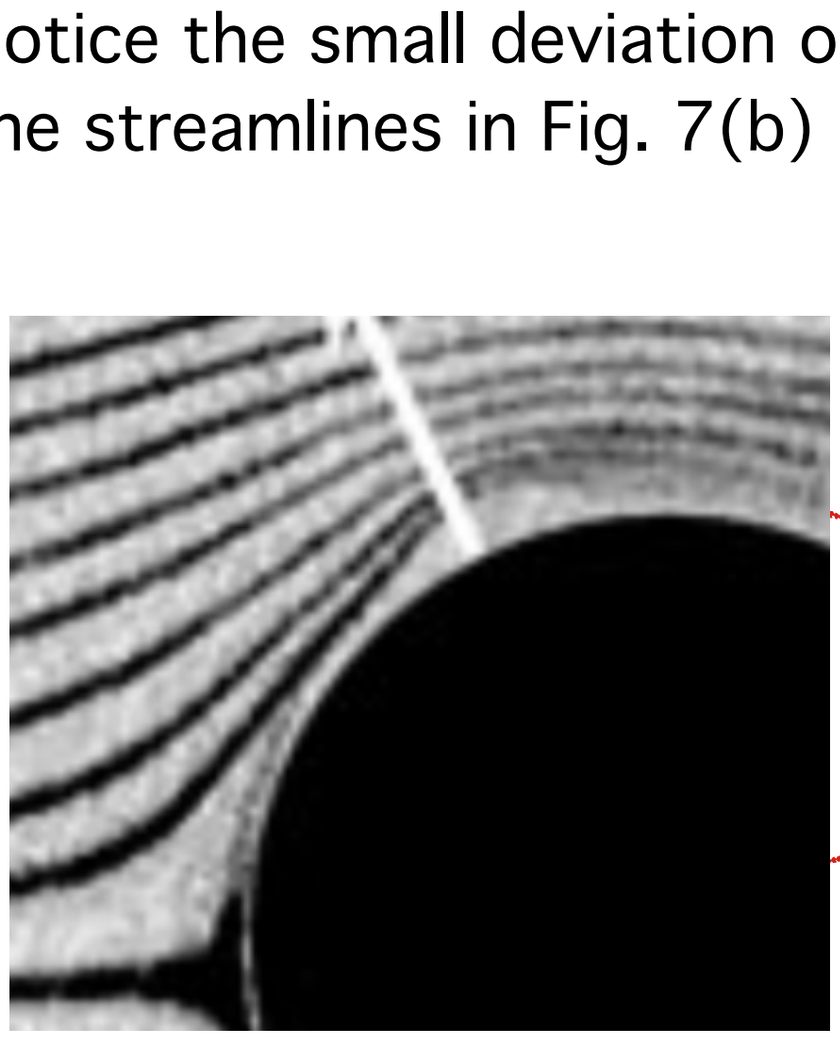

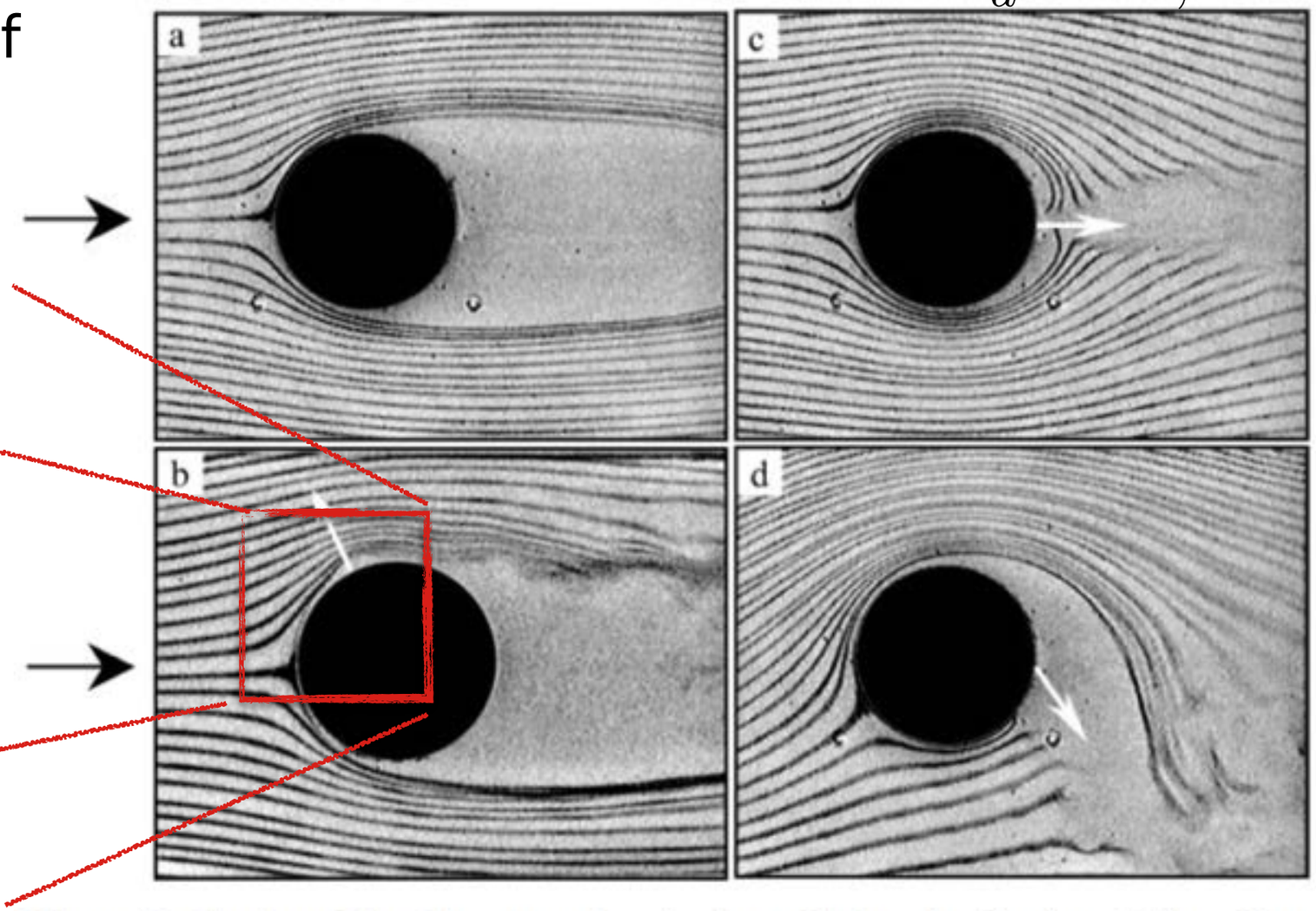

Figure 7 Smoke of the flow around a circular cylinder visualization: (*a*) baseline; and (*b*) actuated: $\phi = 0$, $\gamma = 60°$ and (*c*) 180°, and (*d*) $\phi = 120°$, $\gamma = 180°$.

Virtual Aerodynamic Shaping

Flow near the exit scales momentum flux ratios and jet width.

For low momentum ratio and Strouhal number, discrete vortices shed.

For high momentum ratio and Strouhal number, a closed recirculation zone forms.

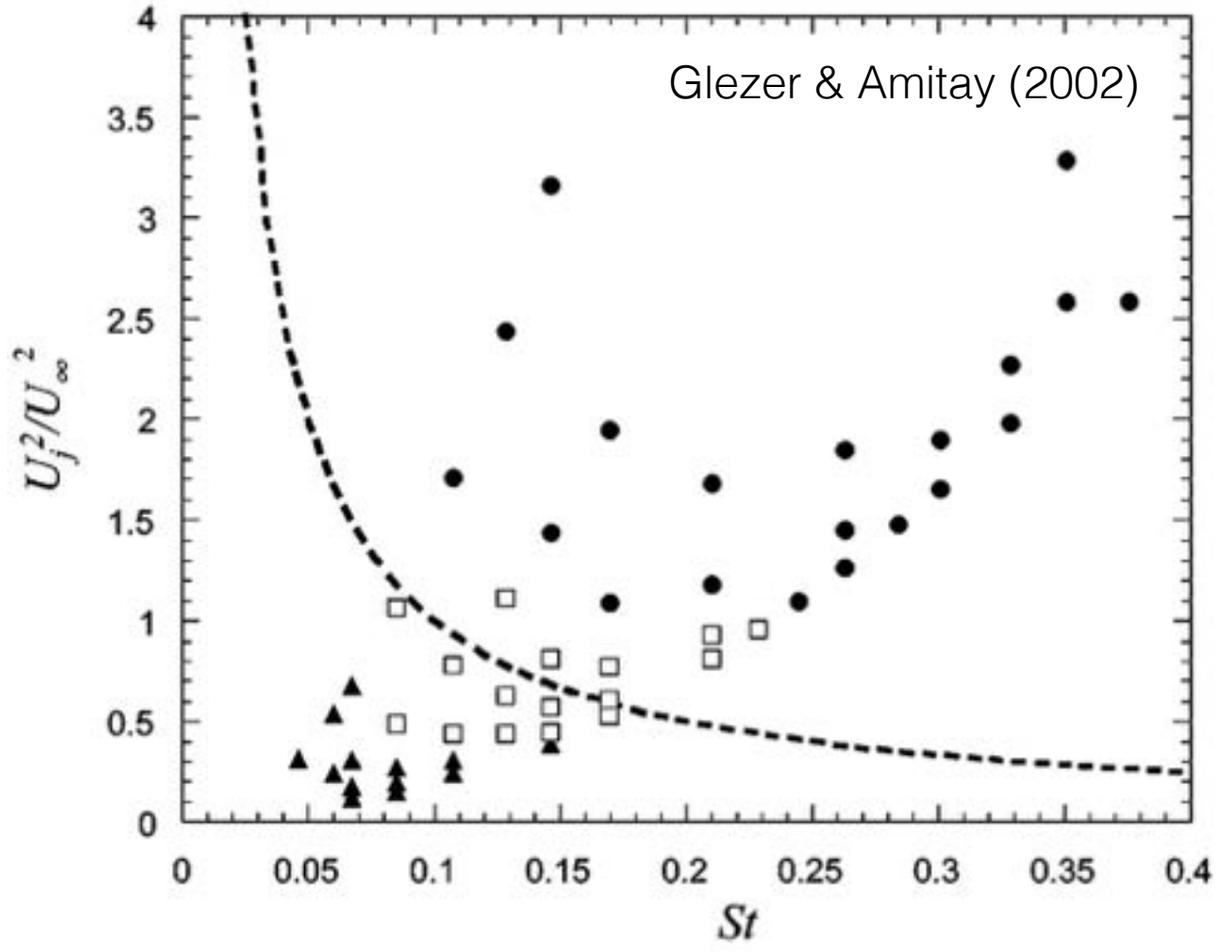

Figure 12 Interaction domain map. (▲) Discrete vortices, (□) transitory, (●) closed recirulation. Dashed line corresponds to $\hat{f} = 0.1$.

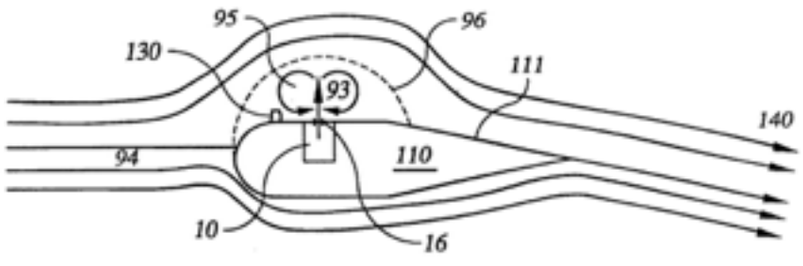

Virtual Aerodynamic Shaping

Baseline flow on top. Separates at about 83°

With excitation, separation moves to 110°

CW vortices convect along the surface, transporting high momentum fluid near the wall

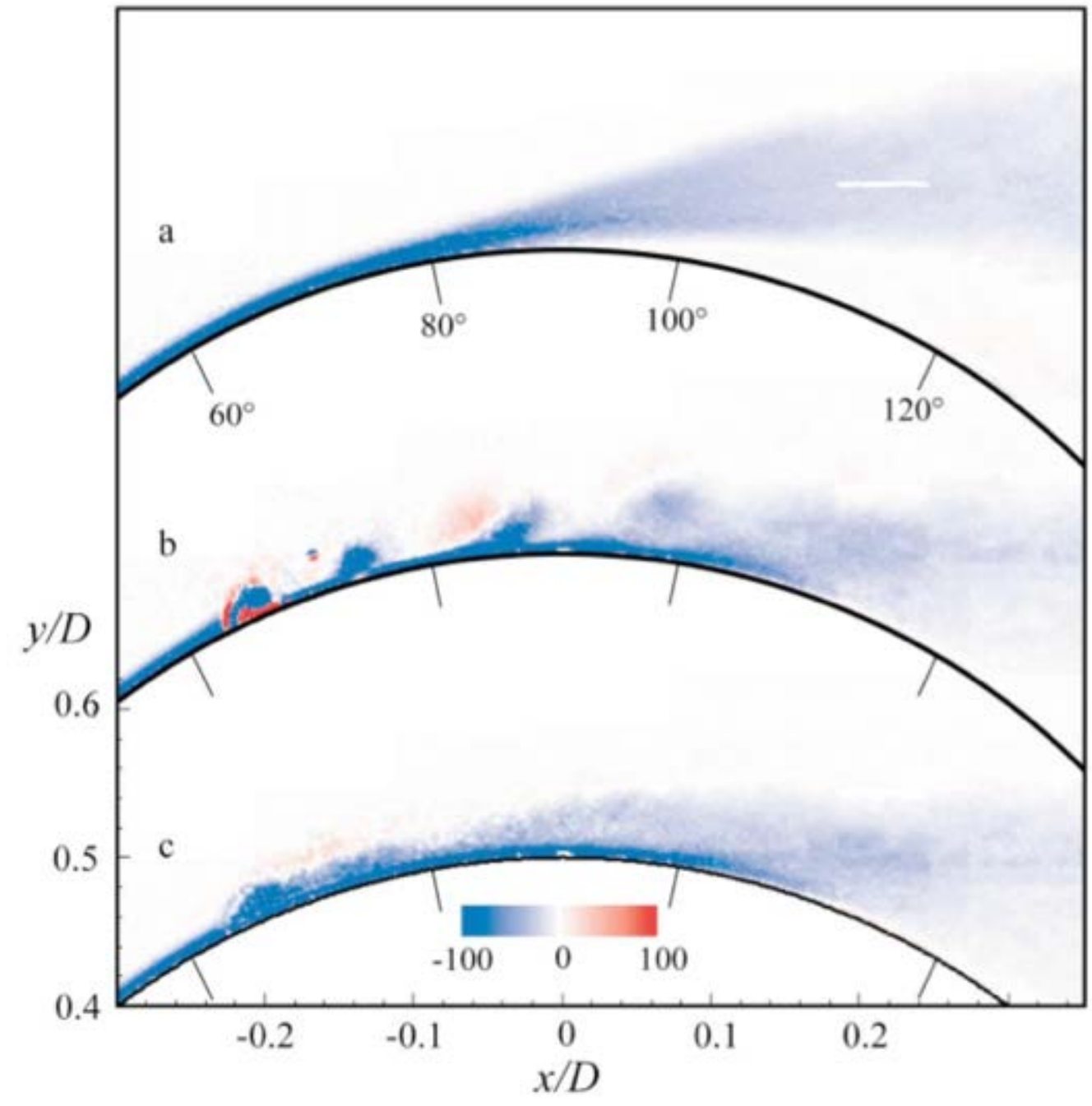

Figure 14 Normalized vorticity. $Re_D = 21{,}500, \gamma = 63^0, C_\mu = 5.1 \times 10^{-2}, \hat{f} = 0.035$. (*a*) baseline; actuated: (*b*) phase locked and (*c*) time averaged.

Low vs High Frequency Forcing

NACA 0025 at Re = 10^5
and 10° angle of attack
Forcing at separation

$$St_e(= f^+) = 58$$

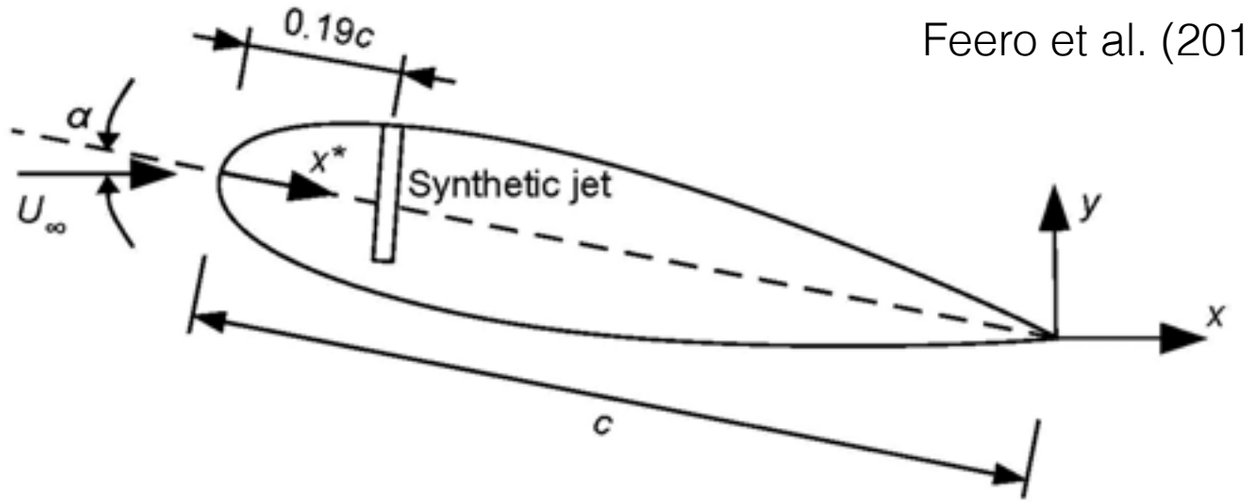

Feero et al. (2015)

Uncontrolled

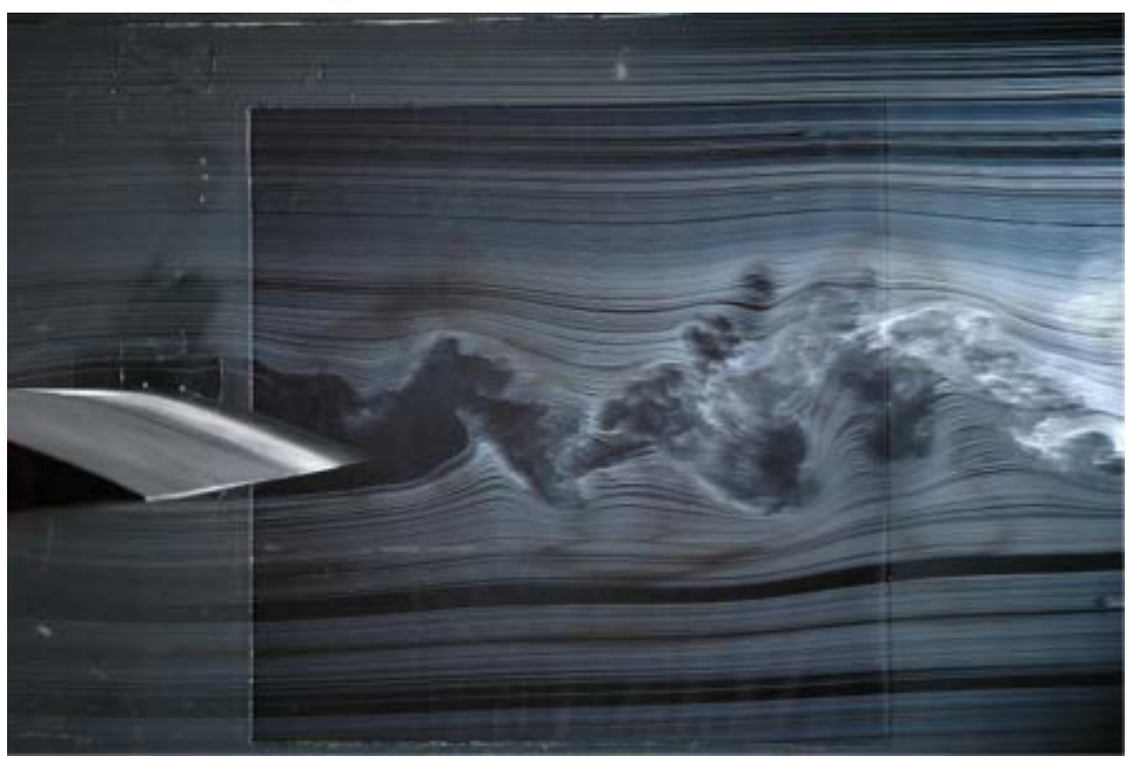

Forced

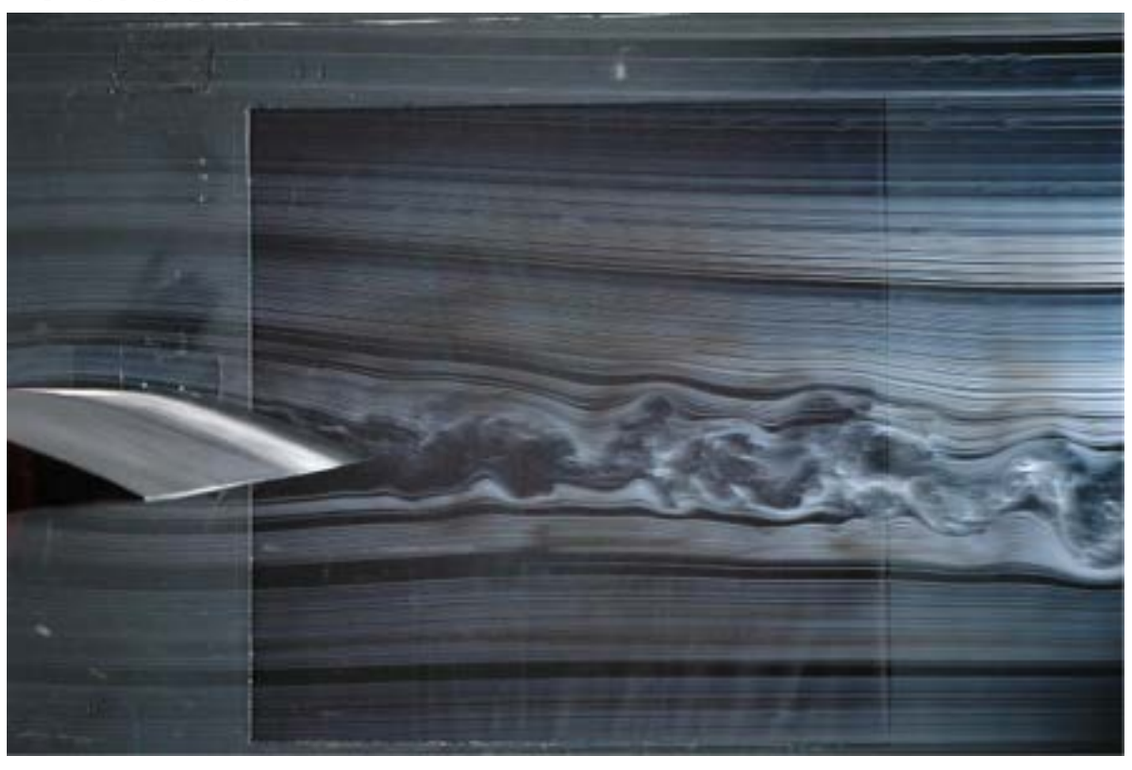

Low vs High Frequency Forcing

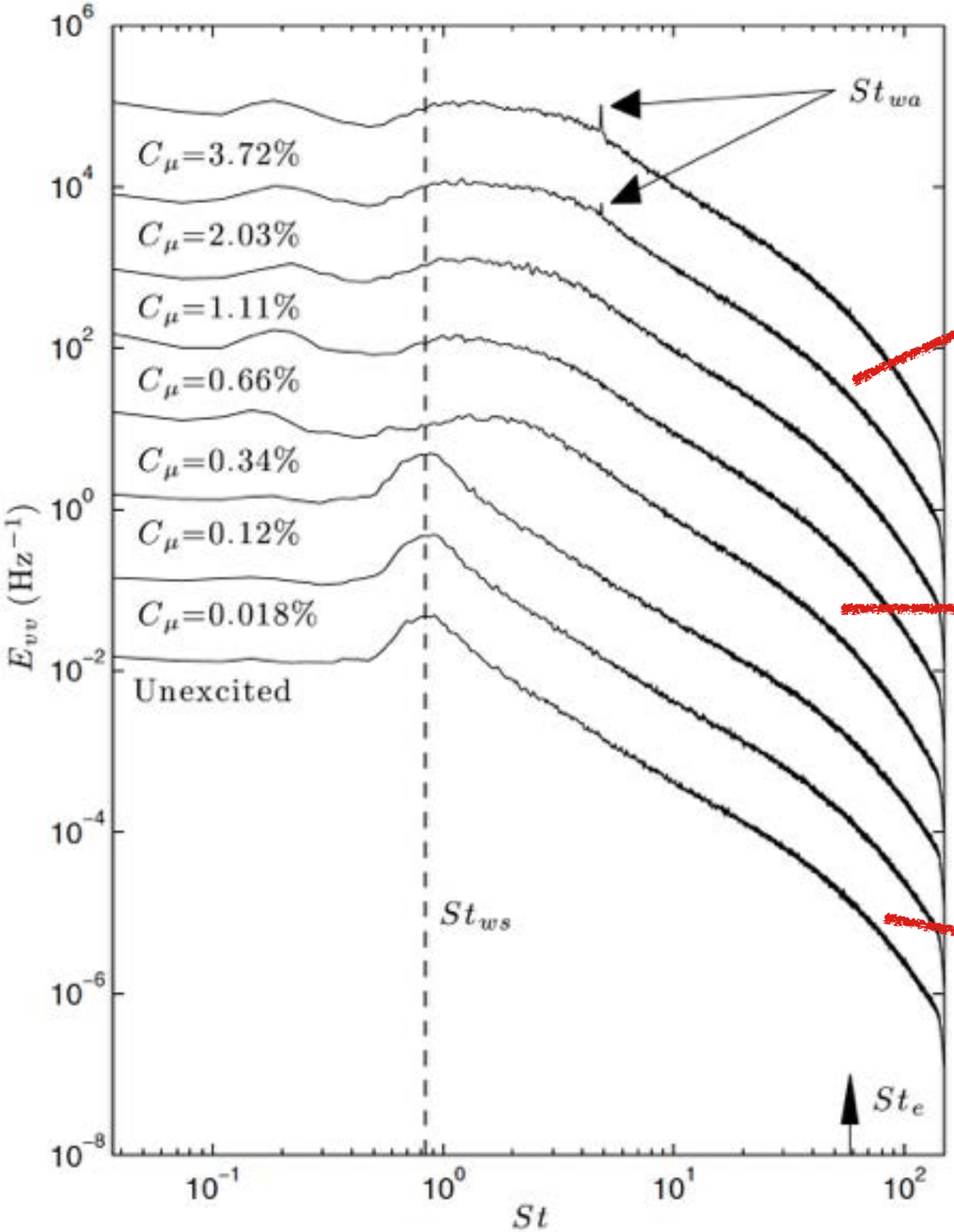

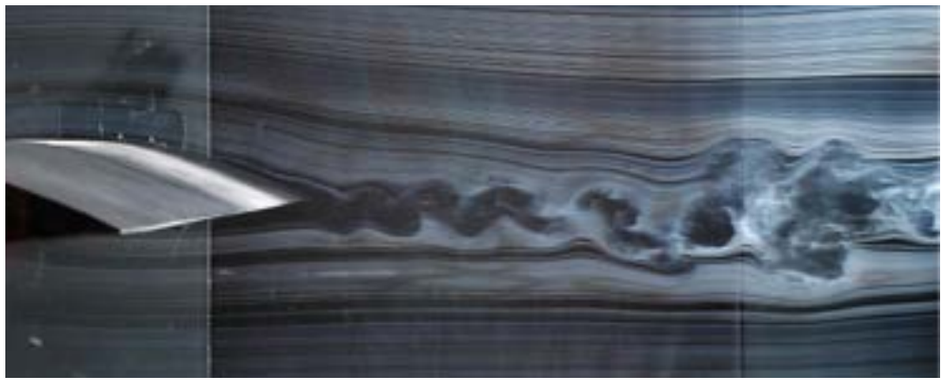

Feero et al. (2015)

Pulse Modulated Forcing

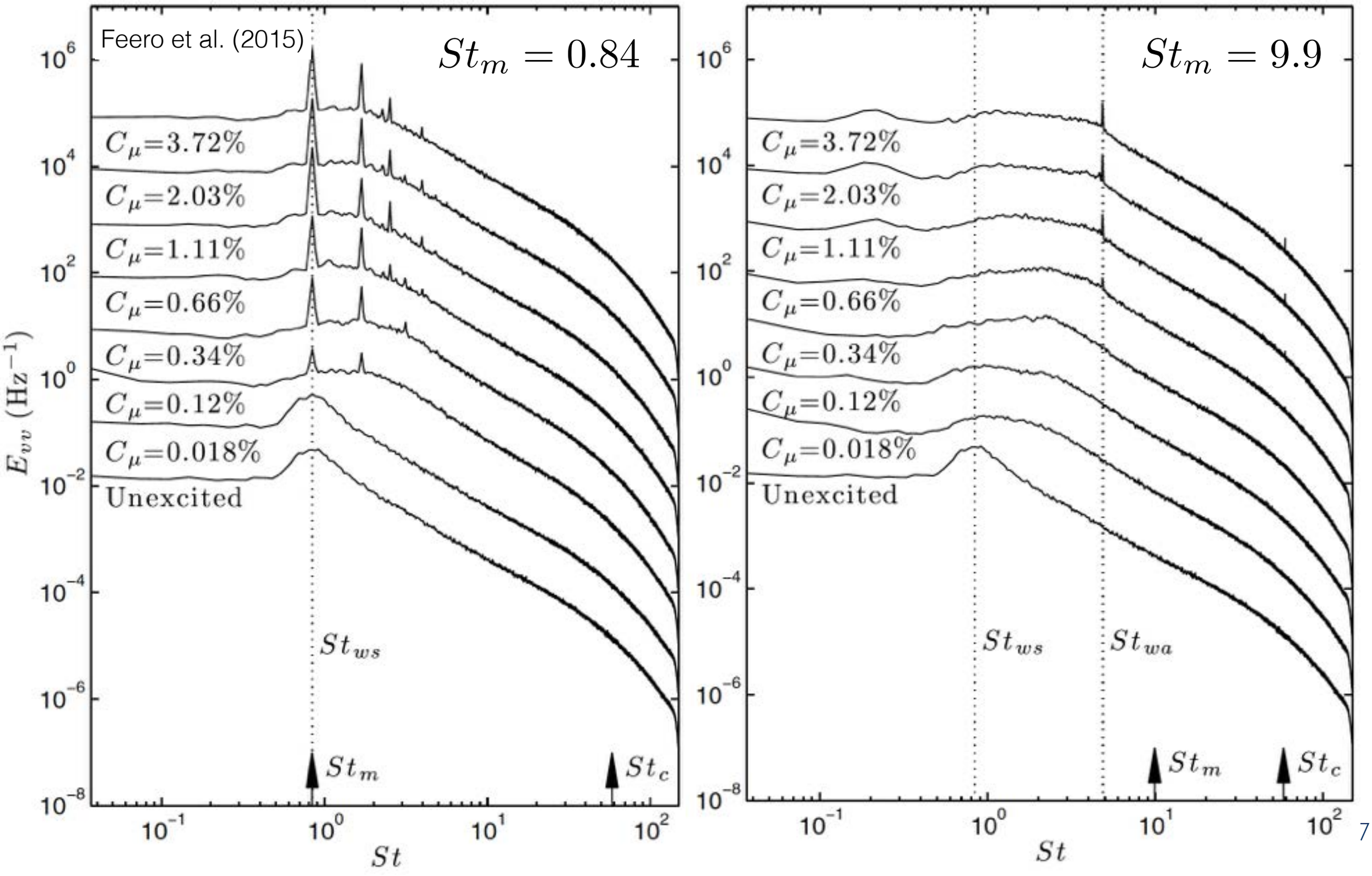

Low vs High Frequency Forcing

- Low frequency forcing ($f^+ = \mathcal{O}(1)$) produces a stronger periodic component in the flow
  - the train of vortices observed previously
  - can produce more “unsteady” aerodynamic forces
  - flow reattached at lower forcing than $f^+ = \mathcal{O}(100)$

- High frequency forcing ($f^+ = \mathcal{O}(10)$) produces more steady reattachment
  - No significant periodicity in the wake except with over actuation
  - Reattachment at lower forcing amplitude as other frequency cases

- Non-linear interactions between structures of different scales play an important and complex role in the reattachment of the flow.

NASA/Boeing ERA Control

Active flow control used on vertical tail.

Lin et al. (2016)

Good point for introduction of technology on a real aircraft

- non-critical application
- can demonstrate reliability

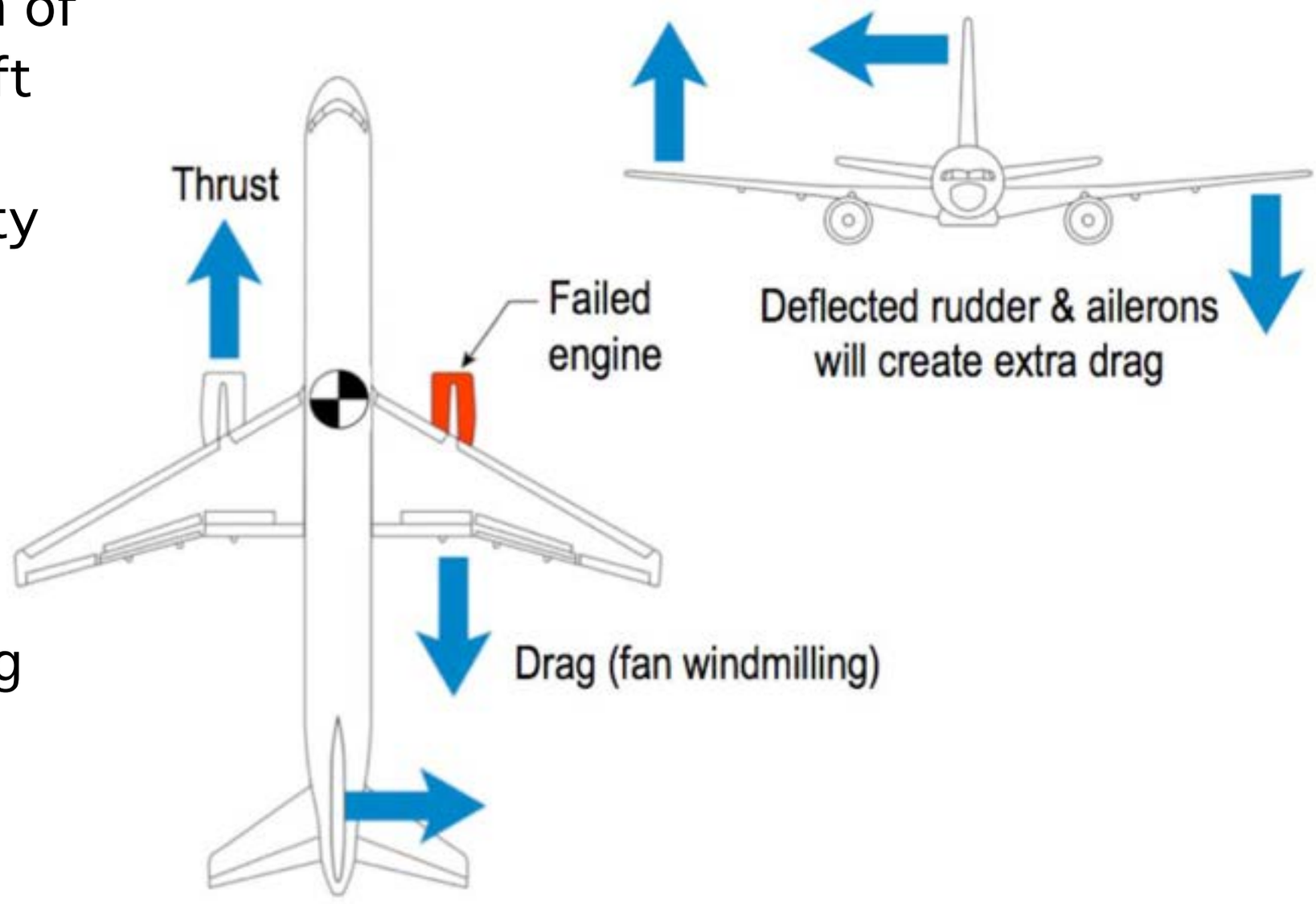

Potential for about 1% drag reduction.

NASA/Boeing ERA Control

Multi-scale, multi-stage effort to move technology from the lab to flight!

Lin et al. (2016)

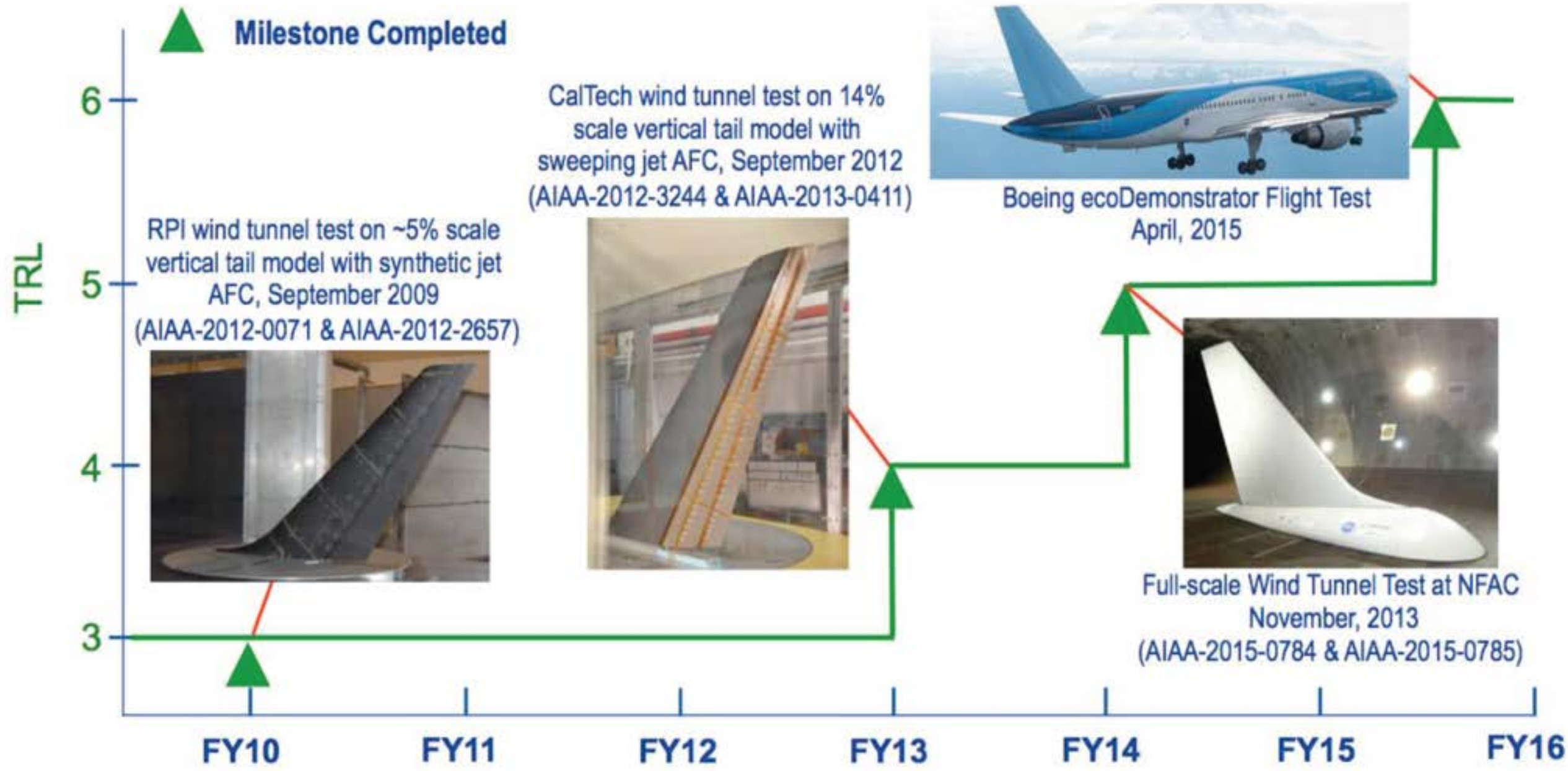

NASA/Boeing ERA Control

For full-scale wind tunnel testing, 37 fluidic oscillators are applied upstream of the rudder hinge.

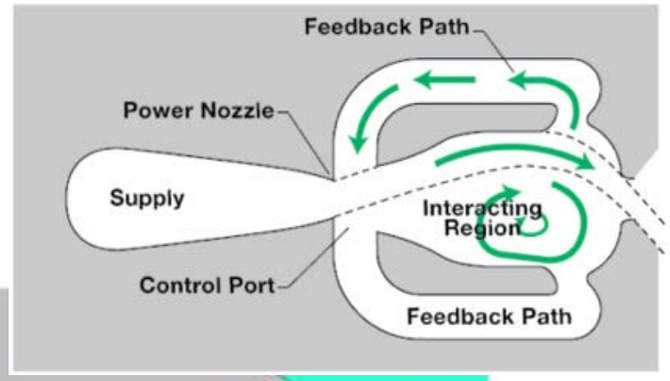

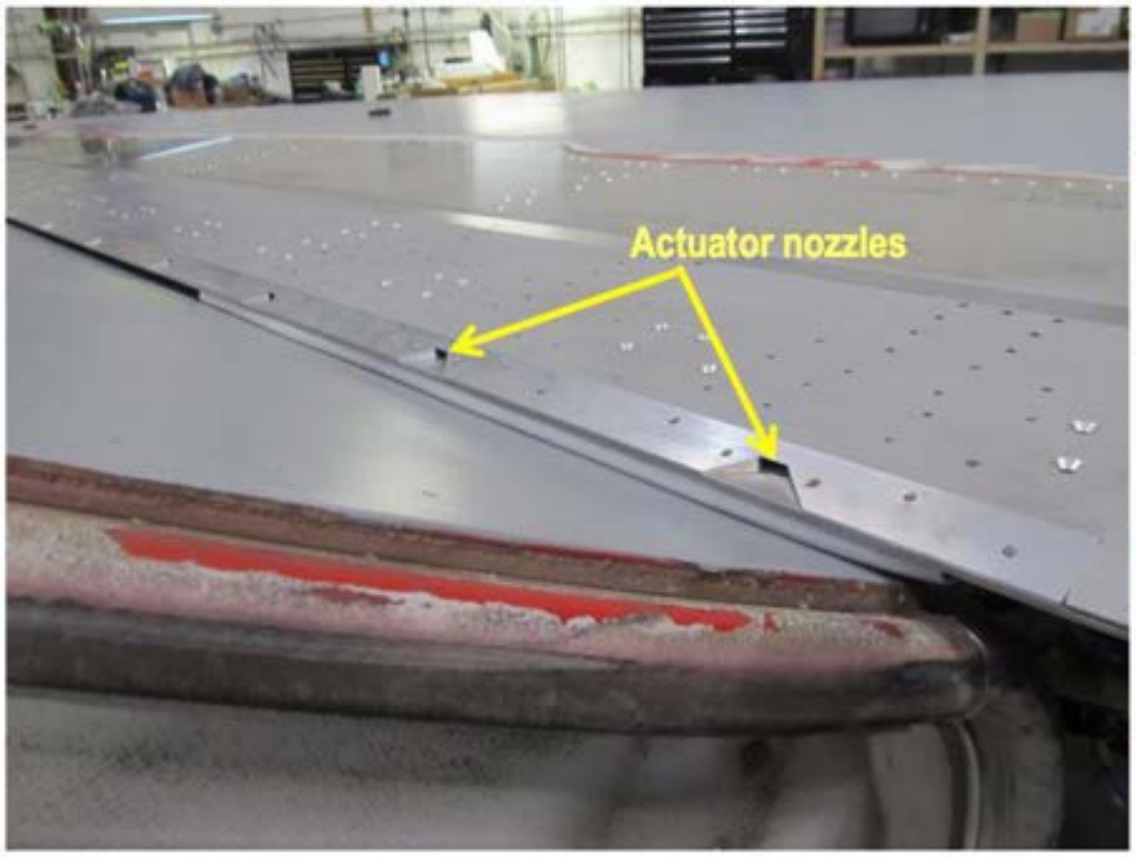

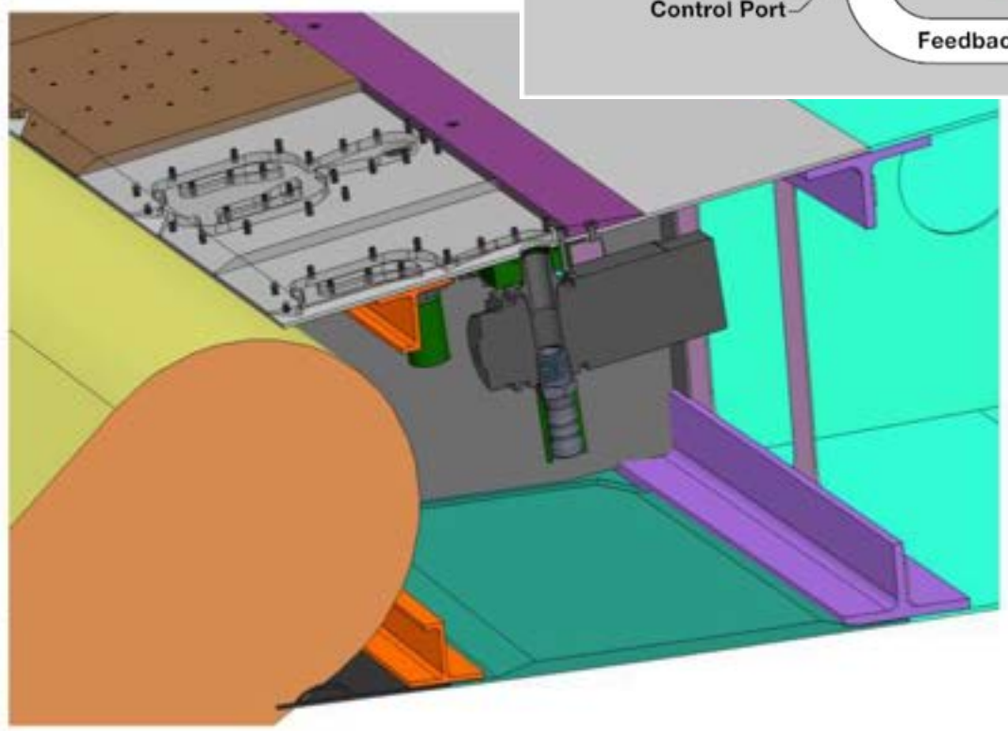

Close-up view of actuators

Whalen et al. (2015)

NASA/Boeing ERA Control

For full-scale wind tunnel testing, 37 fluidic oscillators are applied upstream of the rudder hinge.
20% increase in side force (more than twice what vortex generators give)

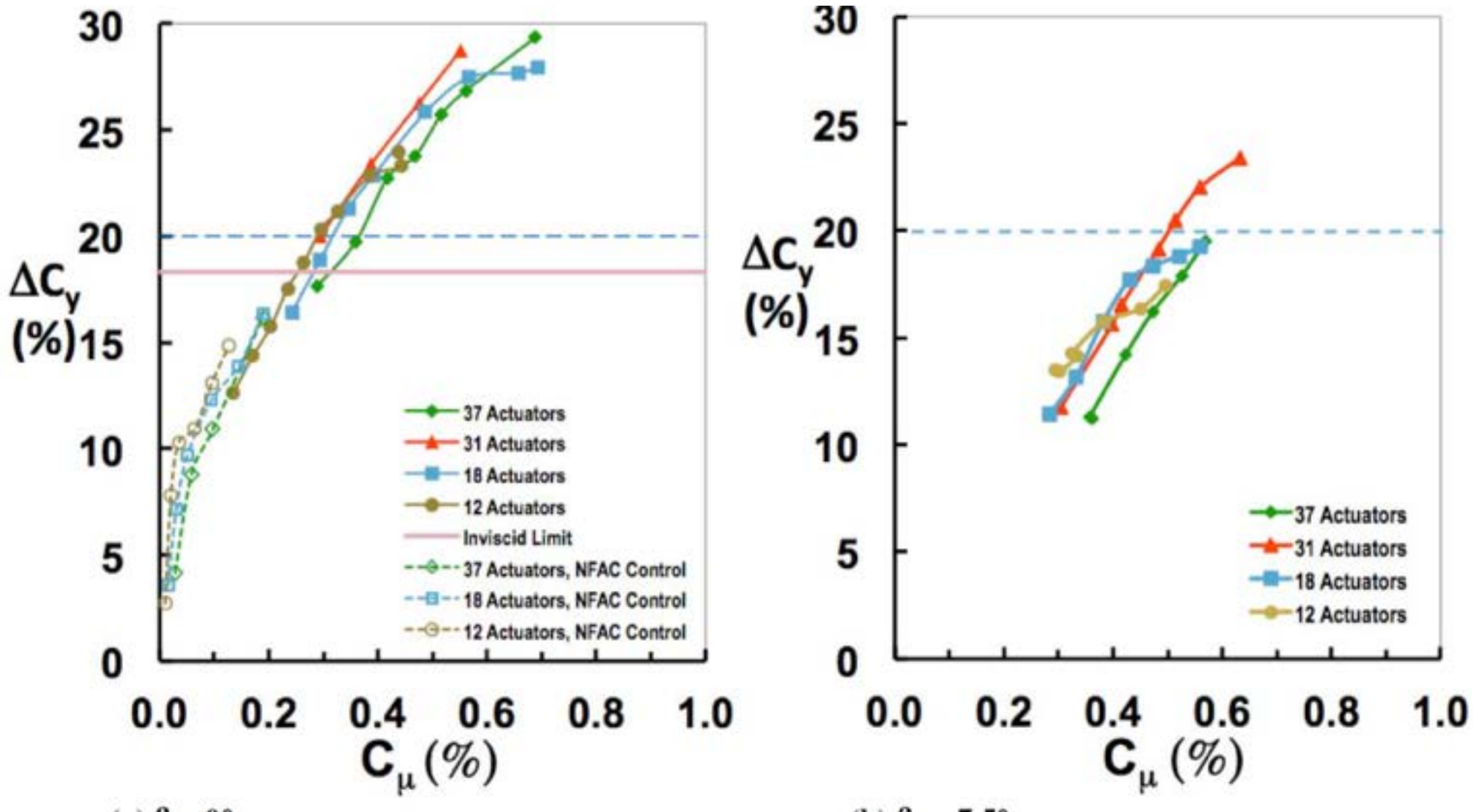

Whalen et al. (2015)

NASA/Boeing ERA Control

For flight tests, 31 actuators used on the 757 ecoDemonstrator

13-16% increase in side force.

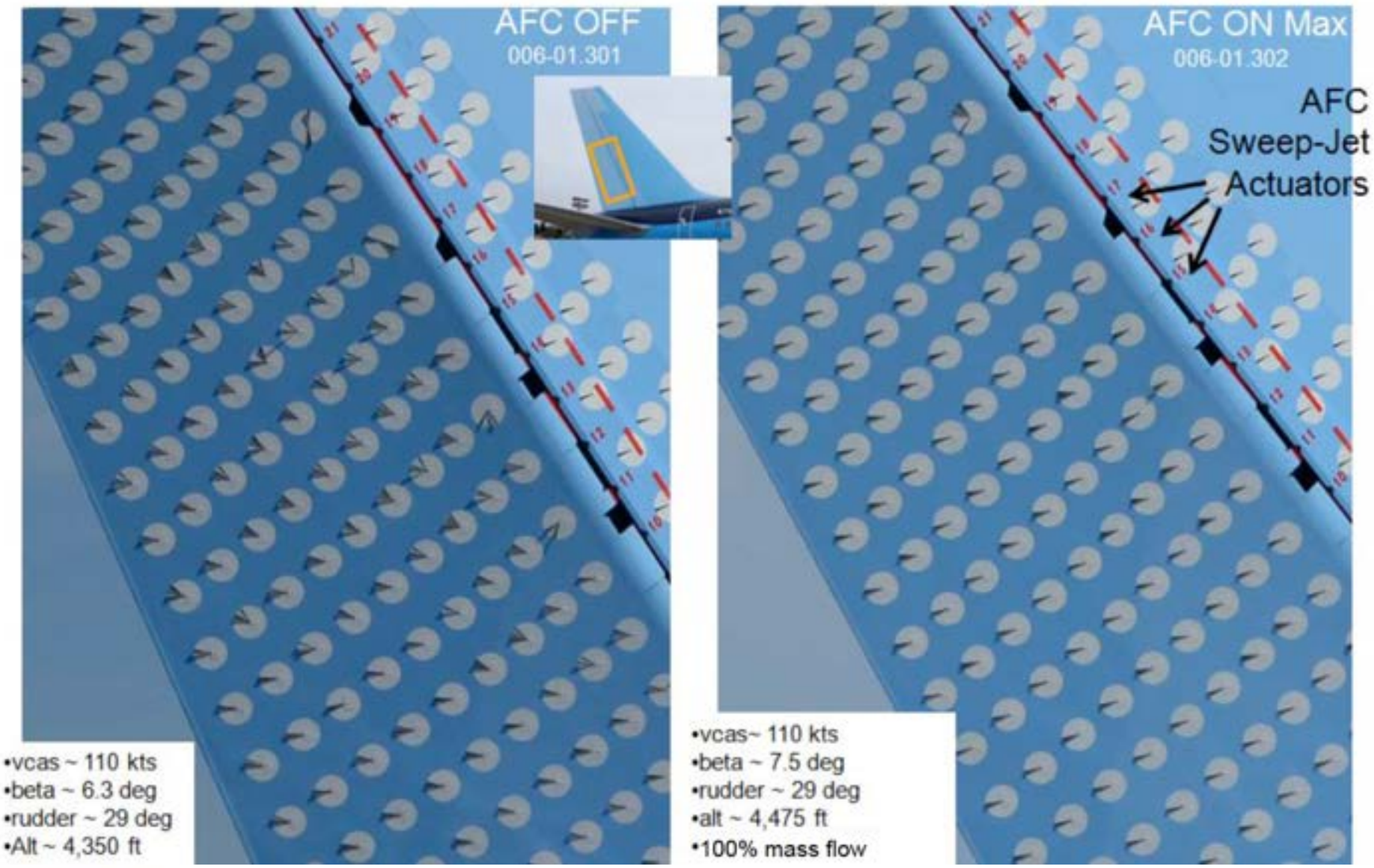

Lin et al. (2016)

3D Nature of Separation

So far, separation is more or less discussed as a 2D phenomena, but it is not!

$Re_c = 10^6$

$\alpha = 16^\circ$

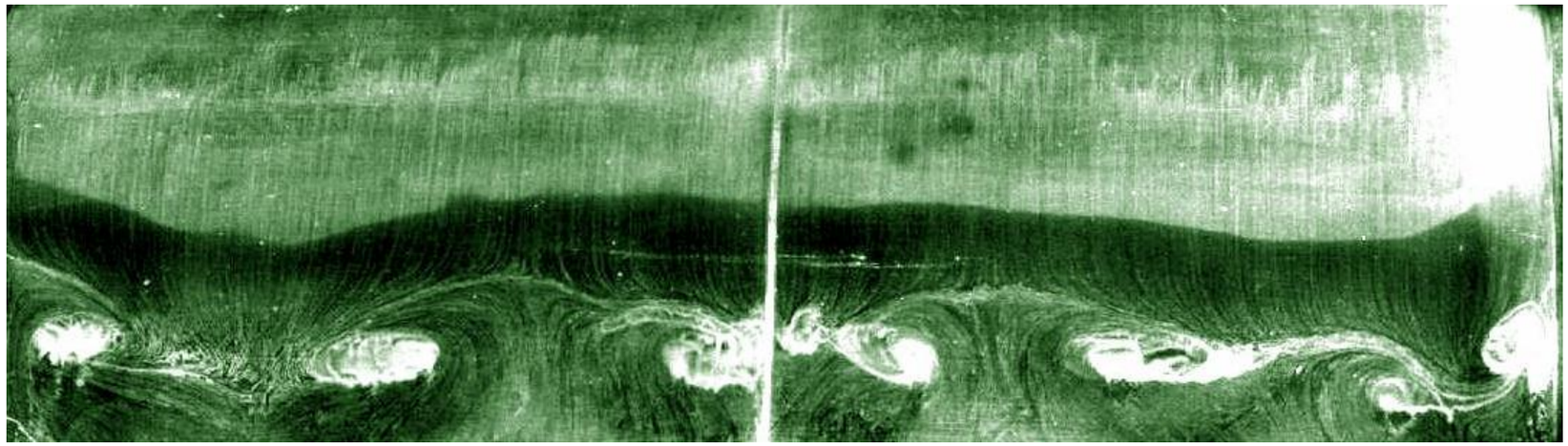

$Re_c = 10^6$

$\alpha = 18^\circ$

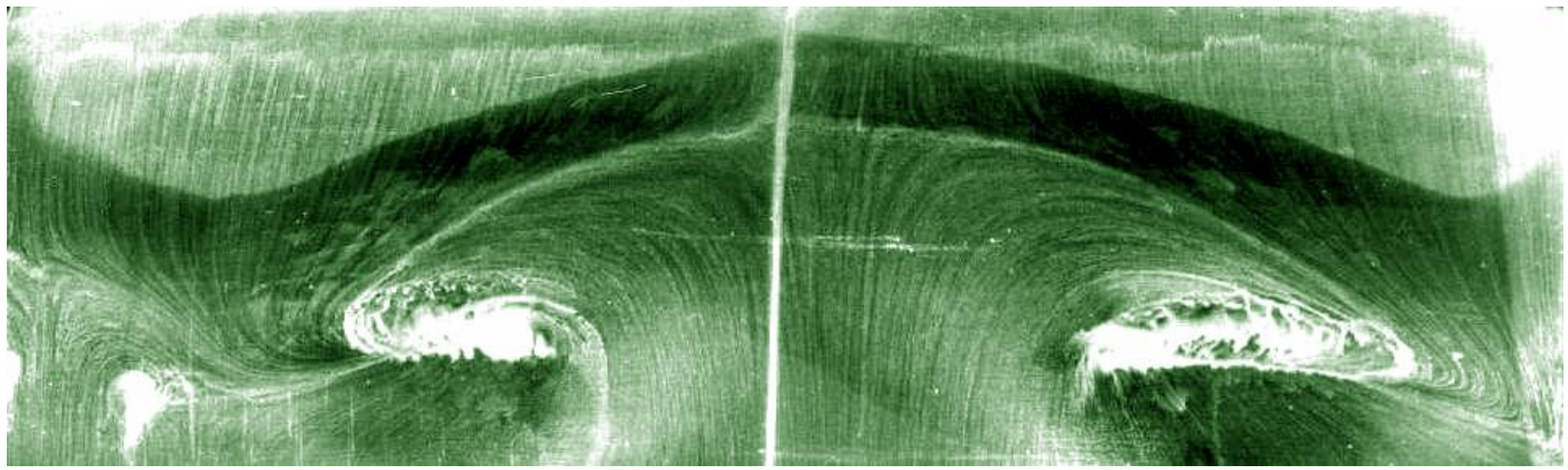

Images courtesy of JF Morrison (Imperial College)

3D Nature of Separation

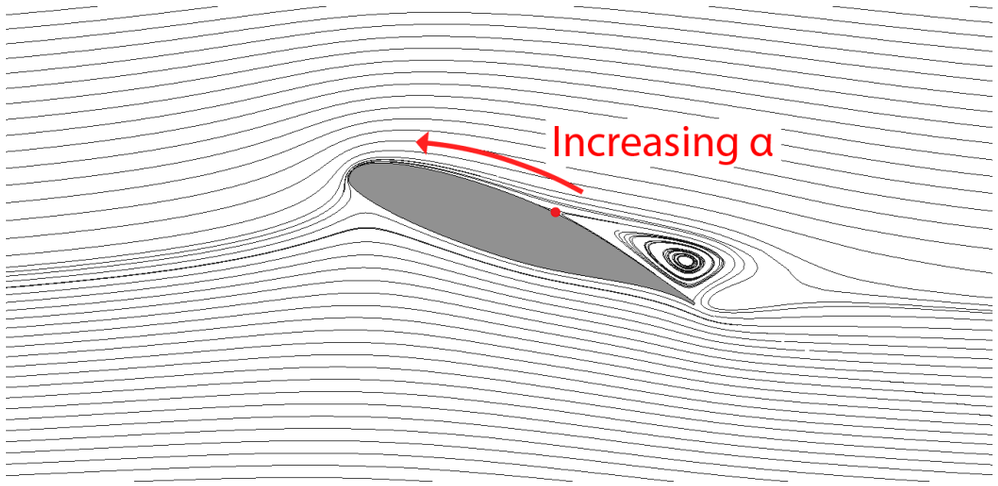

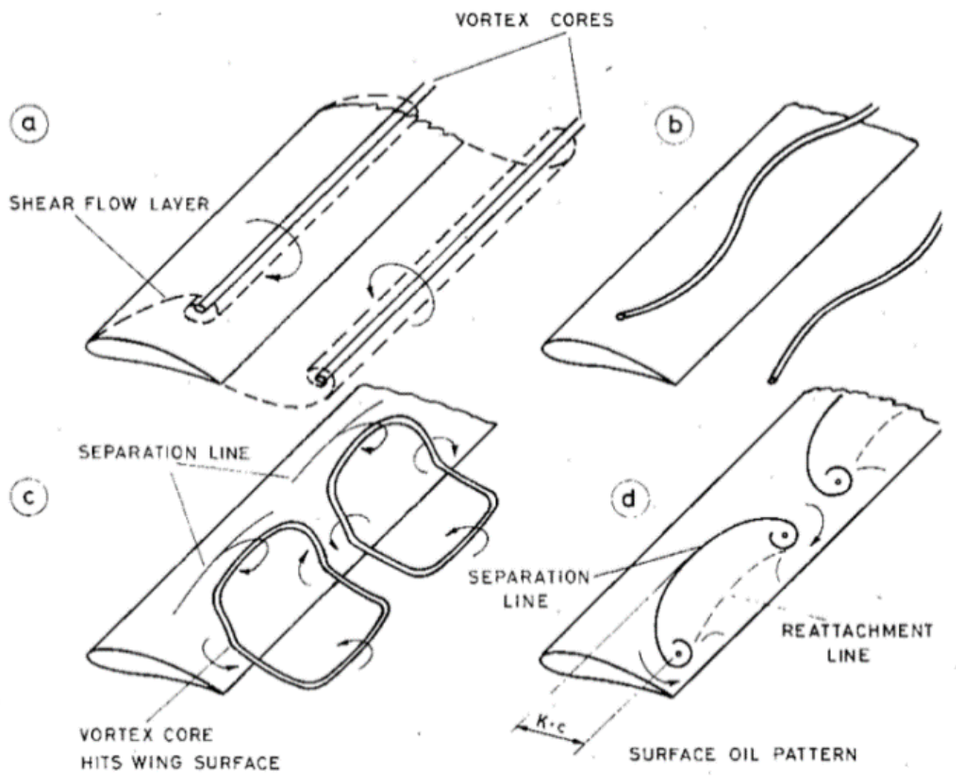

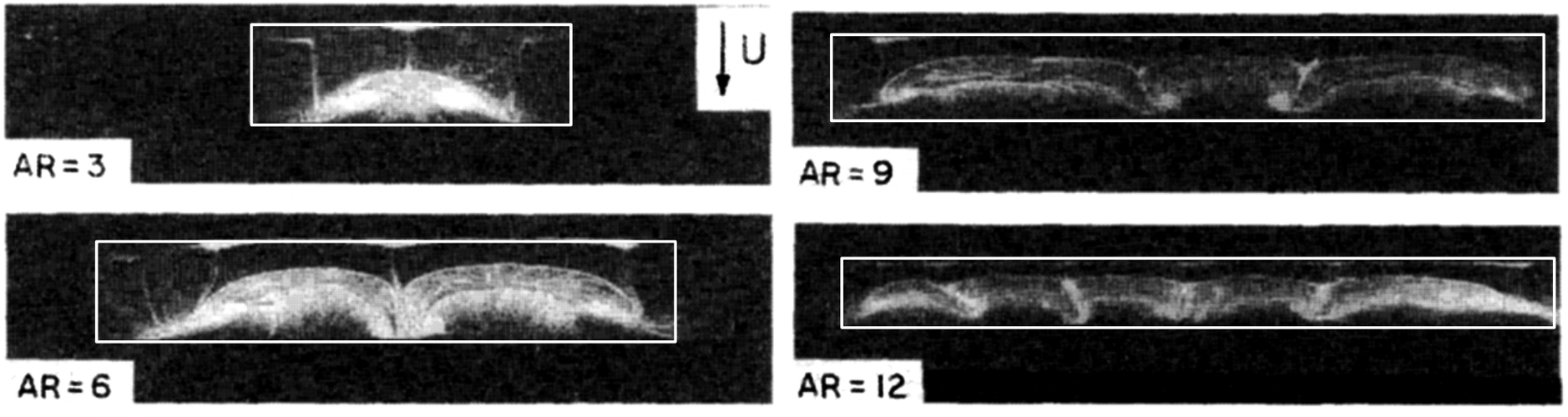

Winkelman & Barlow (1980)

3D Nature of Separation Control

Nominally 2D actuator spanning 1/3 of model span.

Significant 3D effect and rapid reduction of the reattached region downstream of the actuators.

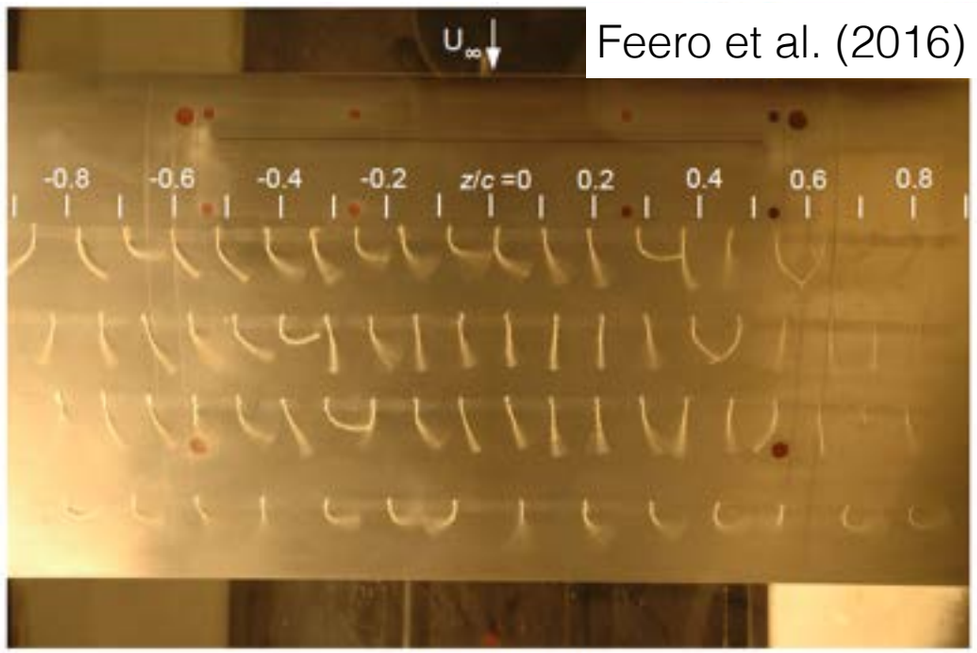

Feero et al. (2016)

(a) Baseline

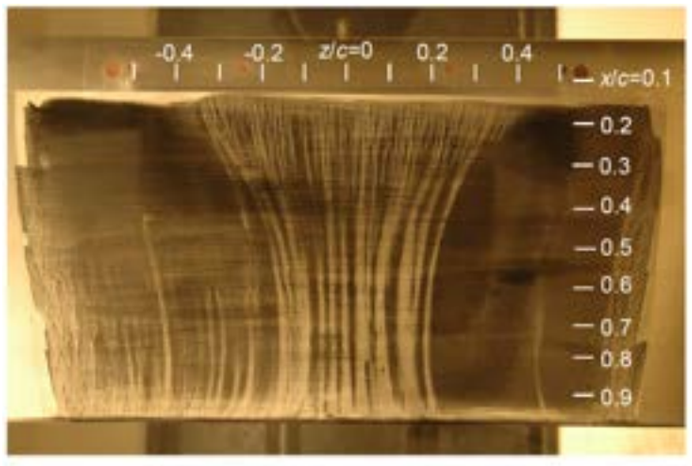

(a) $C_B = 1$

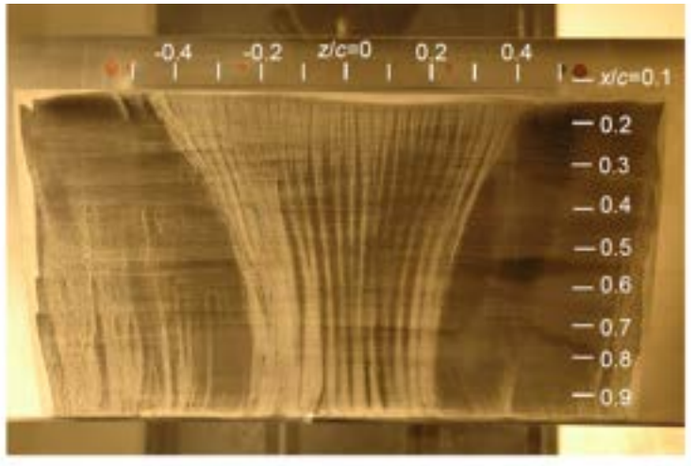

(b) $C_B = 2$

Region of effect increases with actuation amplitude.

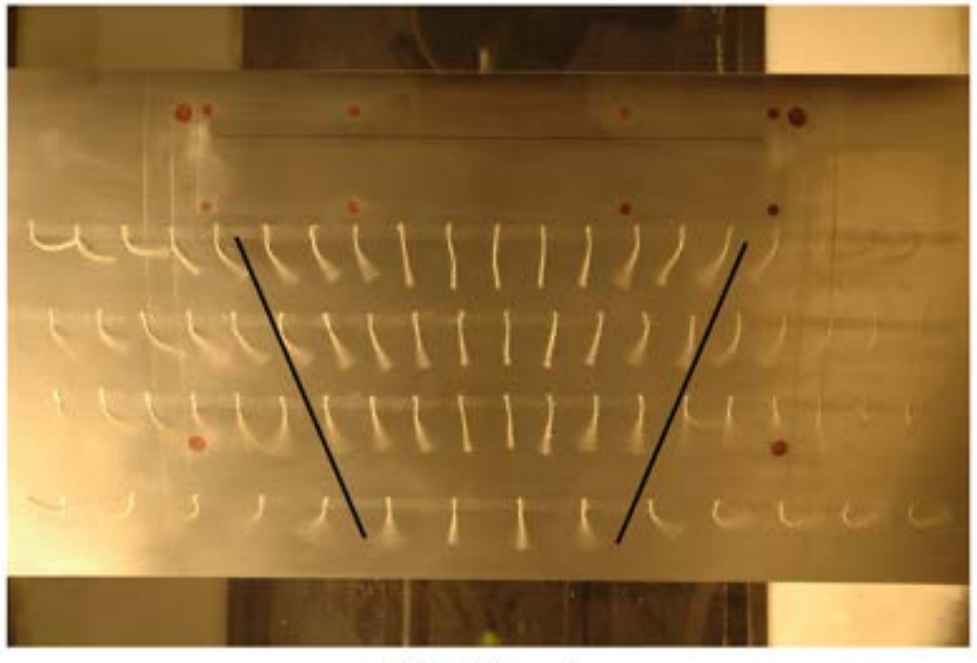

(c) $F^+ = 1$

Control of Bluff Bodies

For bluff bodies, the control strategy will be fundamentally different since the point of separation is either fixed, or very difficult to move.

We will focus primarily on the blunt trailing edge airfoil here, but will bring in some other canonical flow examples.

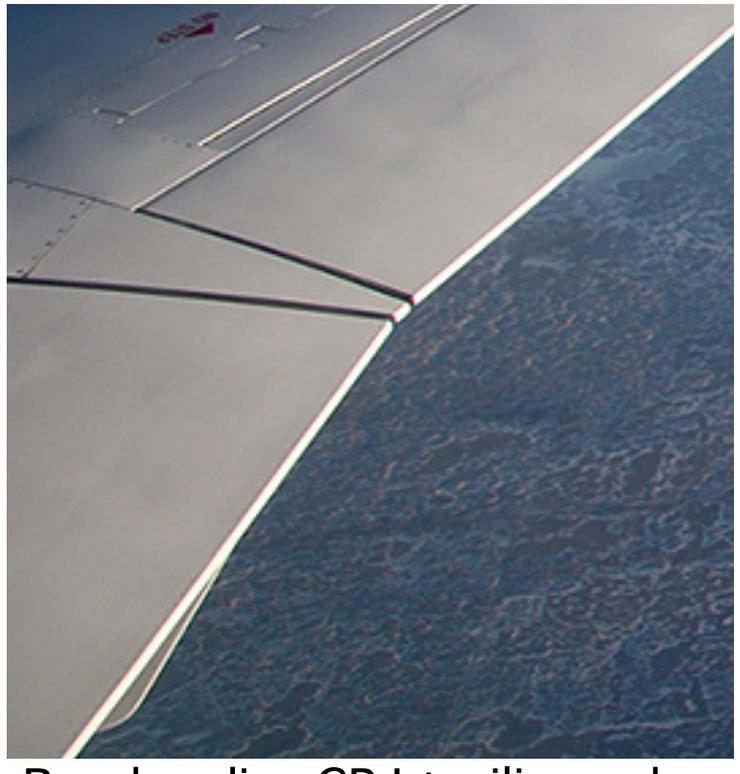

Bombardier CRJ trailing edge

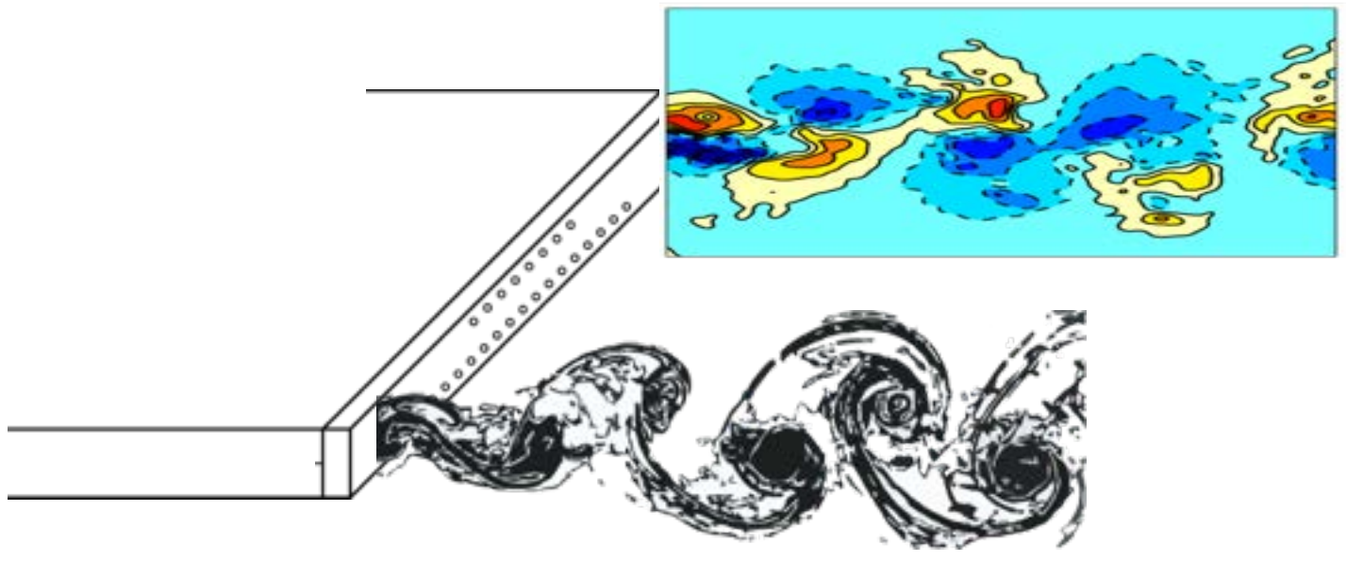

Other Bluff Bodies

A few other bluff bodies of interest.

Landing gears involve a number of them:

- Struts (cylinders)
- Wheels (blocks and cavities)
- Landing gear bay (cavity)
- Wires and hoses (roughness)

Corke & Naguib (IIT)

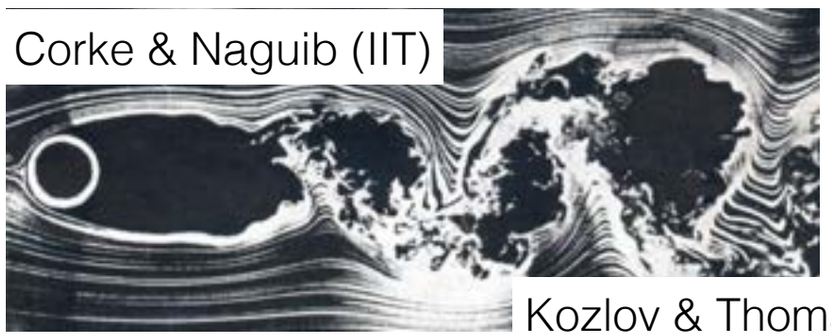

Kozlov & Thomas (2011)

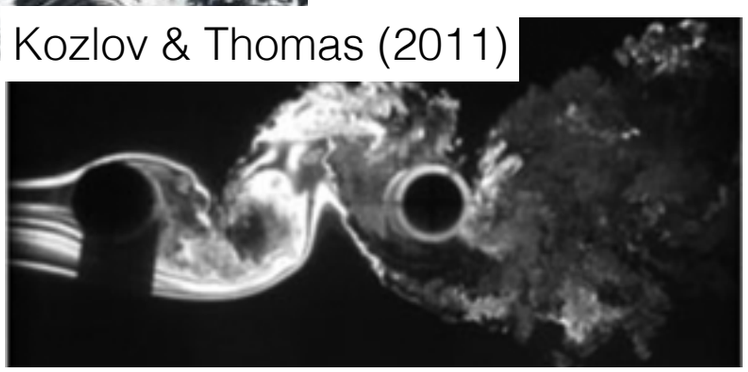

Blunt Trailing Edge Airfoils

Why blunt trailing edge?

- Increased sectional area and sectional moment of inertia for fixed airfoil maximum thickness
- Reduction of adverse pressure gradient on suction side
- Increased $C_{L\alpha}$ and $C_{L\max}$, decreased sensitivity to transition location
- Weaker shock - reduce wave drag

But, increase in drag and unsteady loads associated with vortex shedding, and decrease in base pressure

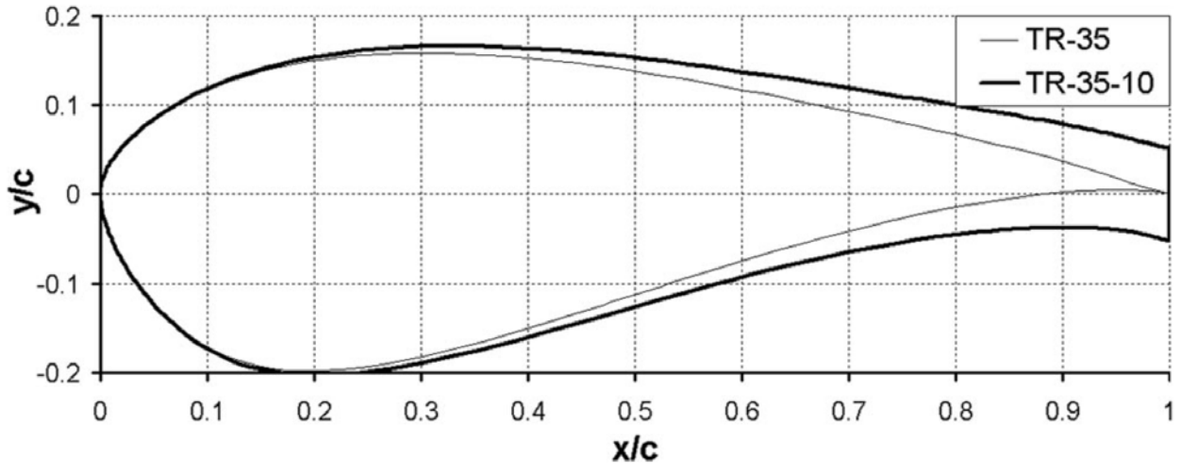

Figures from Standish & van Dam (2003)

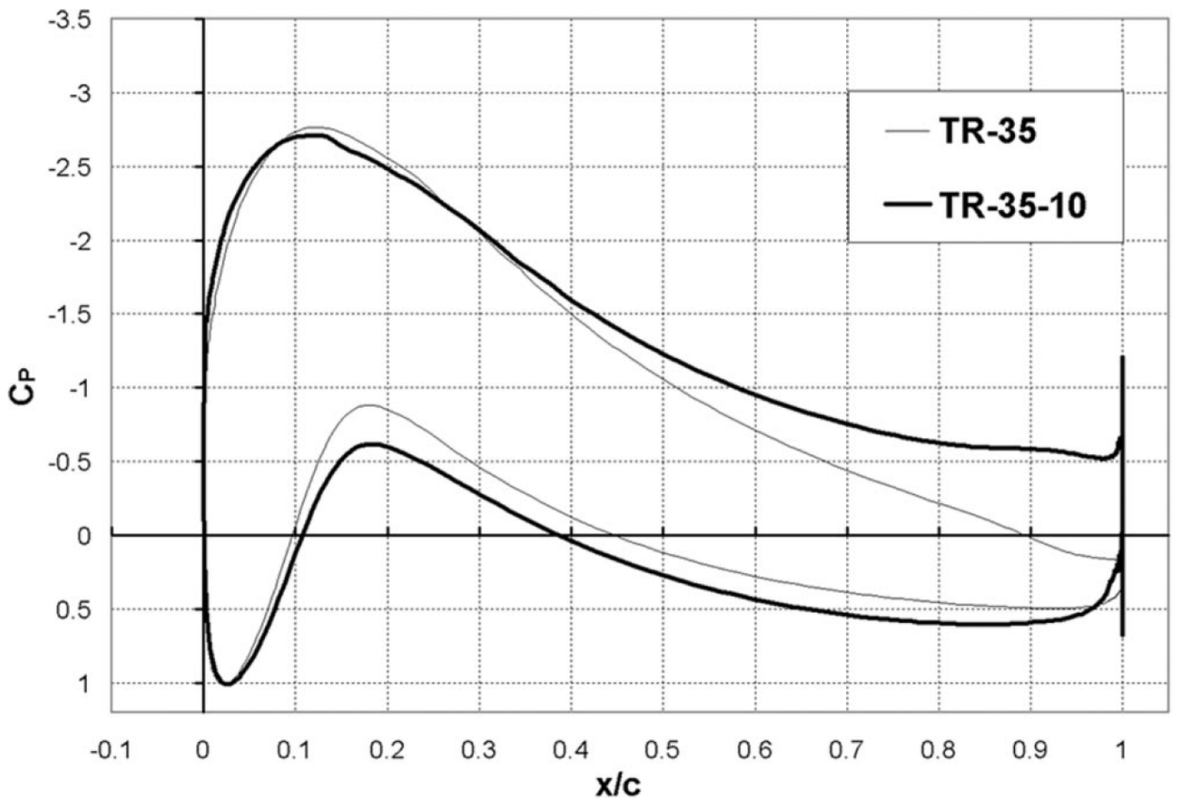

Bluff Body Flow (2D)

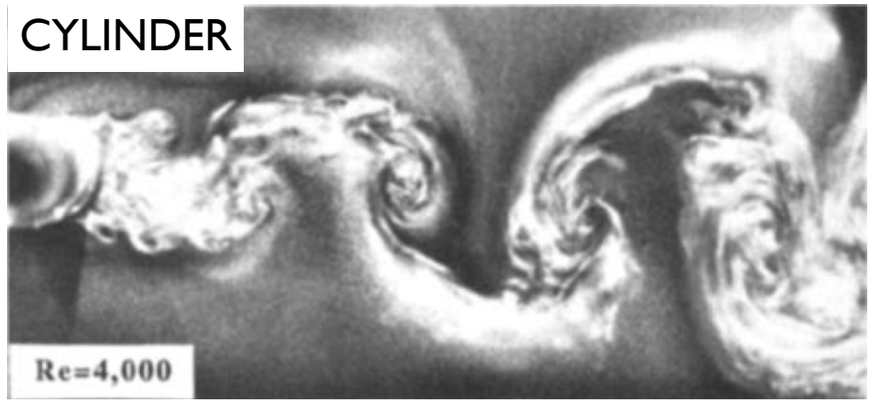

Williamson (1996)

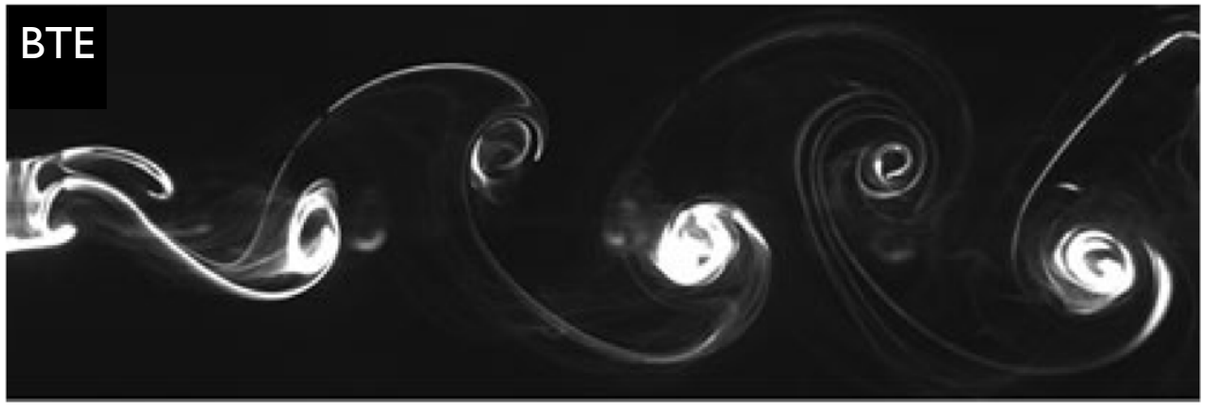

Naghib-Lahouti et al. (2012)

- Vortex shedding occurs above a threshold Reynolds number in wake of nominally two-dimensional bodies
  - Interacting shear layers: vortex grows until fluid with oppositely signed vorticity is entrained from across the wake (Gerrard, 1966)
- Vortex shedding leads to unsteady aerodynamic forces, vibrations and noise
- A convenient and simple way to characterize the strength of the vortex shedding is the vortex formation length, L_f :
  - streamwise distance at which rms velocity fluctuations are maximum

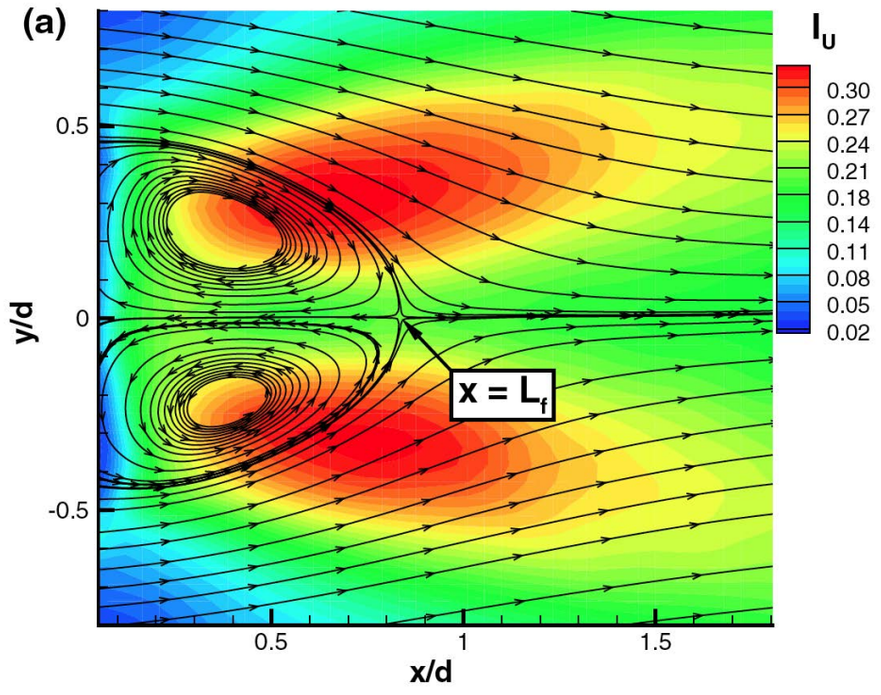

Figures from Naguib-Lahouti, Lavoie & Hangan (2014)

Secondary Instabilities

- Primary vortices are connected by pairs of streamwise vortices with characteristic spacing, λ_z
- Unstable mode topologies depend on body geometry and Reynolds number

- Cylinder wake
  - Williamson (1996): critical Re ≈ 180-190, $\lambda_z \approx 3\text{-}5d$ (Mode B)

numerical

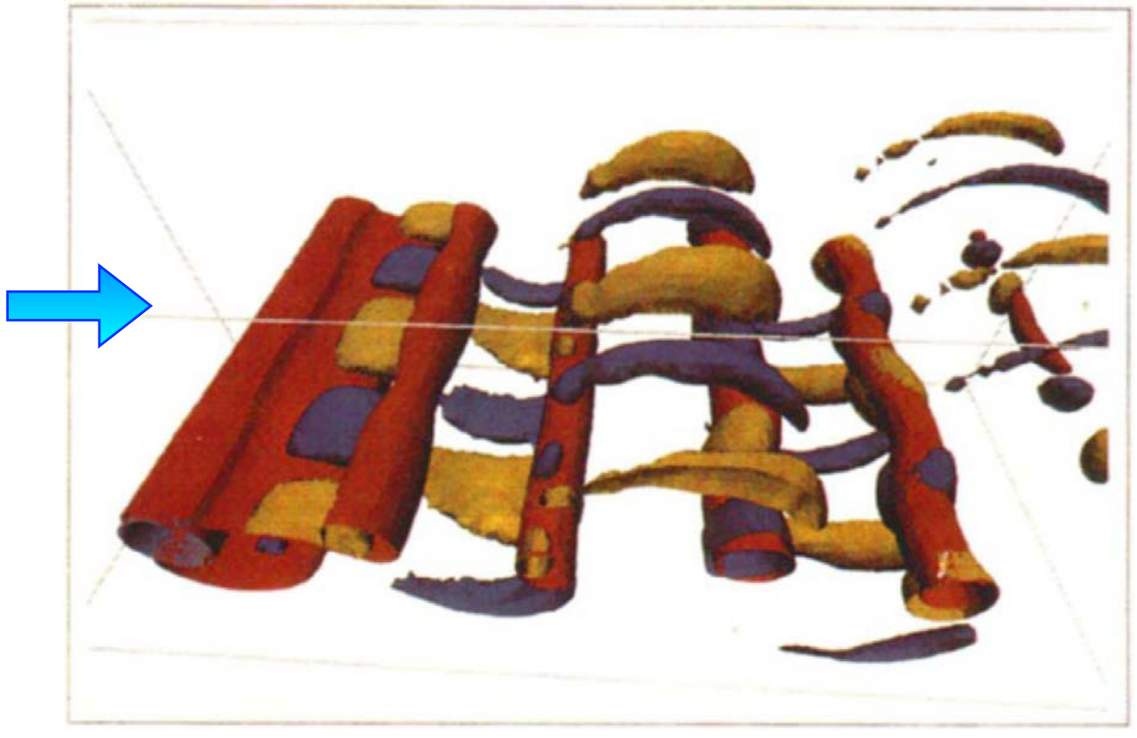

experiment

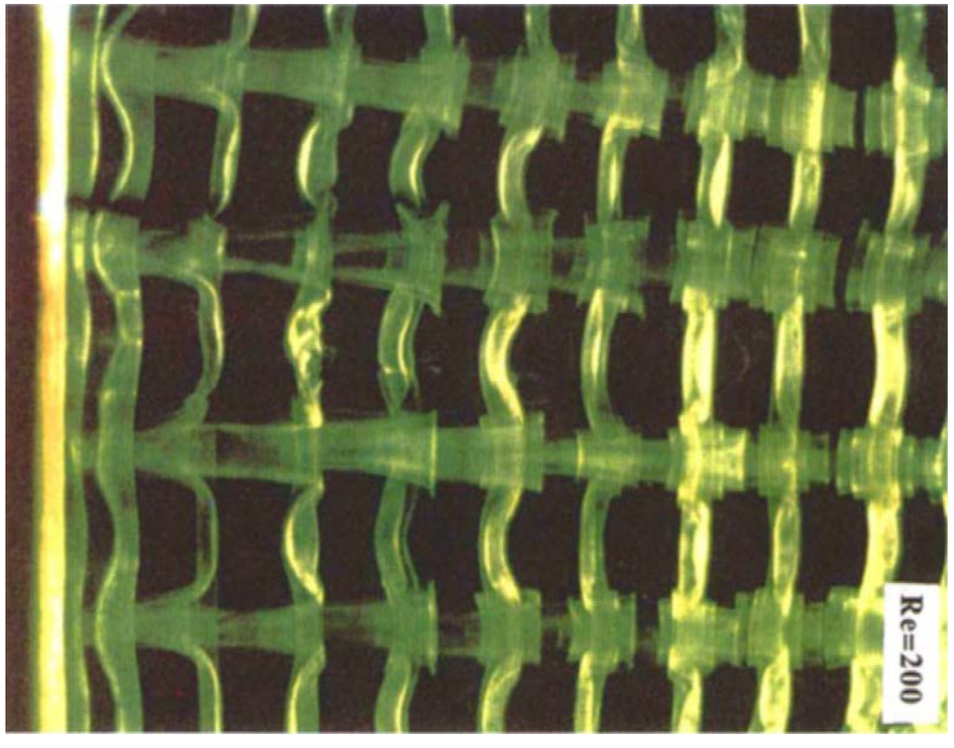

Figures from Williamson (1996)

Secondary Instabilities

- Primary vortices are connected by pairs of streamwise vortices with characteristic spacing, λ_z
- Unstable mode topologies depend on body geometry and Reynolds number
- For BTE geometry with c/d = 12.5, Mode B'
  - Ryan et al. (2005), numerical stability analysis: critical $Re_d \approx 410$, $\lambda_z \approx 2.2d$
  - Naghib-Lahouti et al. (2012, 2014), experiments: $\lambda_z \approx 2.3$ - 2.5 for Re_d = 2,000 - 30,000

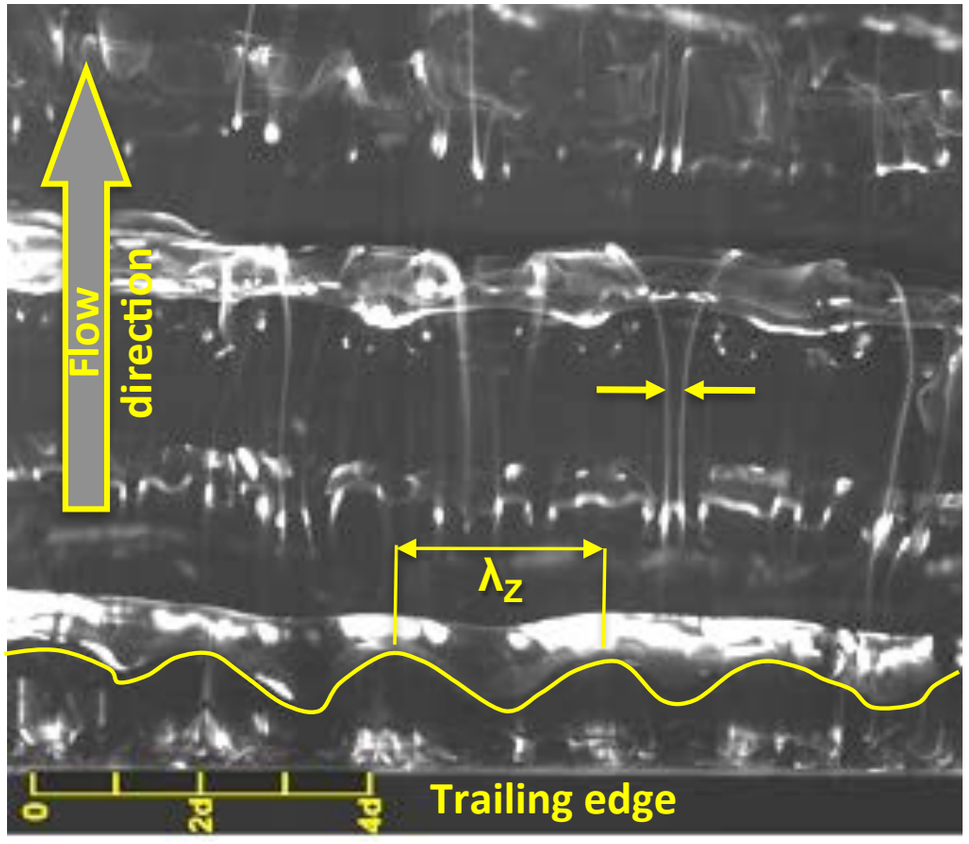

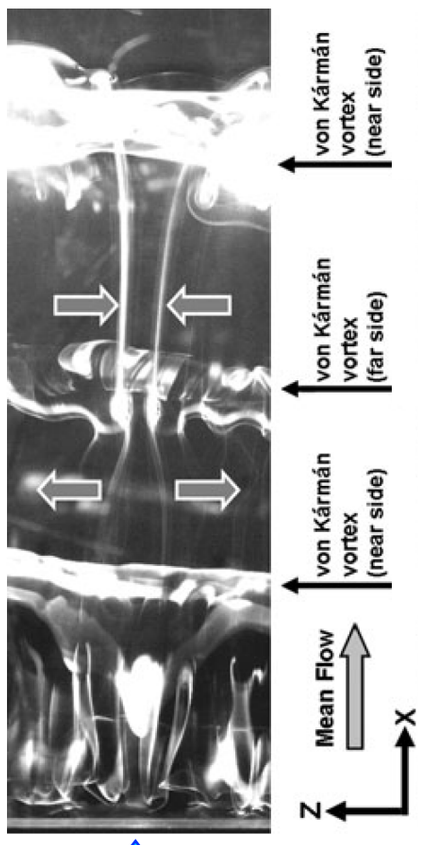

Figures from Naghib-Lahouti et al. (2012)

Three-dimensional Effects

- Low-frequency modulation of local measurements and global properties
- Henderson (1997), cylinder flow: modulation of lift from "phase dislocations," occurs in "bursts at irregular intervals"
- Darekar & Sherwin (2001), wavy square cylinder: flow switches between two states, mildly or highly 3D
- Najjar & Balachandar (1998), normal flat plate: two states correspond to different L_f and C_p
- Increasing wake 3-dimensionality

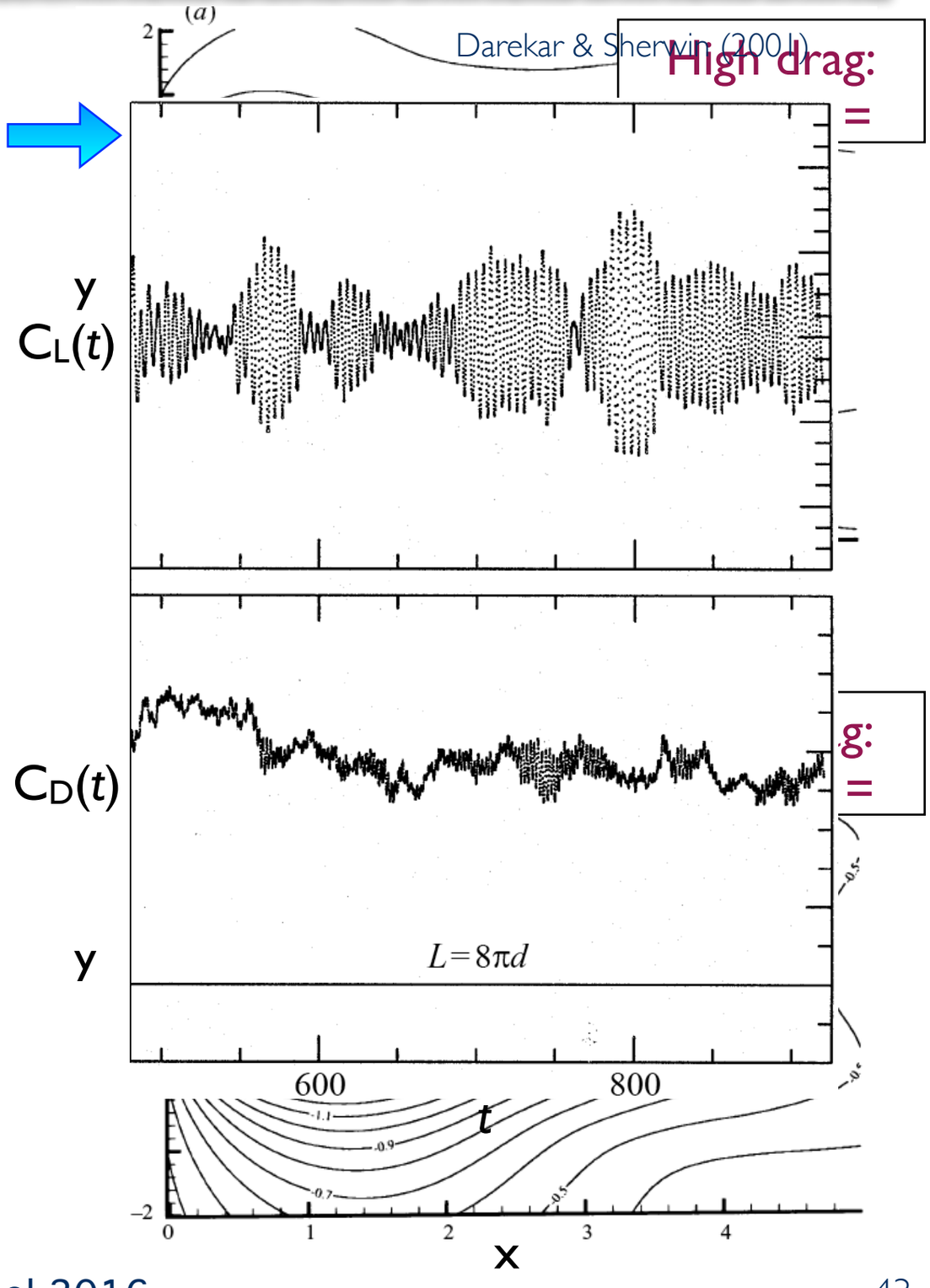

L_f ↑ → base pressure ↑ → drag ↓

Control of Bluff Body Wake

- Considerations for wake modification: drag reduction, modify acoustic signature, reduction of unsteady structural loading
- Baker & van Dam (2008): experiments and simulation of BTE airfoil
  - Passive, 2-dimensional forcing with splitter plate to increase L_f

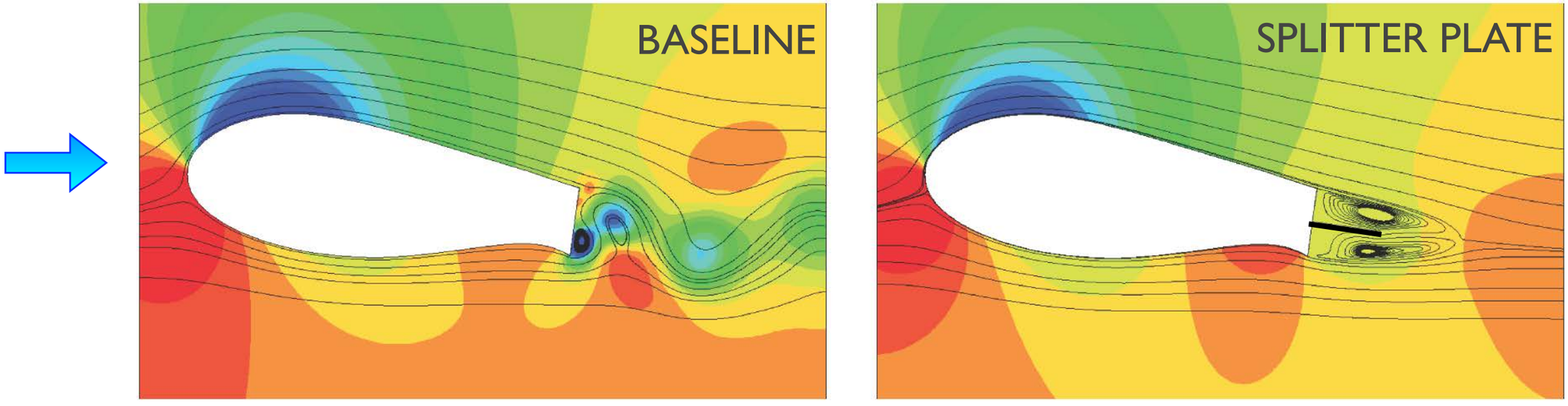

Control of Bluff Body Wake

- Considerations for wake modification: drag reduction, modify acoustic signature, reduction of unsteady structural loading
- Choi et al. (2008): reviewed control methods for bluff bodies
  - Passive, 3-dimensional forcing to leverage intrinsic secondary instability

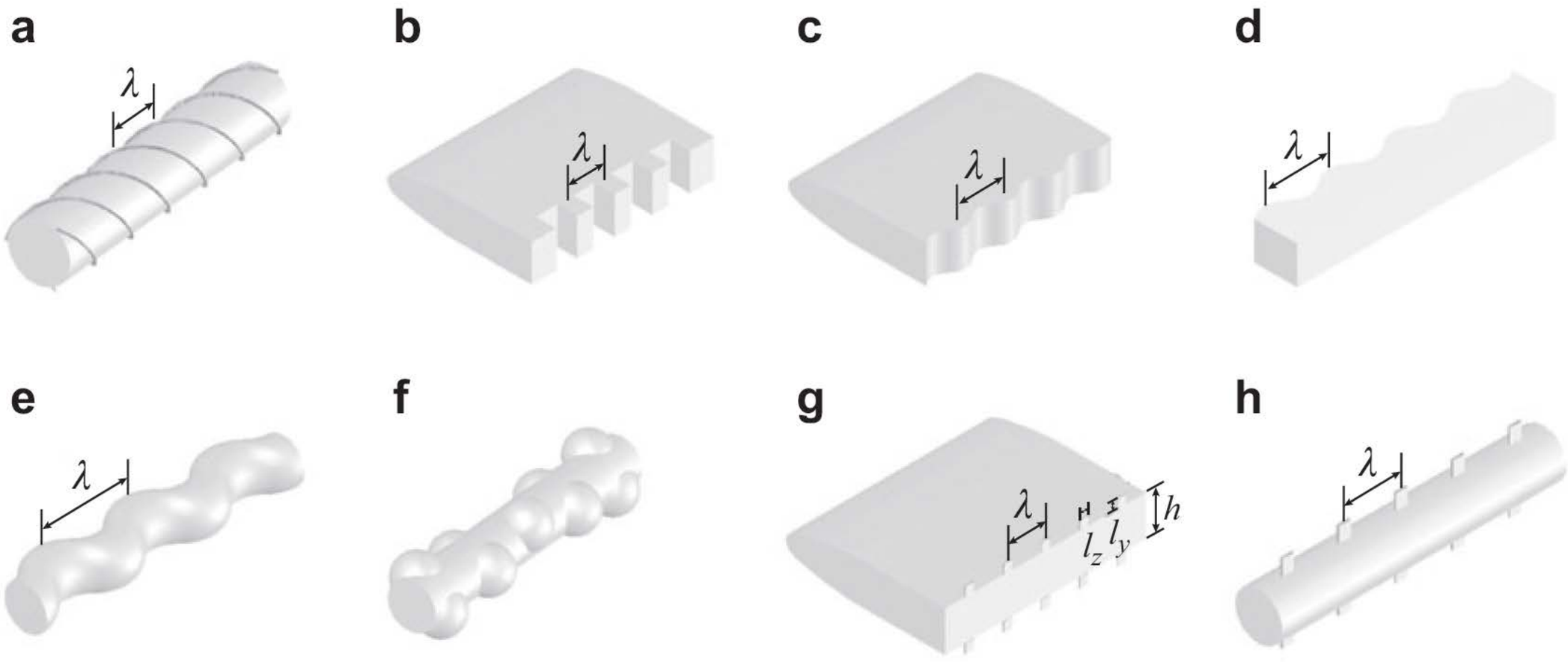

SLIDE TITLE

- Considerations for wake modification: drag reduction, modify acoustic signature, reduction of unsteady structural loading
- Kim & Choi (2005): open loop, spatially sinusoidal suction and blowing
  - Attenuation or annihilation of vortices reduced mean and fluctuating drag

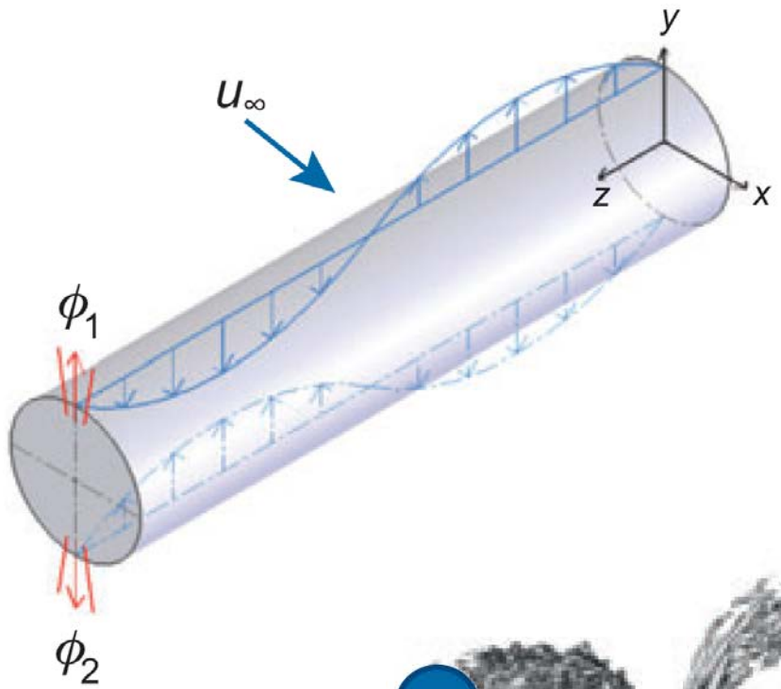

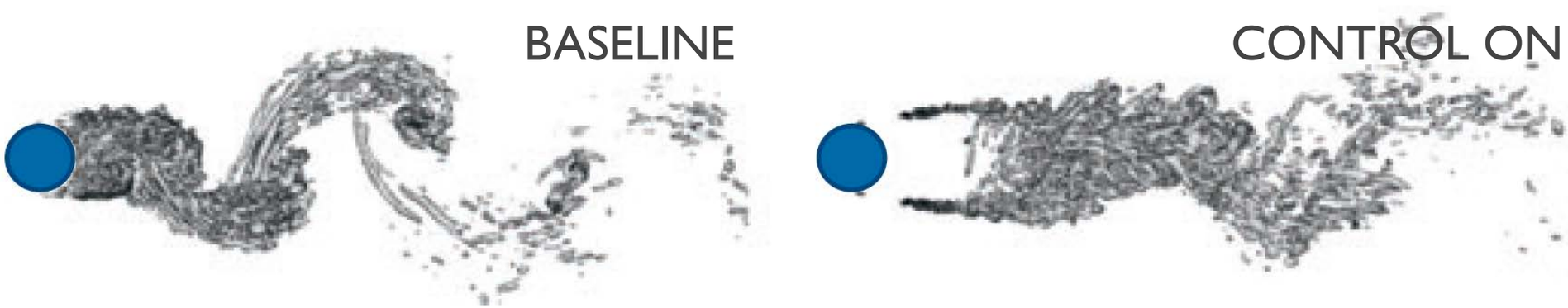

Closed-loop Control

- Considerations for wake modification: drag reduction, modify acoustic signature, reduction of unsteady structural loading

- Pastoor et al. (2008): closed-loop, spanwise uniform actuation
  - Disrupted alternating shedding to increase L_f and decrease drag by 15%
  - Actuation on one side only and over half span of model

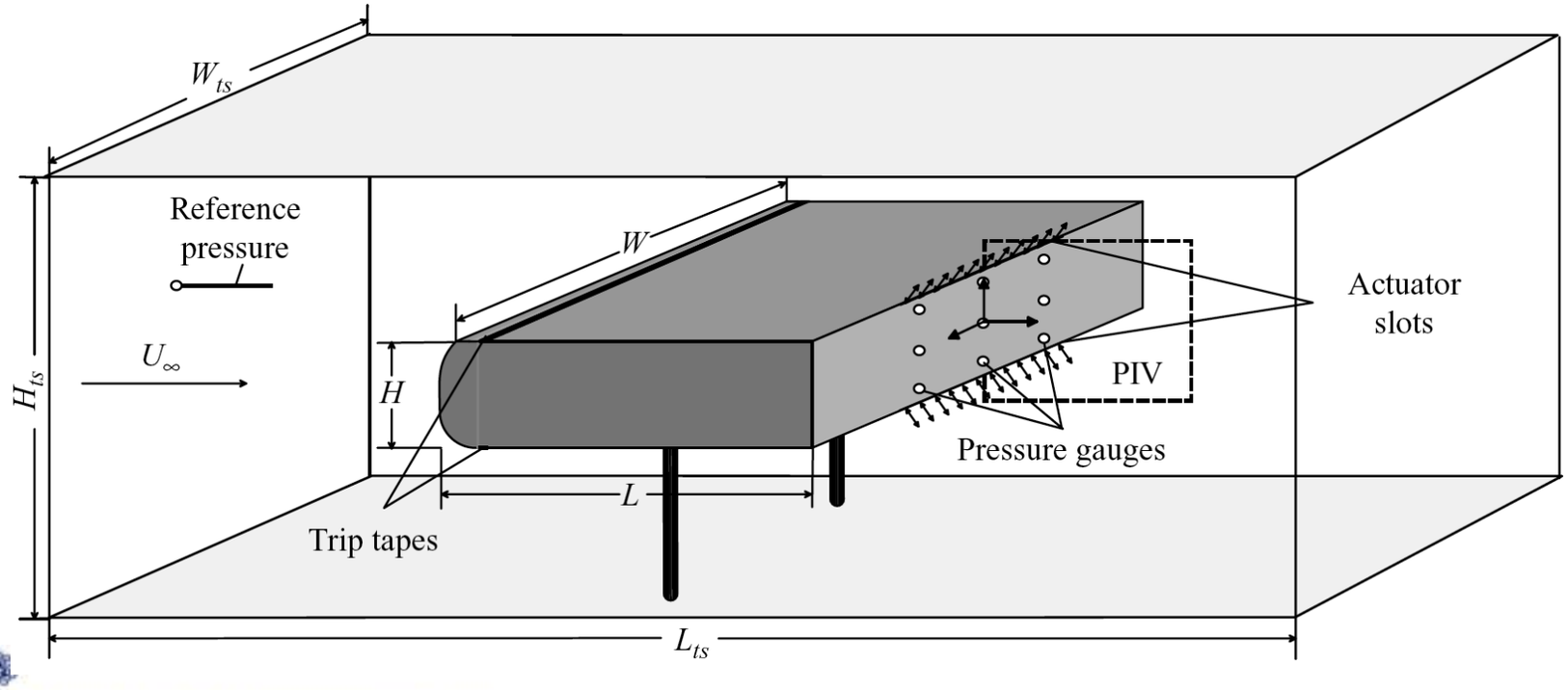

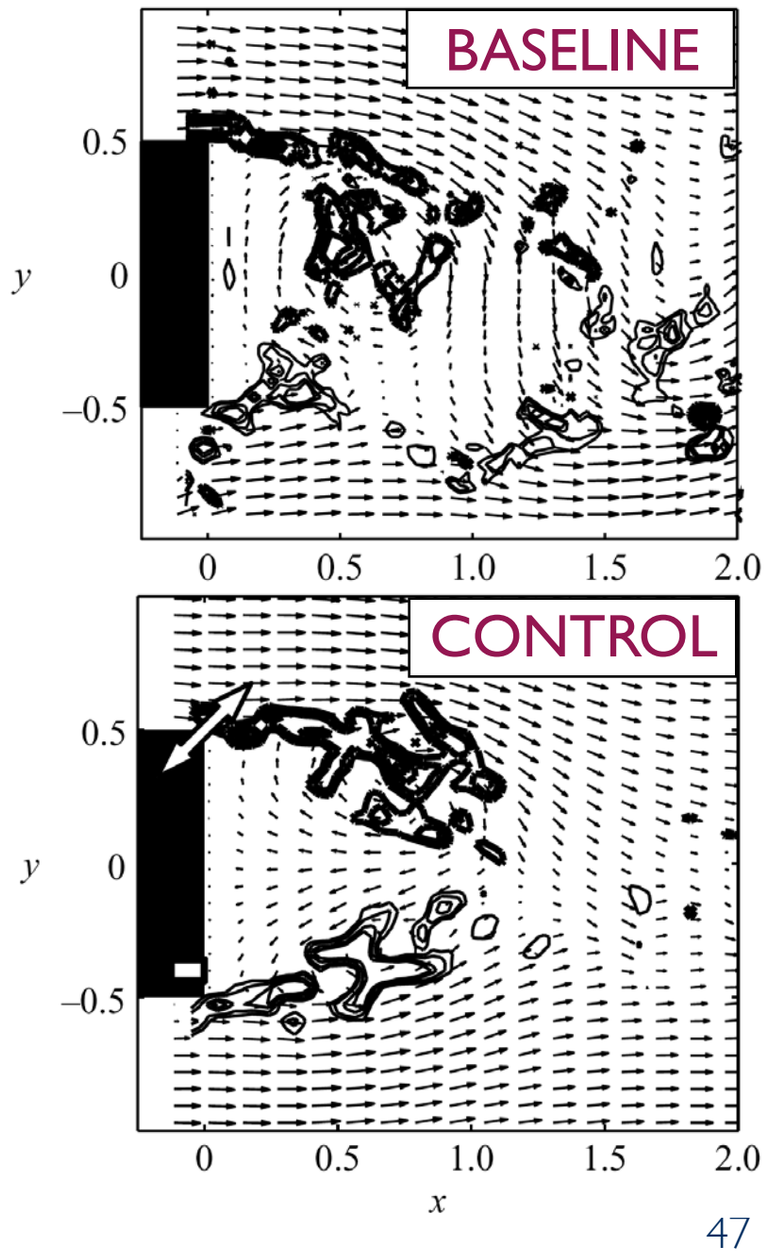

Distributed Forcing via Plasma

- Focus on simplified, canonical geometry
- Elliptical leading edge, flat plate section of thickness *d* with blunt trailing edge
- Chord =12.5*d*
- Additional model features:
  - Active flow control via plasma actuators
  - Time-resolved base pressure measurements via microphone array extension

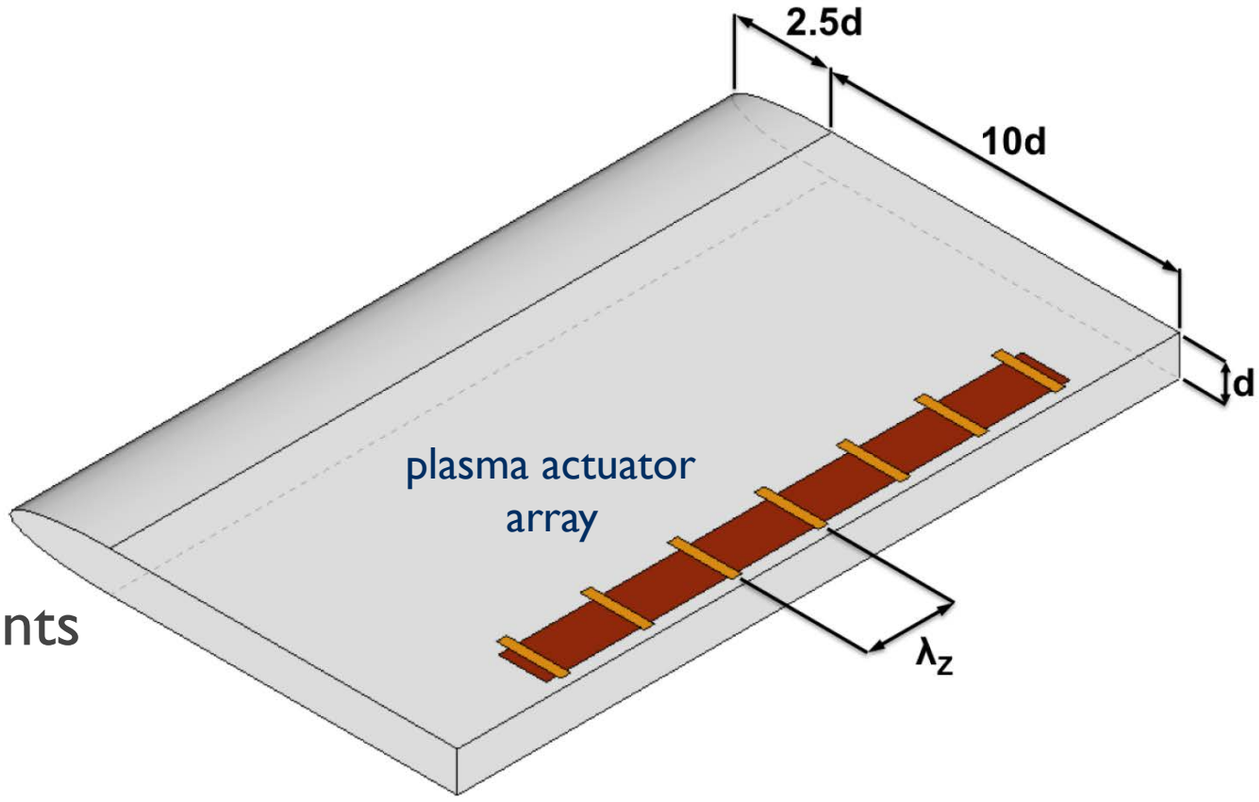

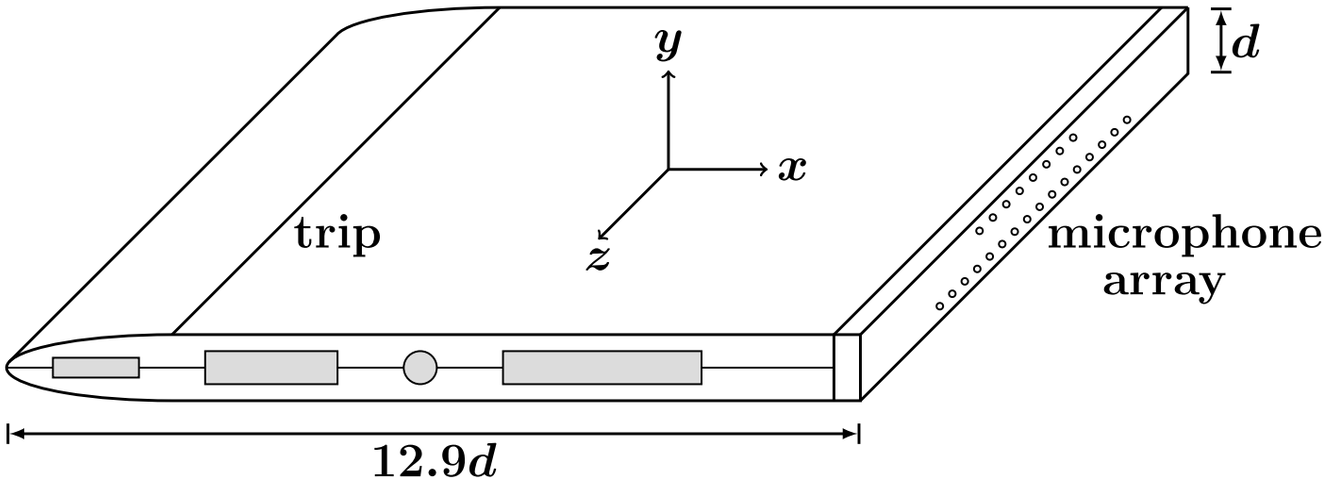

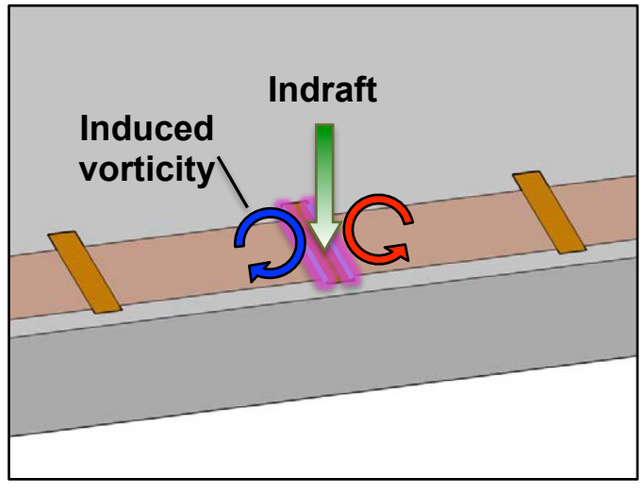

Plasma Actuators

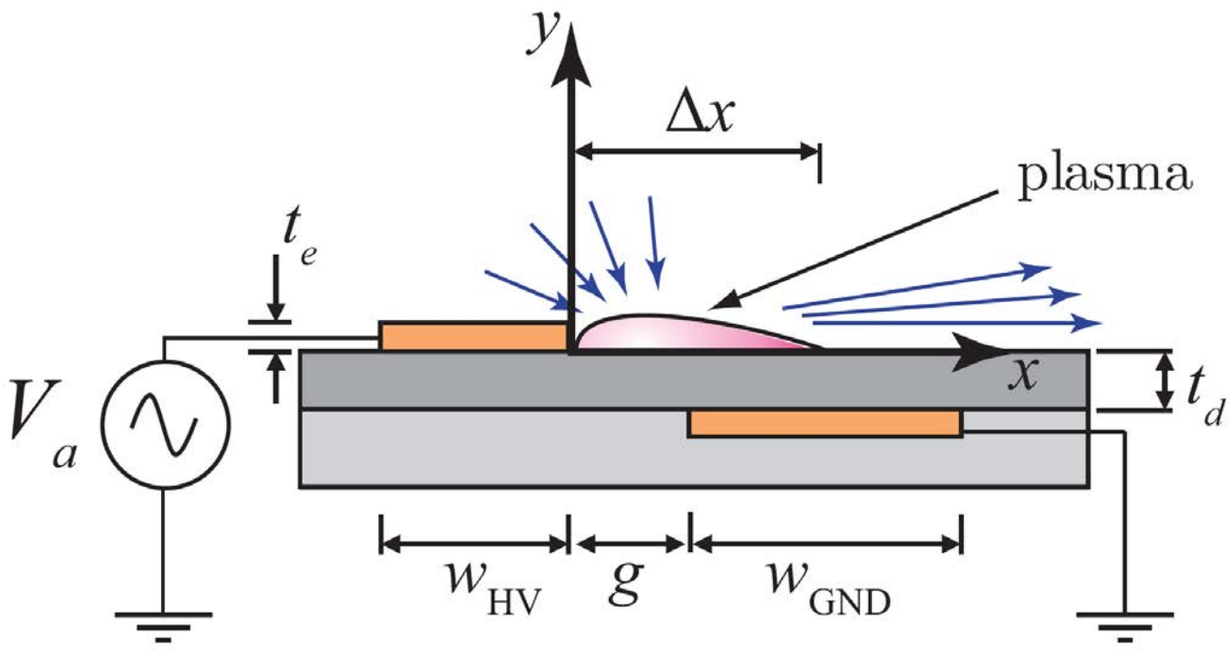

- Electrical input ⟶ fluidic output
- Single actuator produces wall jet

- Actuator array introduces alternating streak disturbance

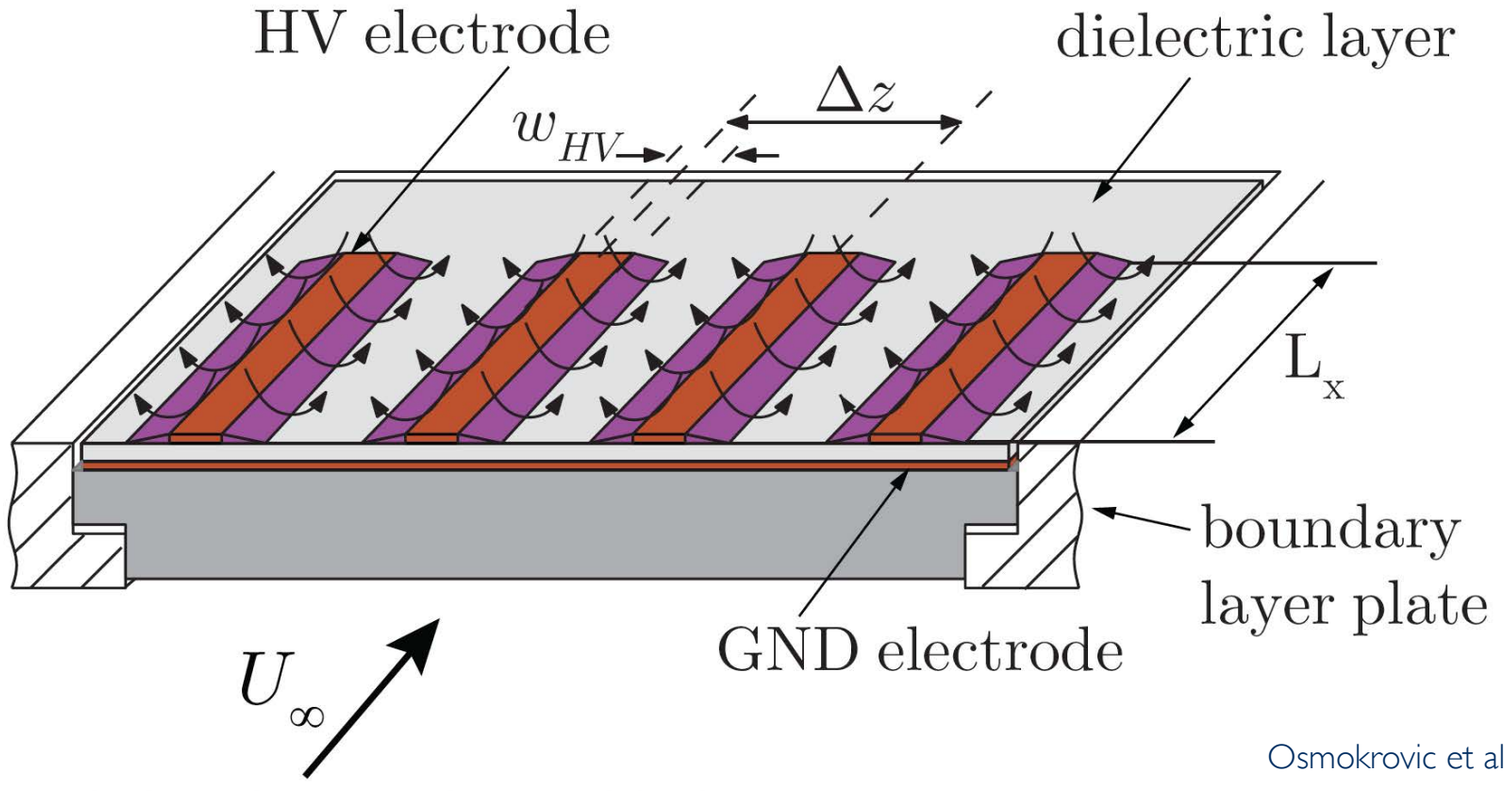

Osmokrovic et al (2012)

POD for Structure Identification

- Naghib-Lahouti et al. (2012, 2014) used POD model to extract dominant structures in wake

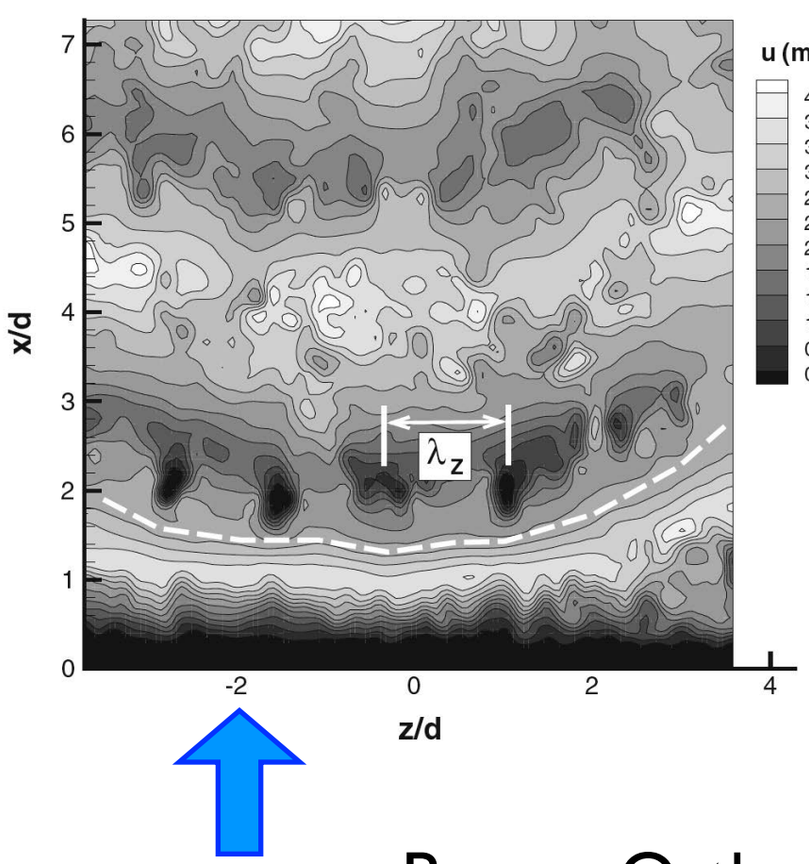

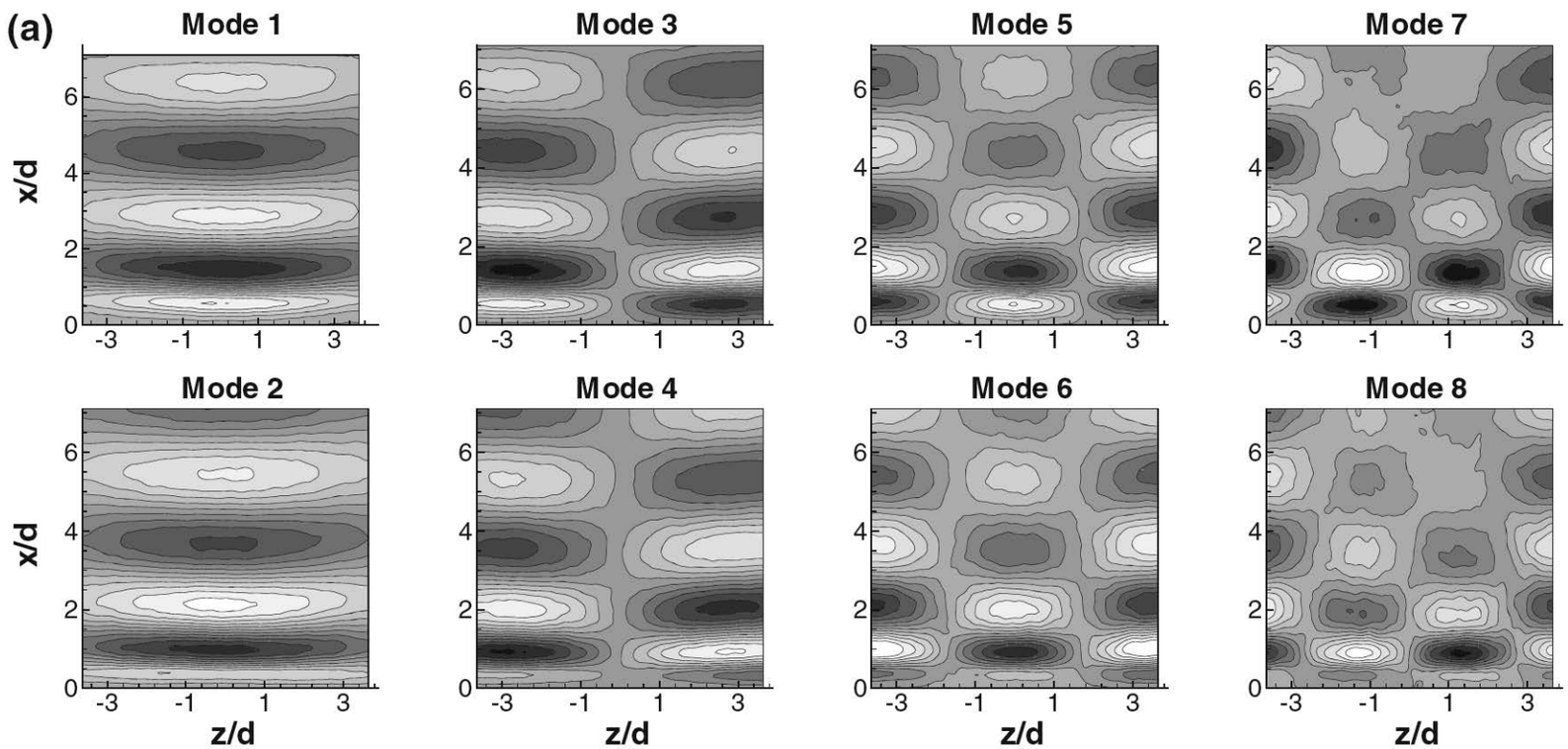

Proper Orthogonal Decomposition (POD) - *in a nutshell*

$$\tilde{u}_i\left(x_i,t\right)=\sum_{n=1}^{M}a^n(t)\phi^n(x_i)$$

$\phi^n(x_i)$: orthogonal eigenfunctions (modes)

$a^n(t)$: time varying coefficient

POD for Structure Identification

- Naghib-Lahouti et al. (2012, 2014) used POD model to extract dominant structures in wake

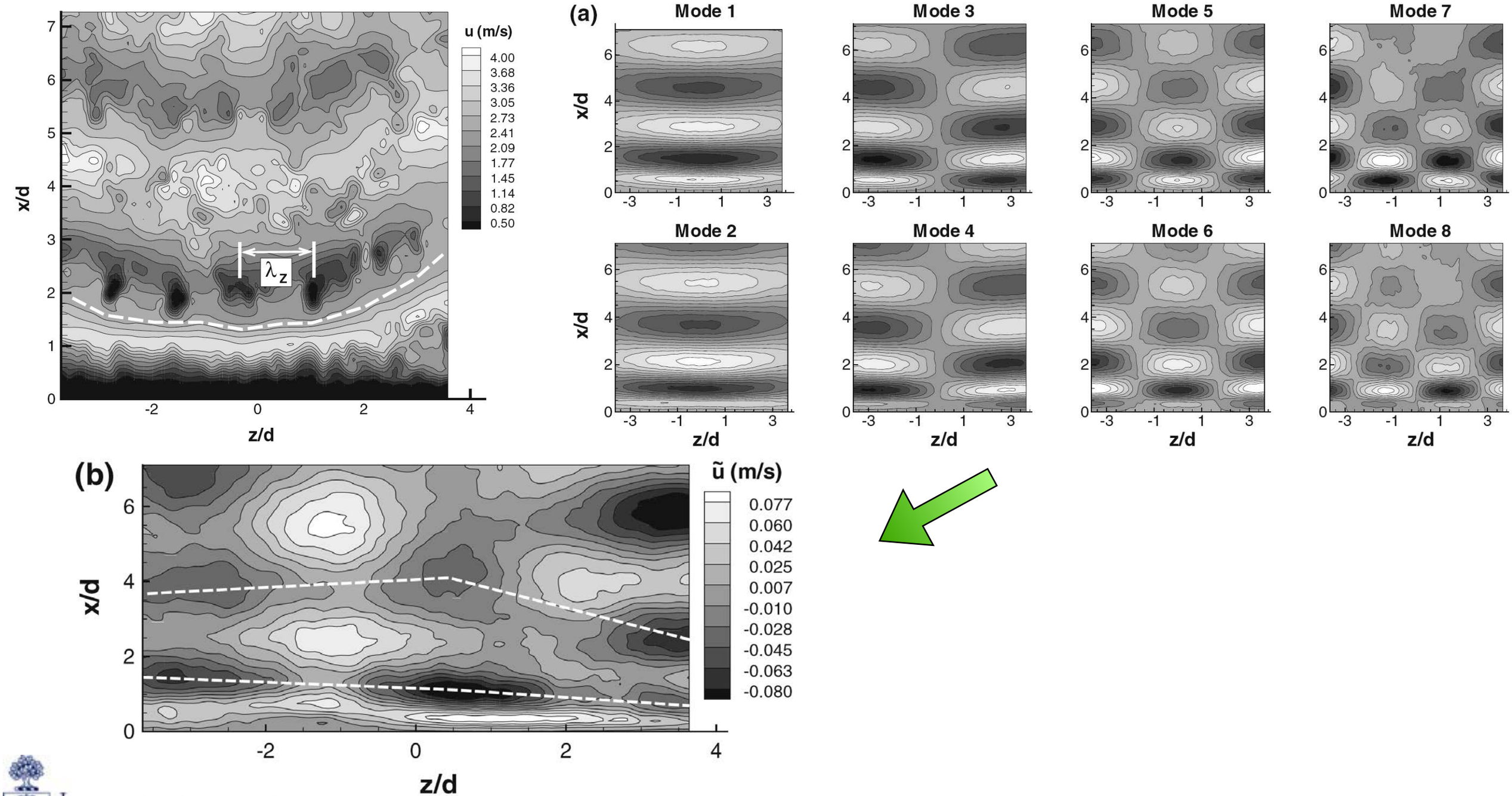

POD for Structure Identification

- Naghib-Lahouti et al. (2012, 2014) used POD model to extract dominant structures in wake

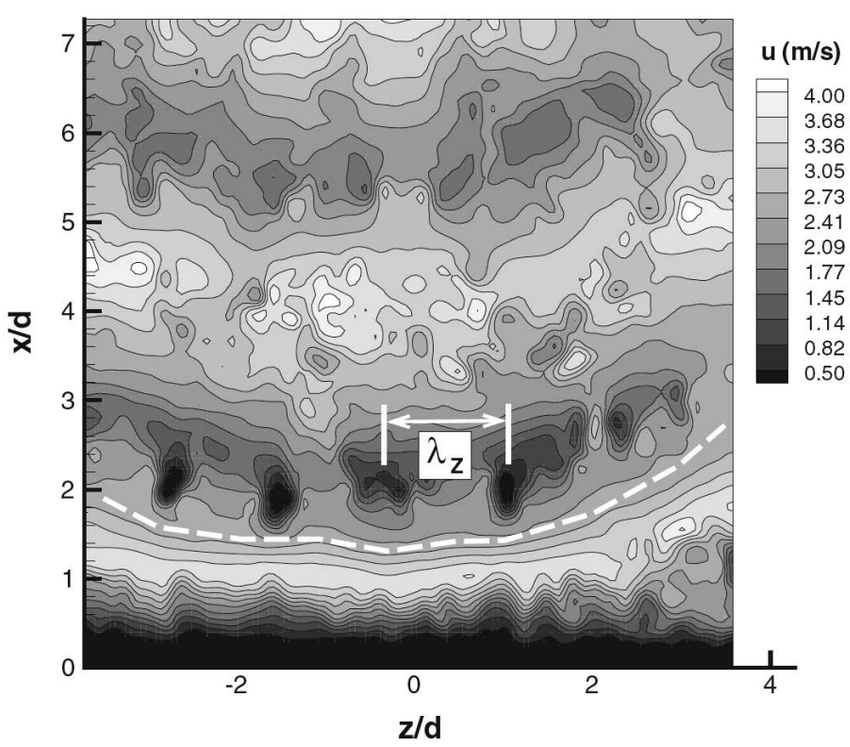

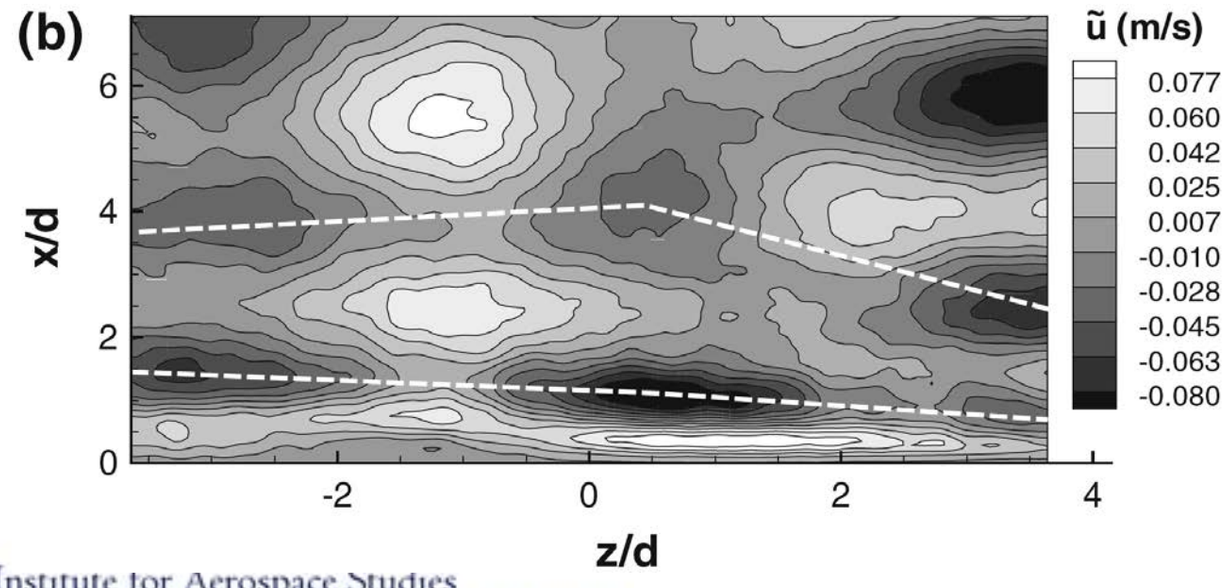

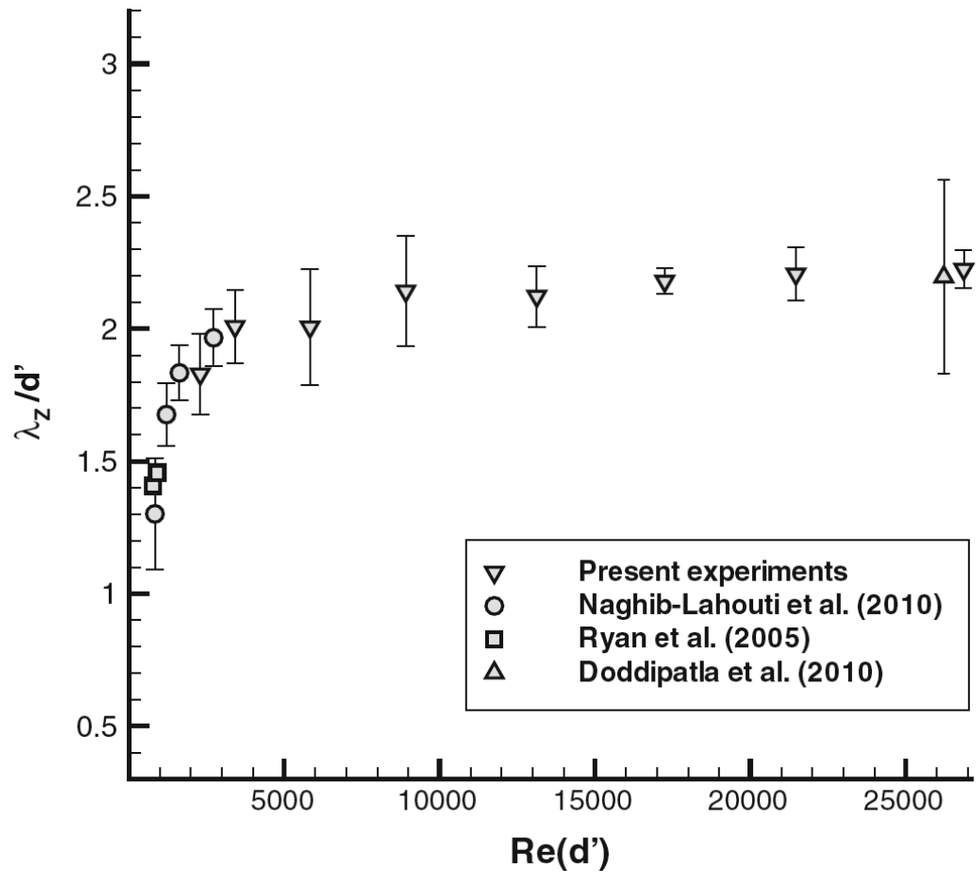

- Instability wavelength, λ_z, relatively constant with Re
  - Implications for distributed forcing in wake control strategy

Plasma Actuator Control

- Re_d = 2,000, 3,000, & 5,000
- Energy input is varied through excitation parameters of actuators

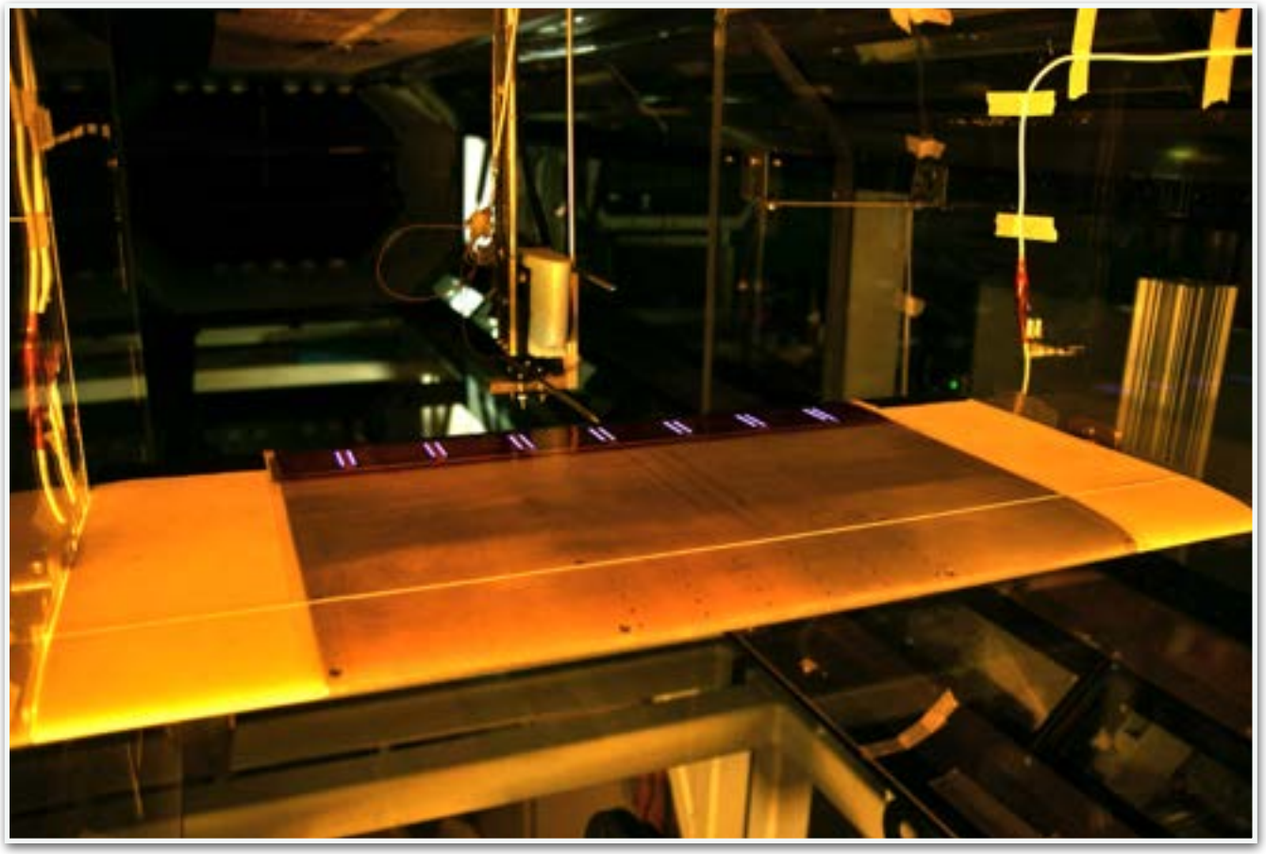

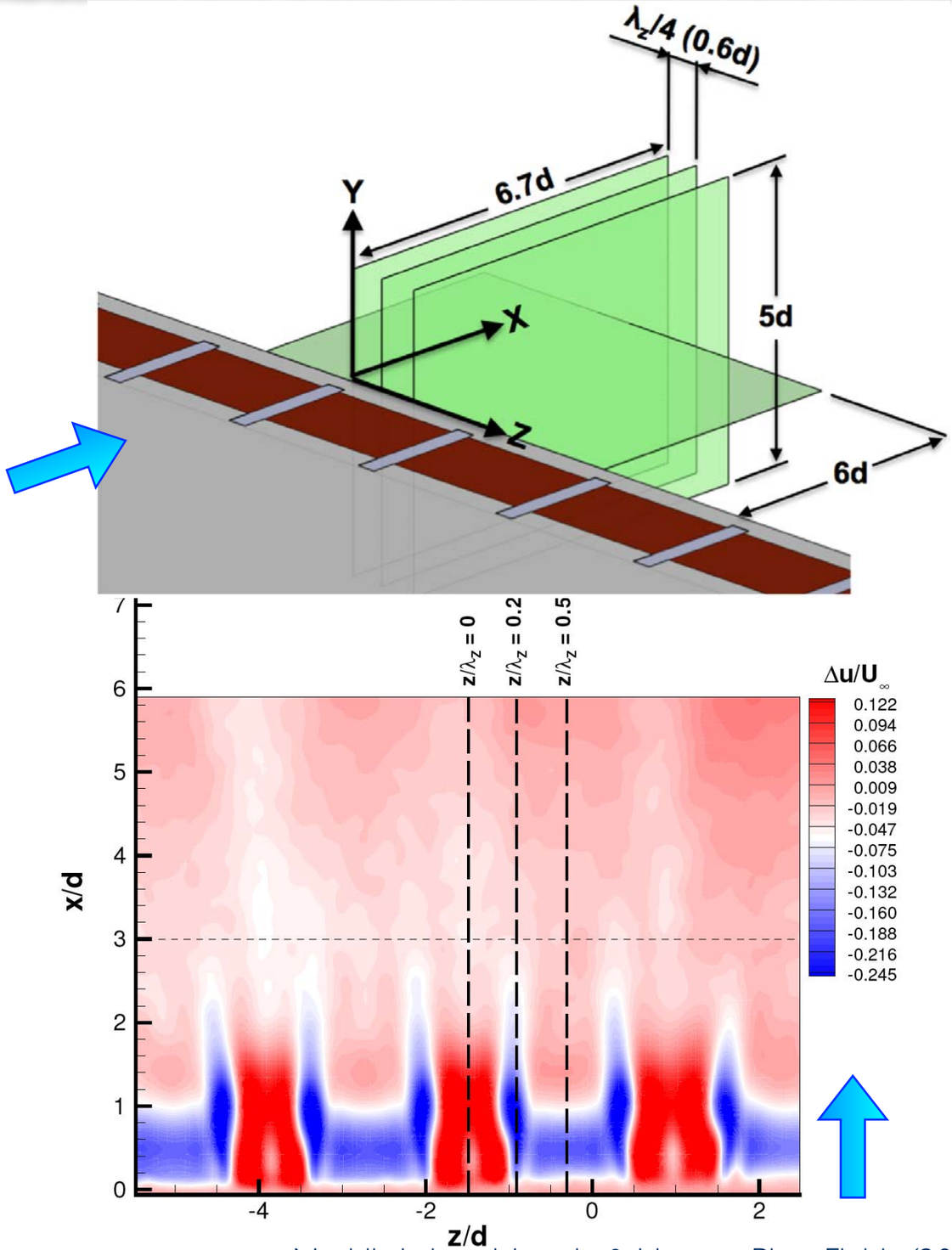

Naghib-Lahouti, Lavoie & Hangan, Phys. Fluids (2015)

Plasma Actuator Control

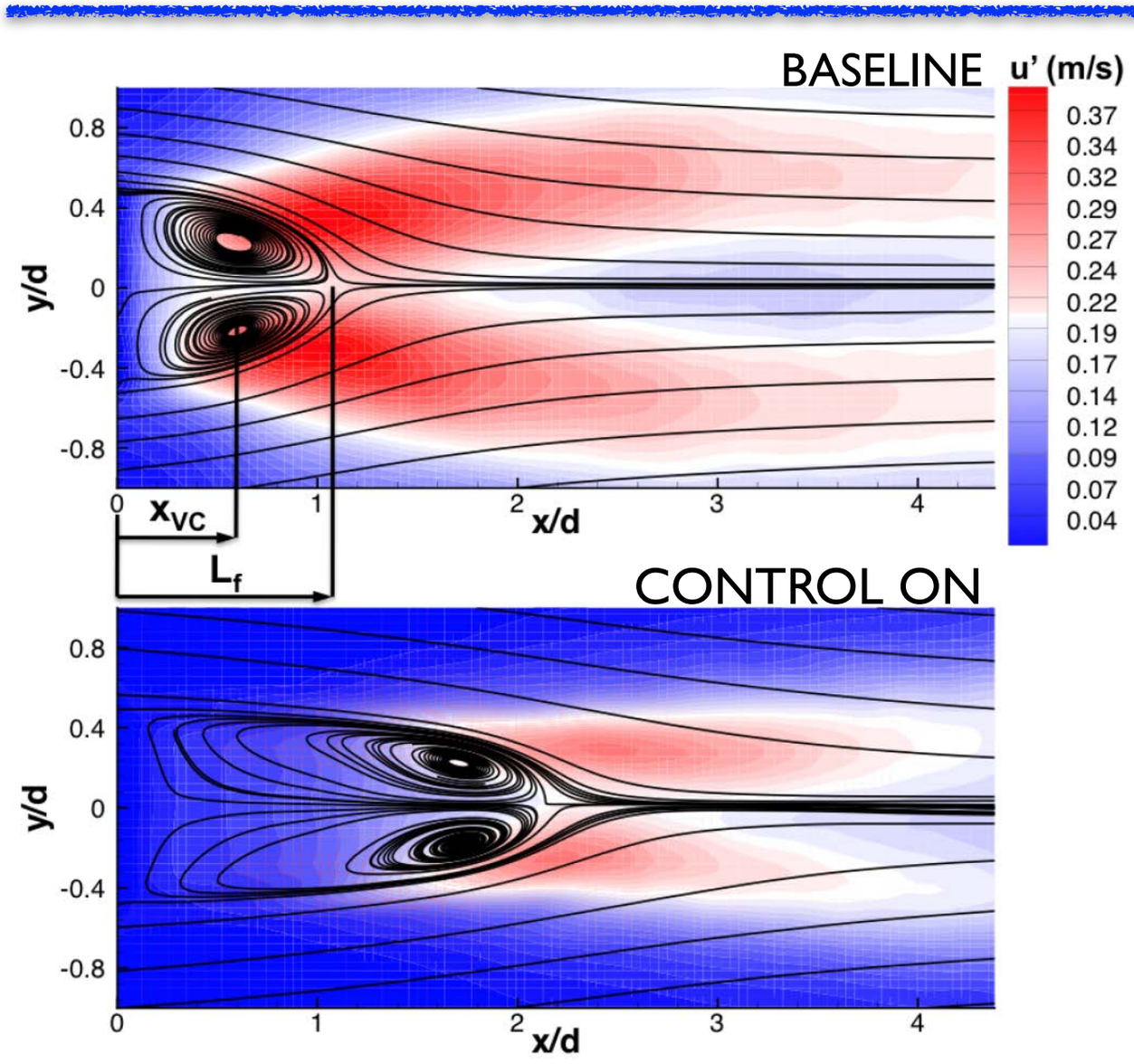

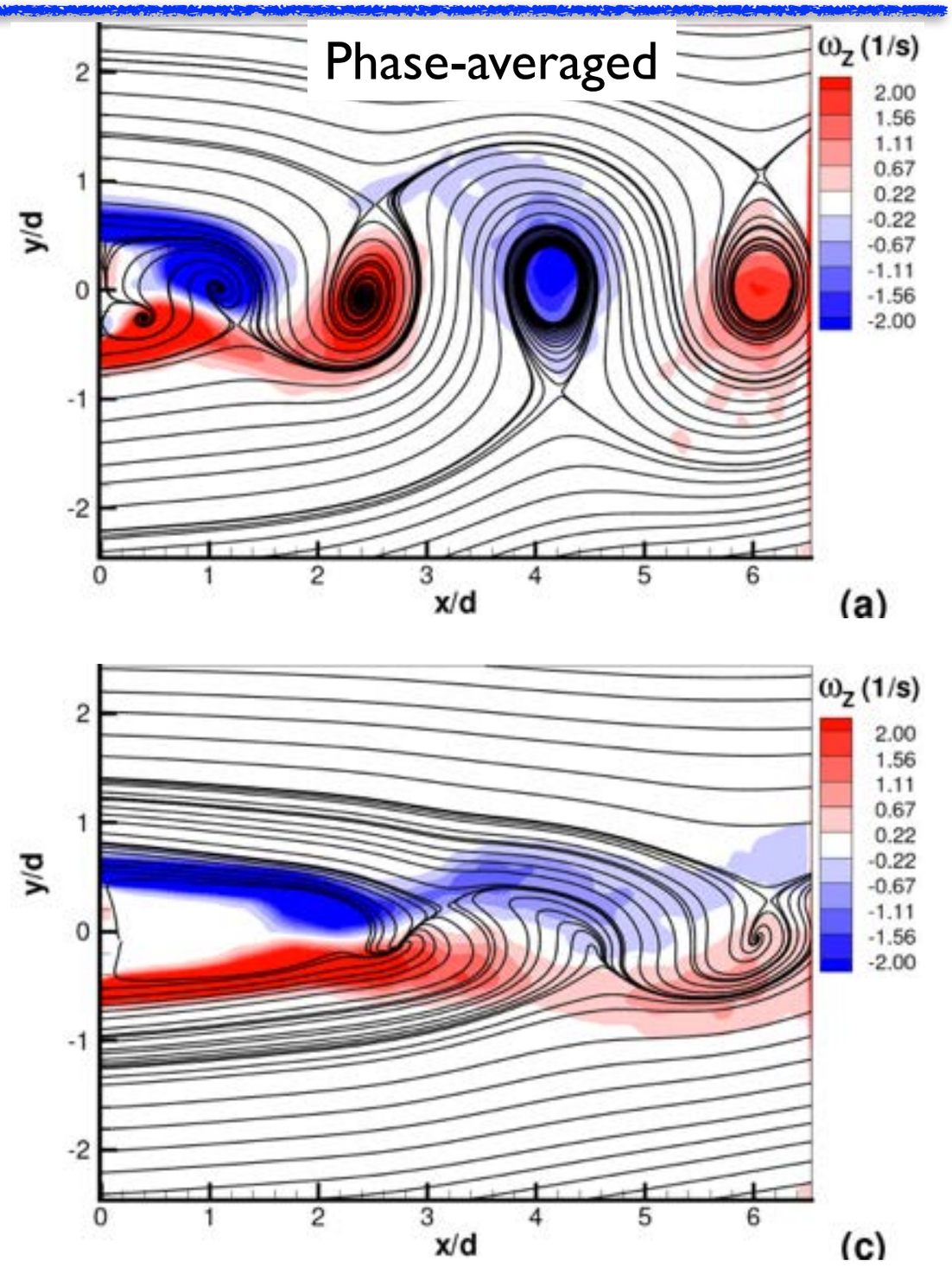

- Formation length extended
- Vortex formation decimated

Naghib-Lahouti, Lavoie & Hangan, Phys. Fluids (2015)

Plasma Actuator Control

Can be seen from the change in the POD modes

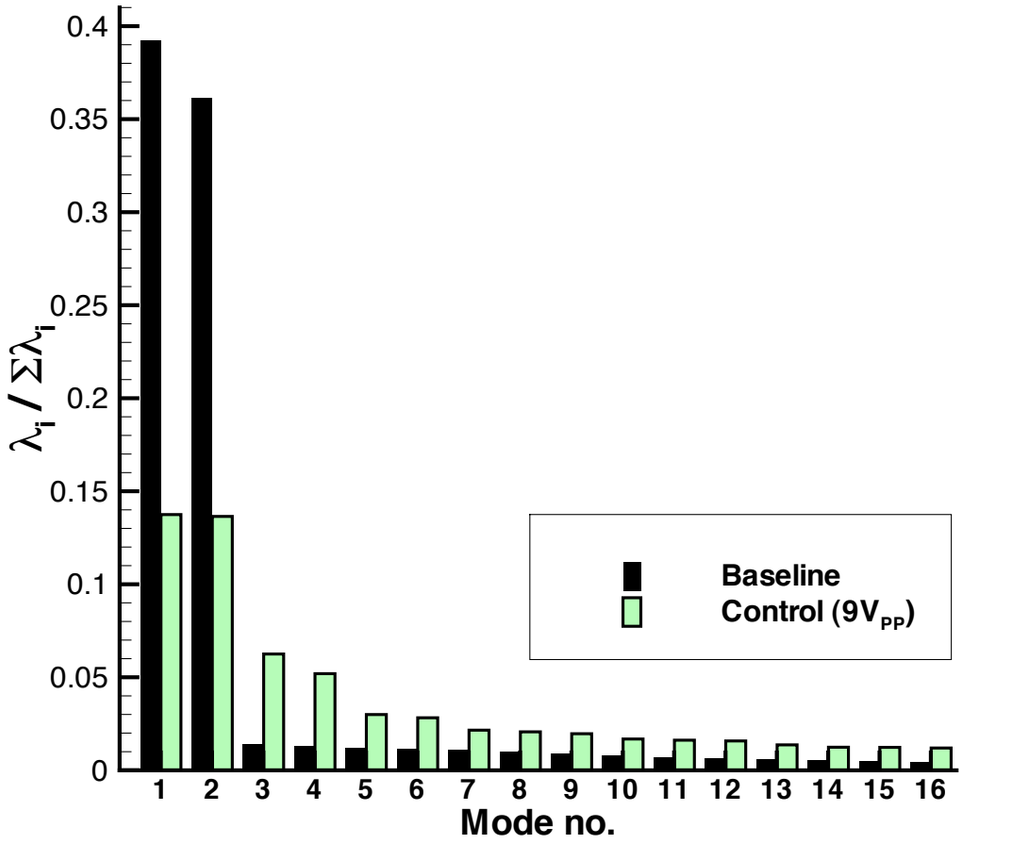

Relative energy of POD modes in (x-y) plane

Re(d) = 2000, z/λ = 0

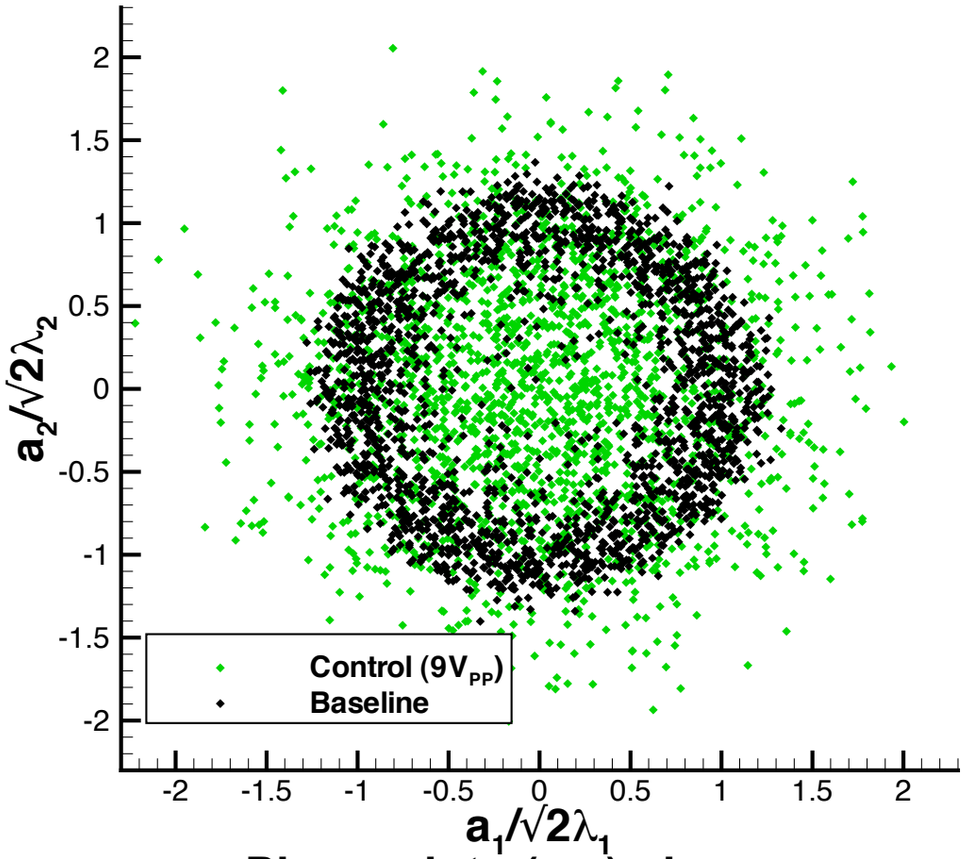

Phase plot - (x-y) plane

Re(d) = 2000, z/λ = 0

- Formation length extended
- Vortex formation decimated

Naghib-Lahouti, Lavoie & Hangan, Phys. Fluids (2015)

Plasma Actuator Control

Effect of forcing extend over the full span.

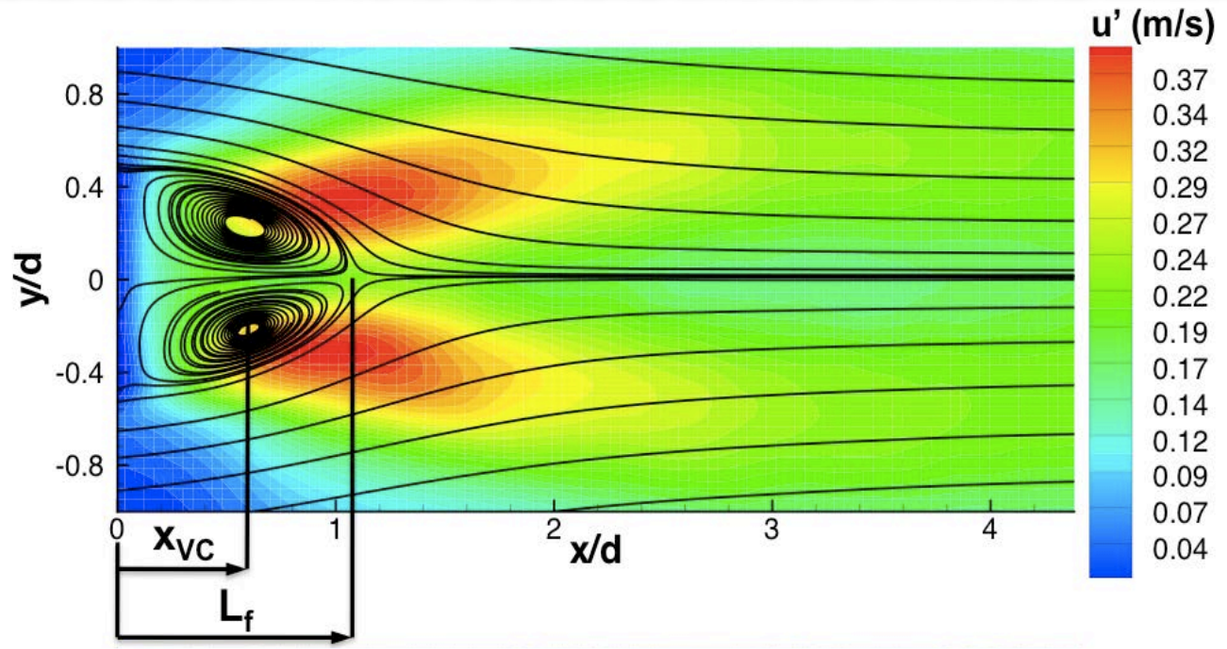

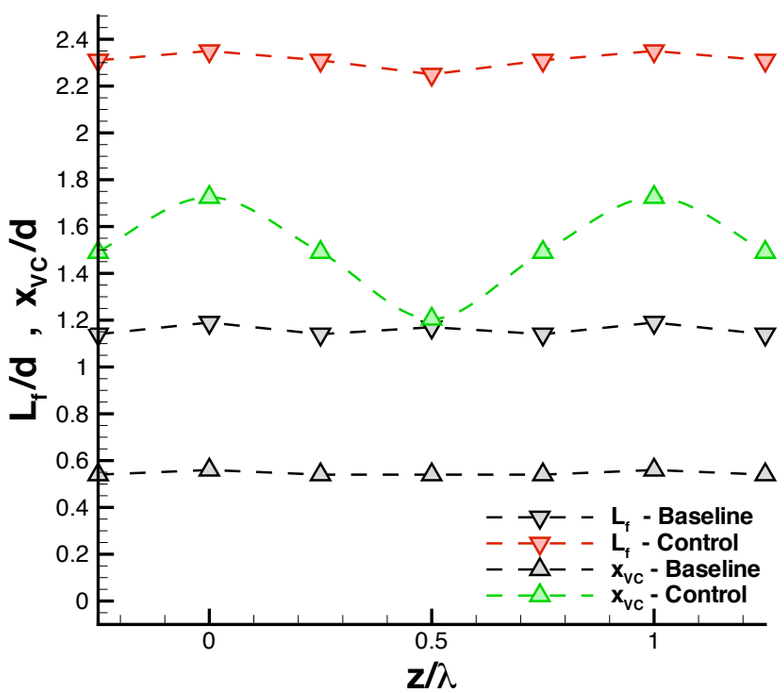

Re(d) = 2000
9kV$_{PP}$

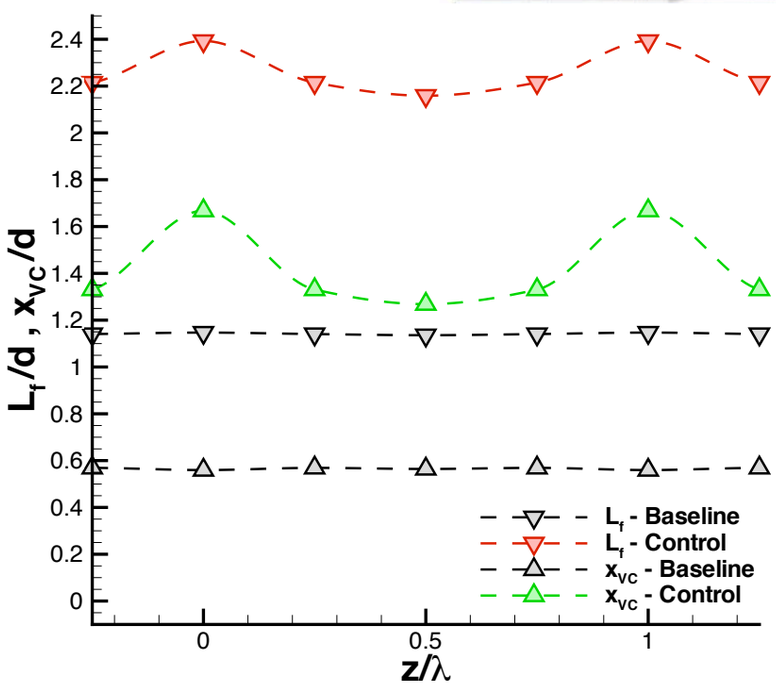

Re(d) = 3000
10kV$_{PP}$

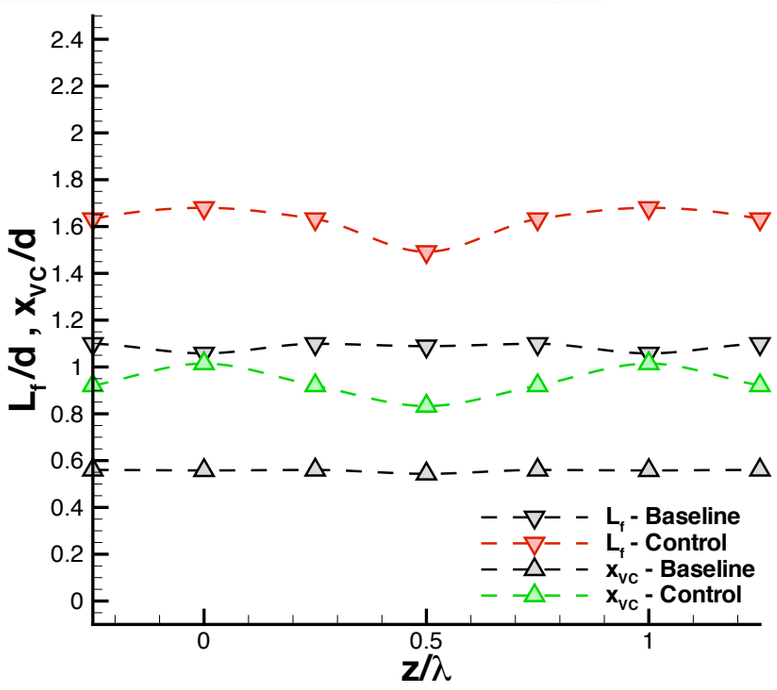

Re(d) = 5000
11kV$_{PP}$

Naghib-Lahouti, Lavoie & Hangan, Phys. Fluids (2015)

Plasma Actuator Control

Base pressure coefficient based on the average pressure measured through 4 ports across the span.

Significant recovery of base pressure, consistent with the behaviour of L_f and x_{vc}

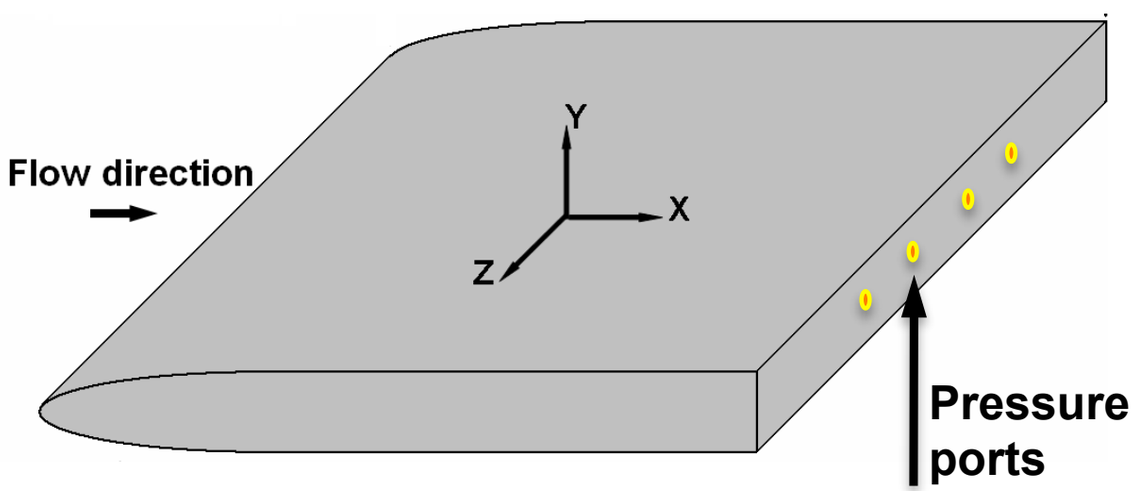

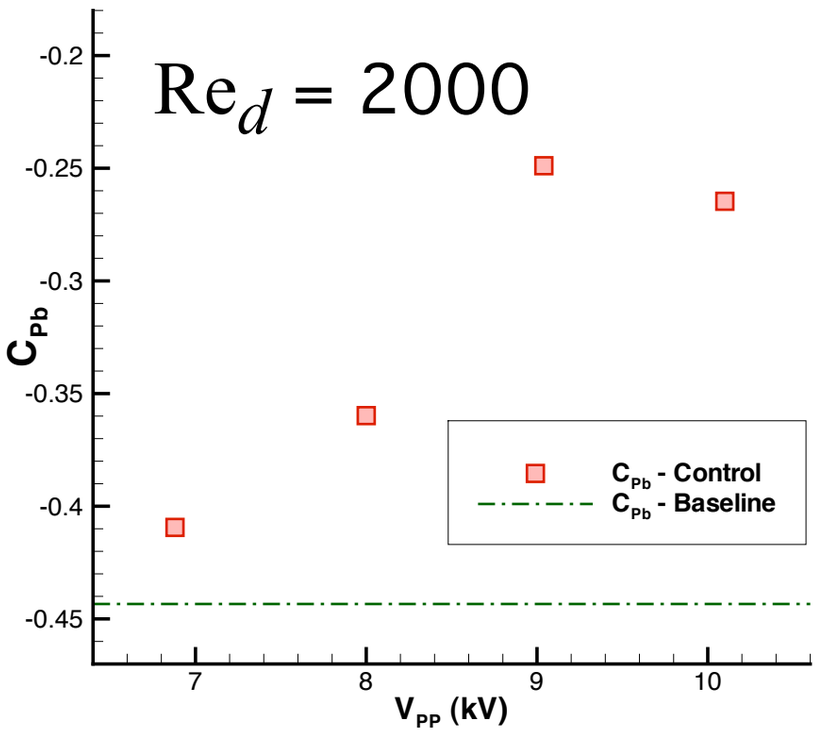

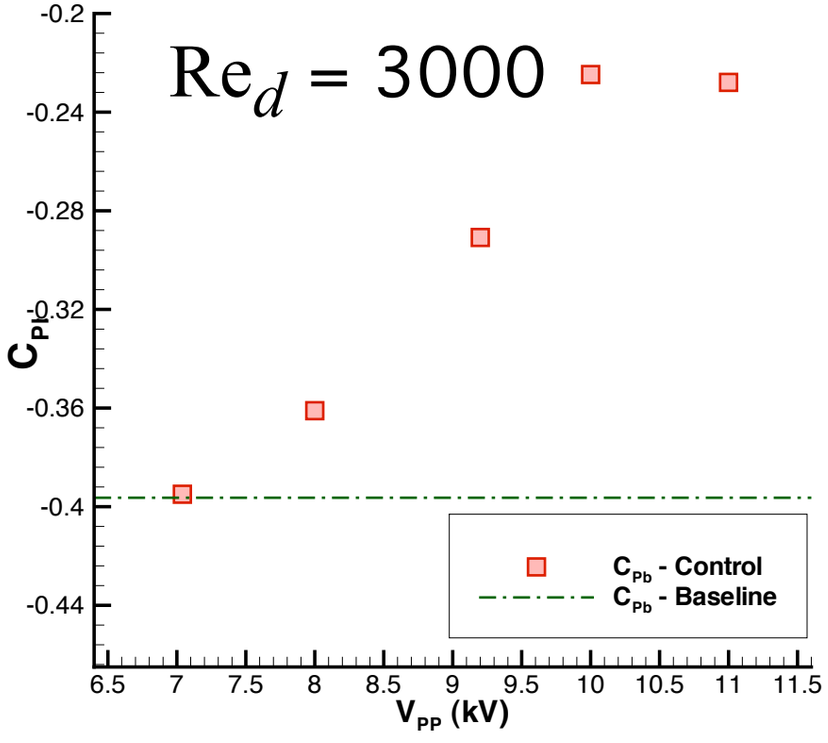

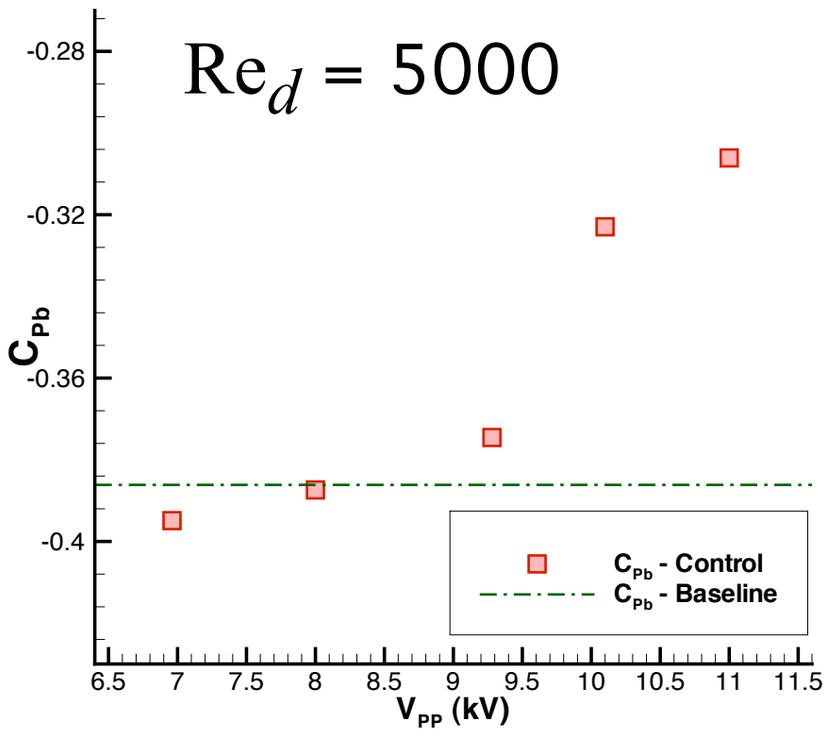

44% recovery

43% recovery

21% recovery

Plasma Actuator Control

Drag estimate based on flow measurements

(van Oudheusden et al., 2007; Bohl & Koochesfahani, 2009)

$\tilde{C}_D$

$$C_D = \frac{2}{A}\int \frac{\overline{u}}{U_\infty}\left(1-\frac{\overline{u}}{U_\infty}\right)\mathrm{d}y \boxed{-\frac{2}{A}\int\left(\frac{u'}{U_\infty}\right)^2\mathrm{d}y+\frac{2}{A}\int\left(\frac{v'}{U_\infty}\right)^2\mathrm{d}y}$$

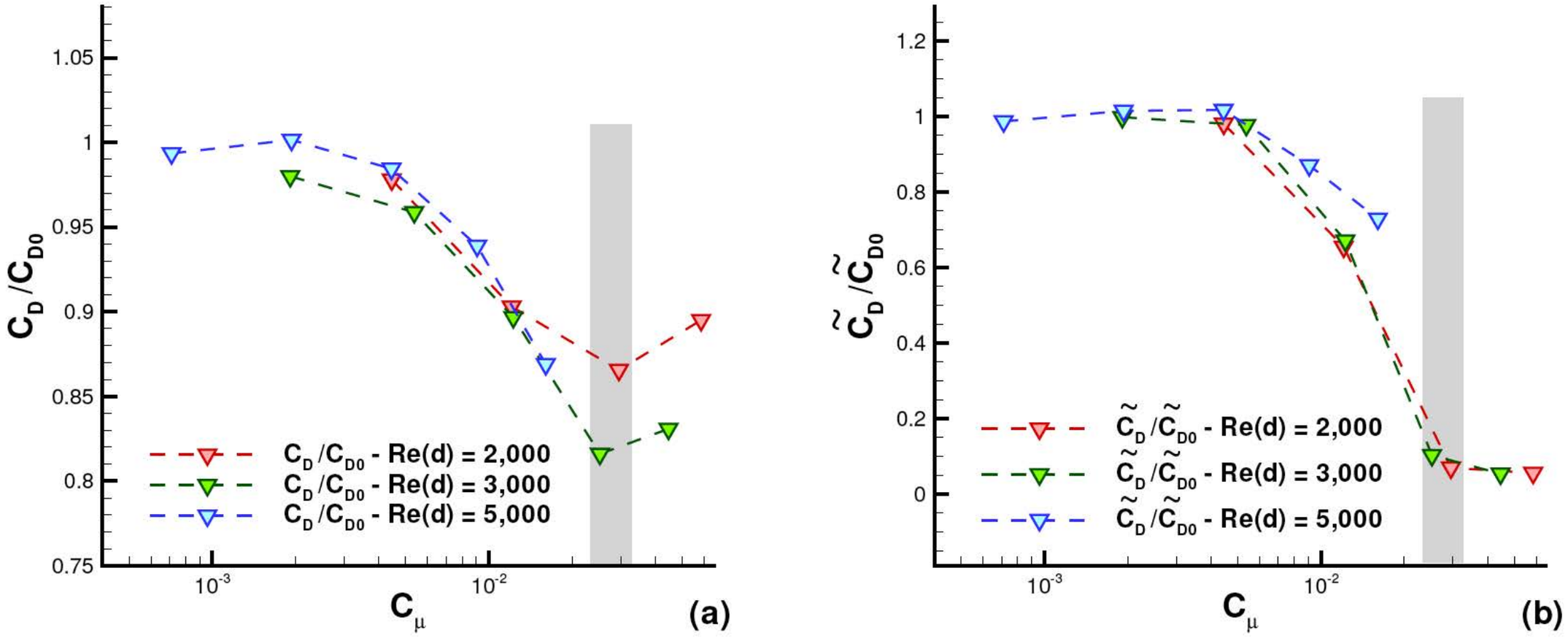

$$C_\mu = \frac{\text{momentum flux induced by actuators}}{\text{freestream momentum flux through base area of body}}$$

Estimation for Control

- Estimation in complex flows: coherent structures analysis and low-dimensional modelling, closed-loop control
- Two broad categories (Cattafesta et al., 2008)
  - static estimator based on empirical mapping
  - dynamic estimator based on physical model

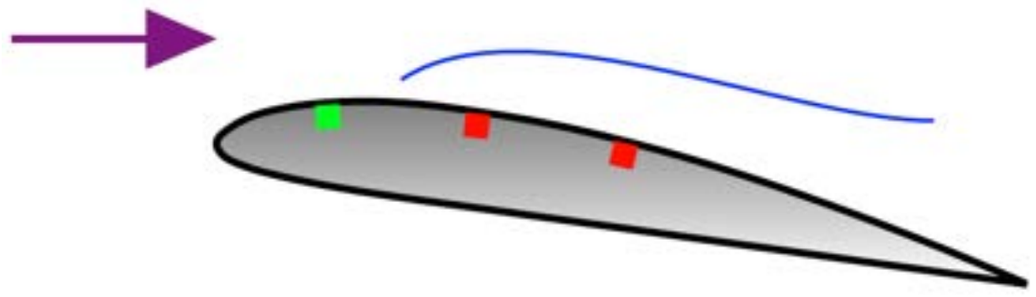

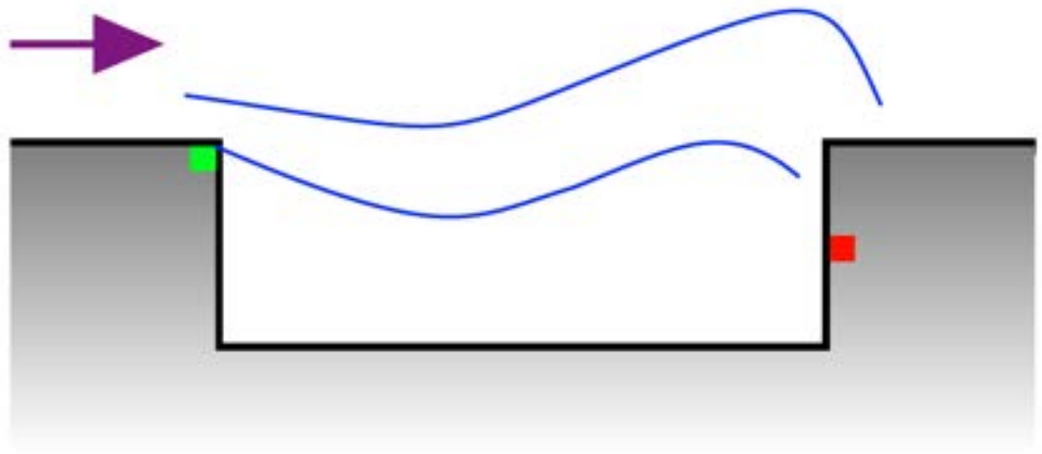

Clark, Naghib-Lahouti & Lavoie, EiF (2014)

Objective:

Estimate states of interest from limited surface sensing

Estimation for Control

- Objective: extend distributed forcing control strategy to closed-loop method

- Actuation depends on state of flow, requires nonintrusive real-time measurements
- Advantages
  - Reduce actuator power consumption
  - Robustness to external disturbances and conditions
- Base pressure fluctuations indicate time evolution of local vortex shedding

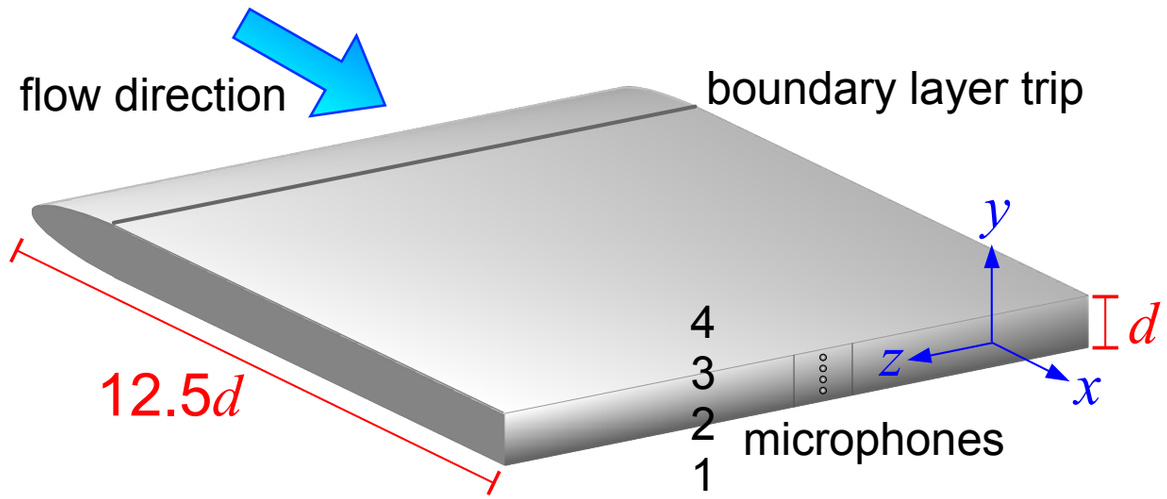

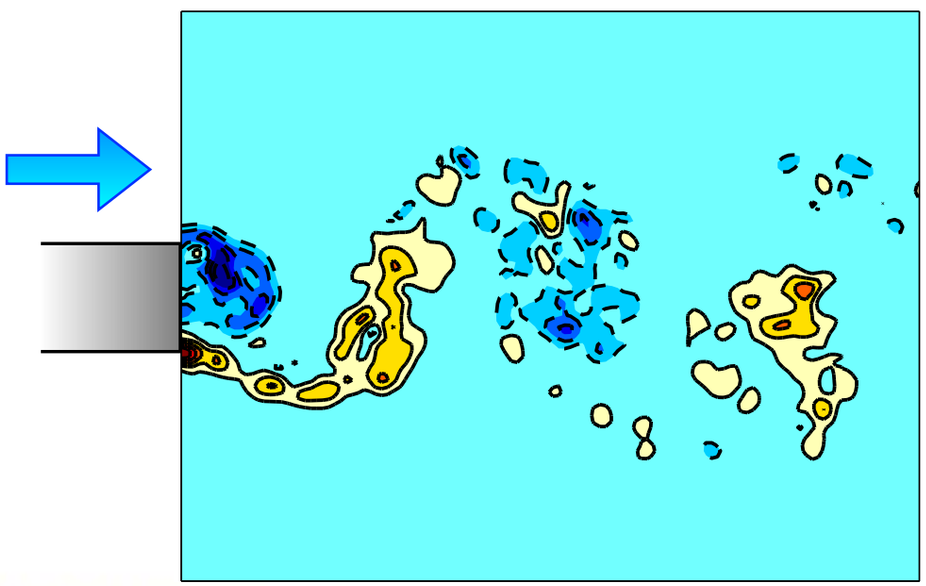

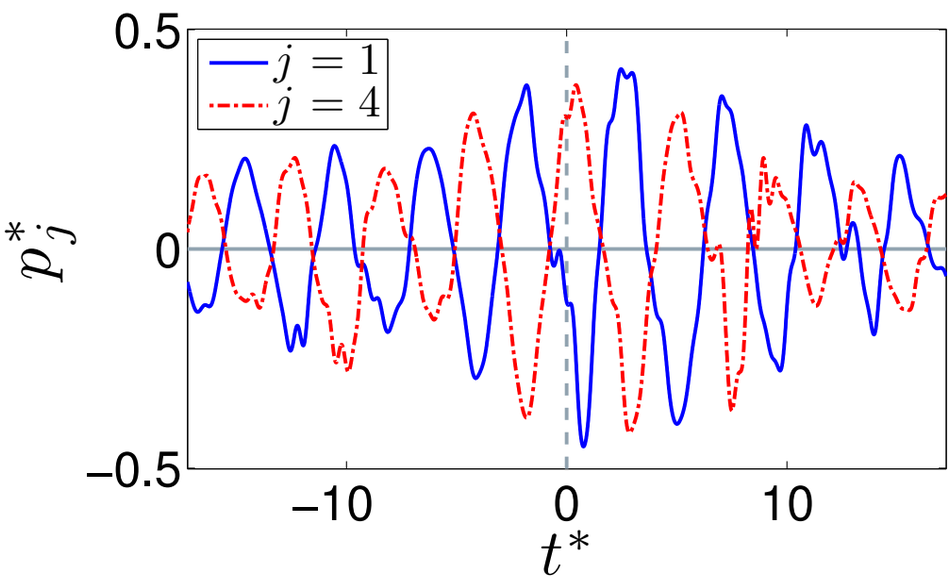

Empirical Estimator

1. Obtain synchronized measurements of velocity and fluctuating pressure in the wake

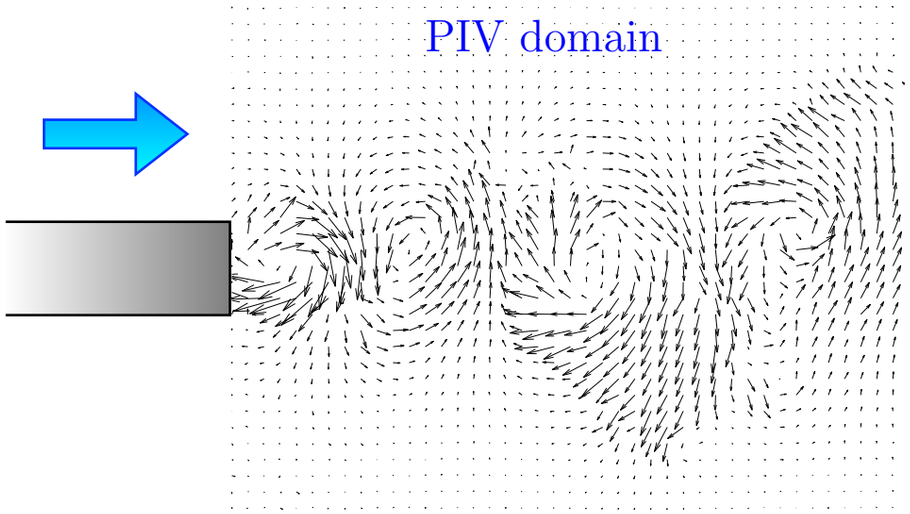

PIV - not time resolved

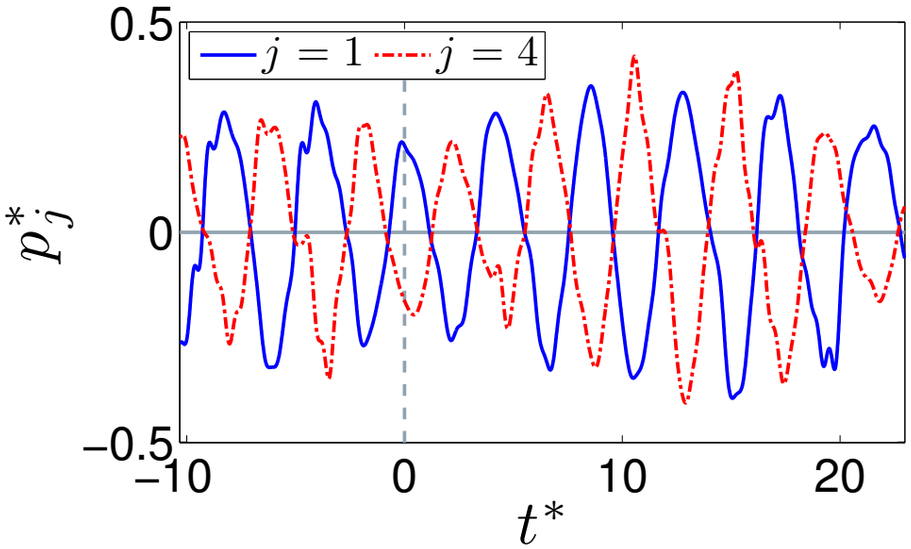

Pressure fluctuations - time resolved

2. Construct model from flow statistics to estimate velocity from pressure signals only

$$p_j(t) \longrightarrow \boxed{\mathcal{F}} \longrightarrow \tilde{\mathbf{u}}(x, y, t)$$

Reduced-order model

POD for Reduced Order Modelling

- Usually not interested in knowing the velocity at every point - can use POD modes to reduce the order of the problem and provide a reduced order model
- Estimate evolution of the large coherent structures only (POD model)
  - Simple model required for real-time feedback control

MEASURED

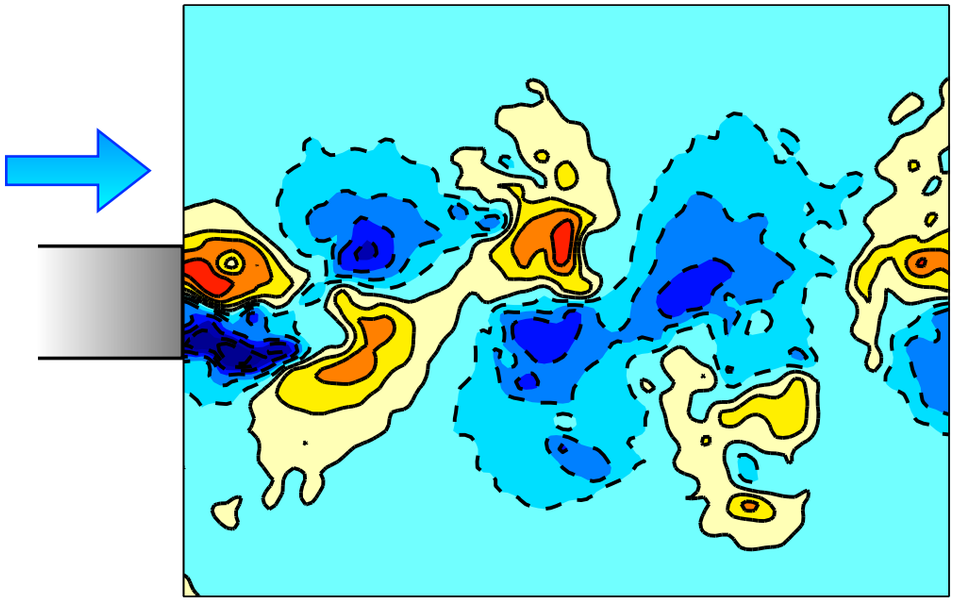

ESTIMATED

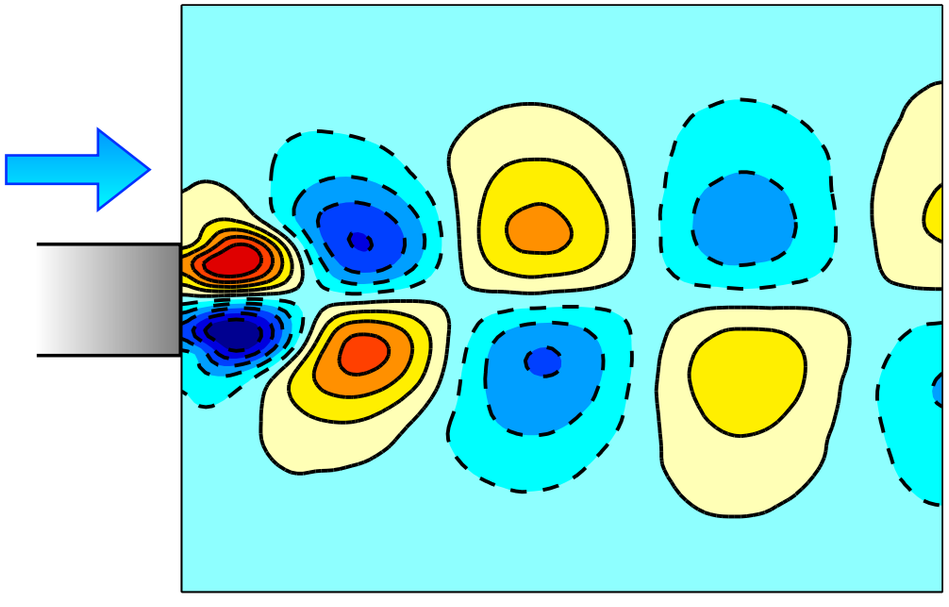

3D Complications

- Low-frequency modulation of base pressure fluctuations
- Wu et al. (2005), normal trapezoidal body; Lemkuhl et al. (2013), cylinder: modulation associated with unsteady variation in vortex formation length

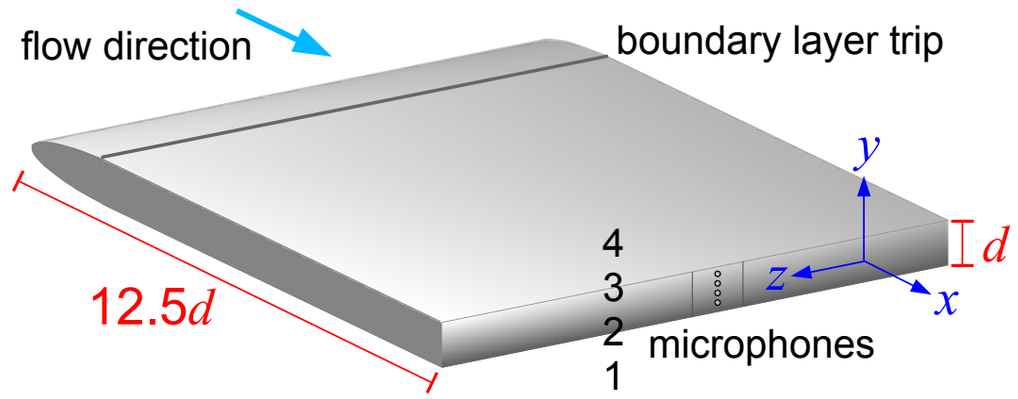

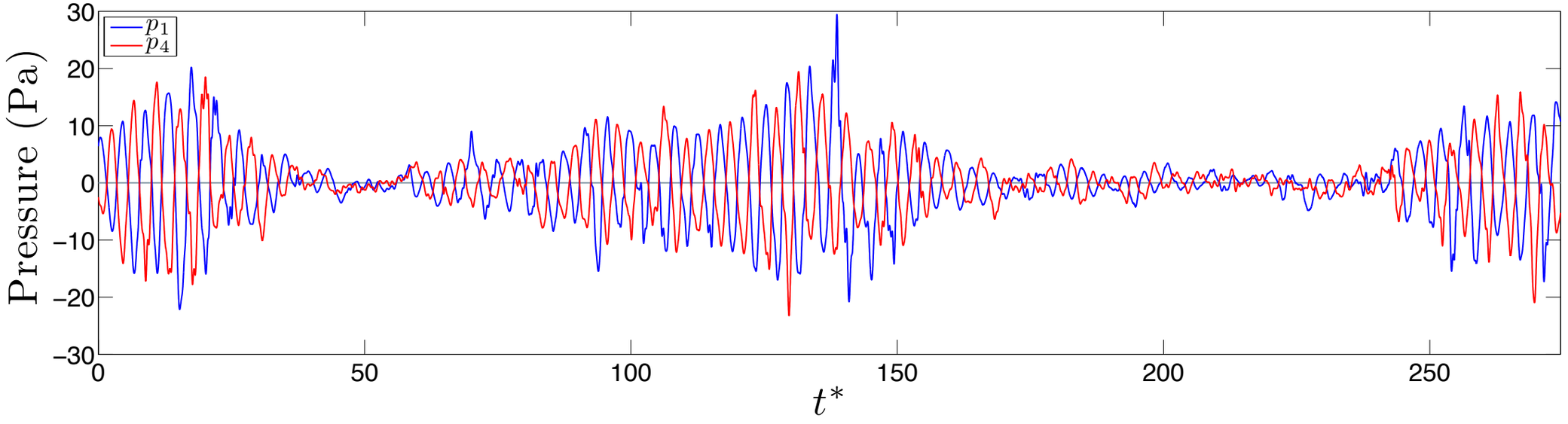

3D Complications

- Low-frequency modulation of base pressure fluctuations
- Wu et al. (2005), normal trapezoidal body; Lemkuhl et al. (2013), cylinder: modulation associated with unsteady variation in vortex formation length

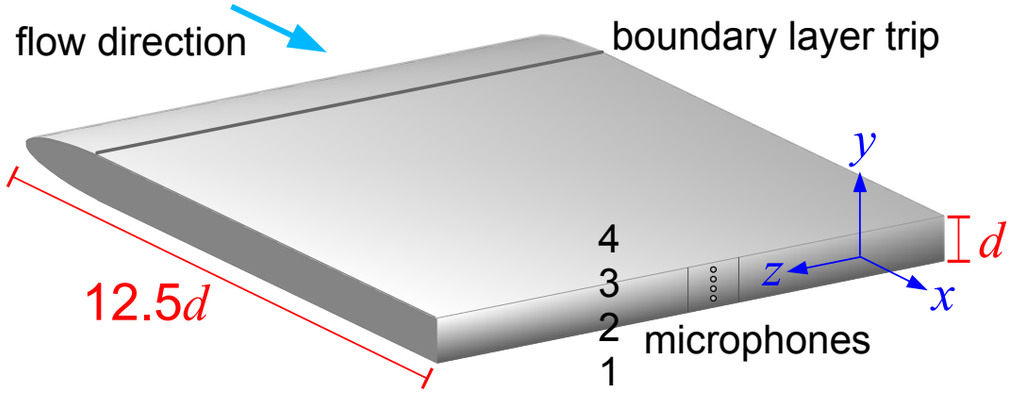

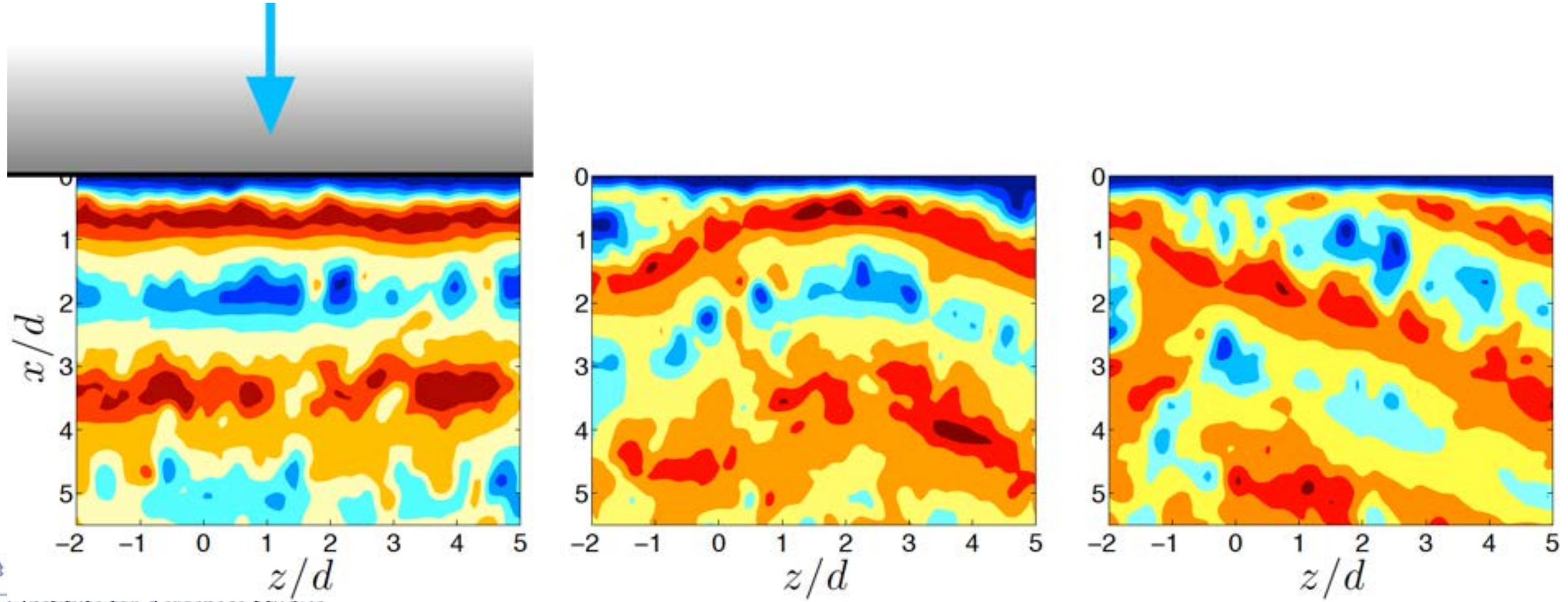

Variable state of shedding

COHERENT

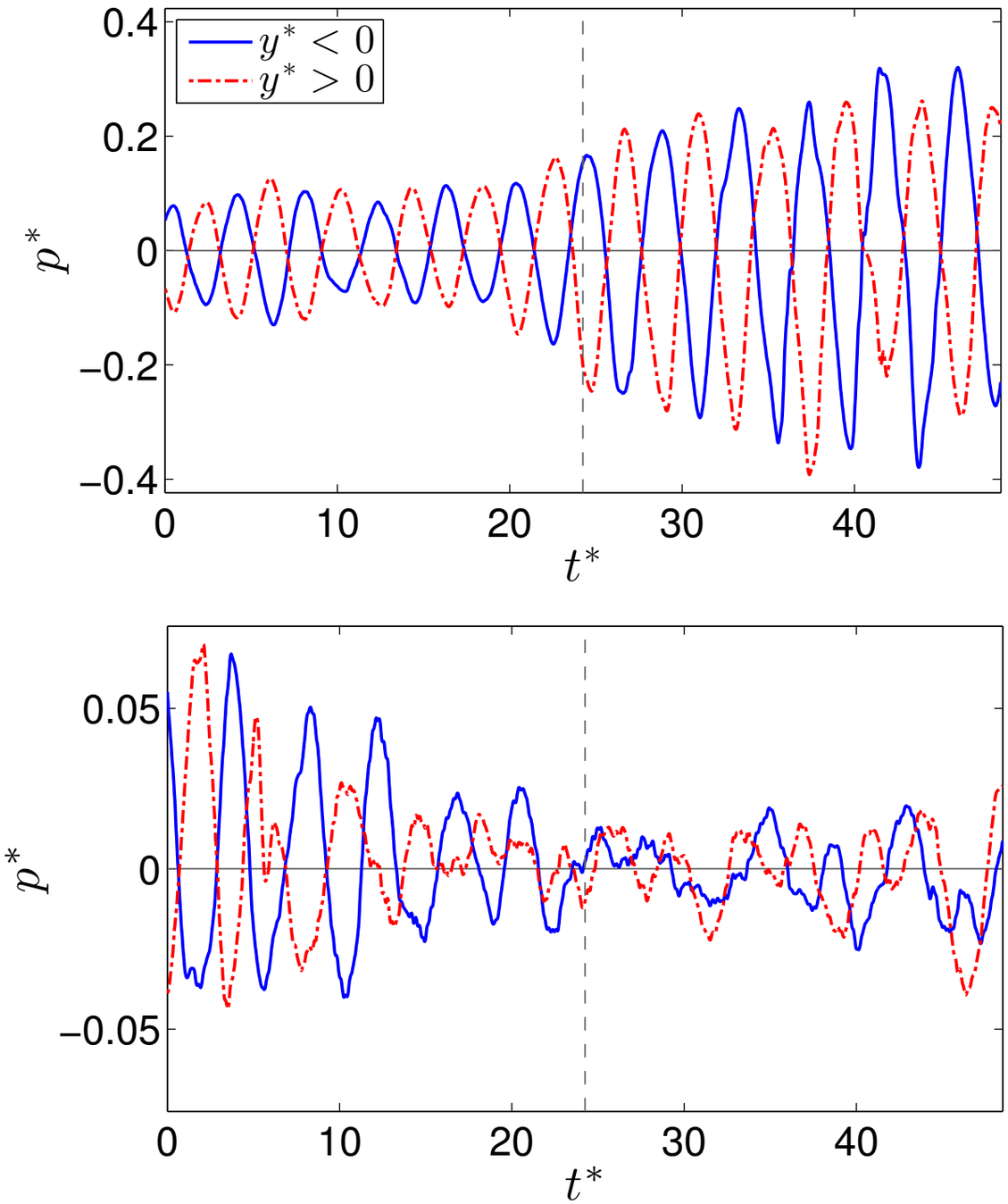

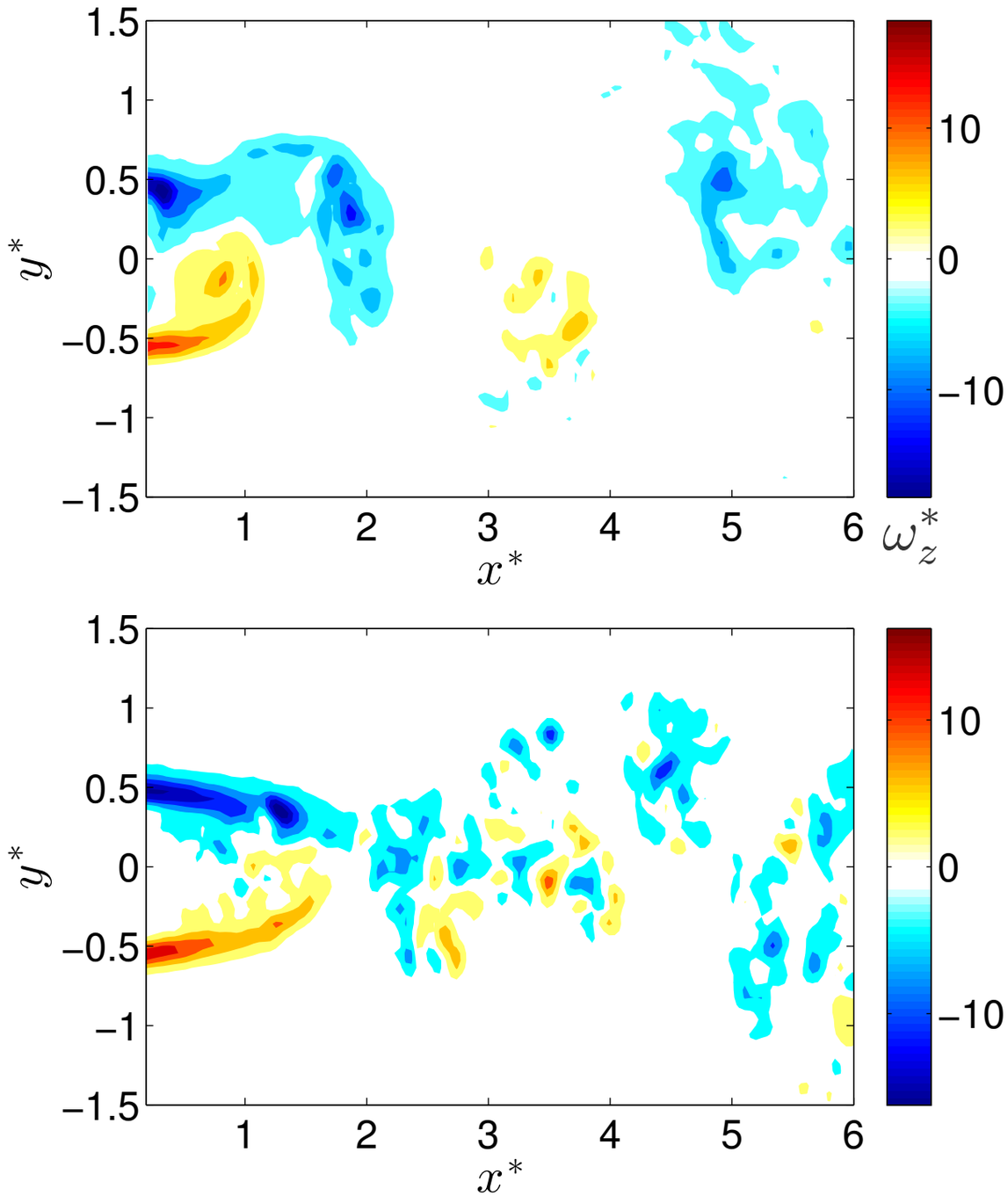

DISORGANIZED

- Phase disorganization typically occurs with low amplitude fluctuations at the same z^*

Amplitude modulation

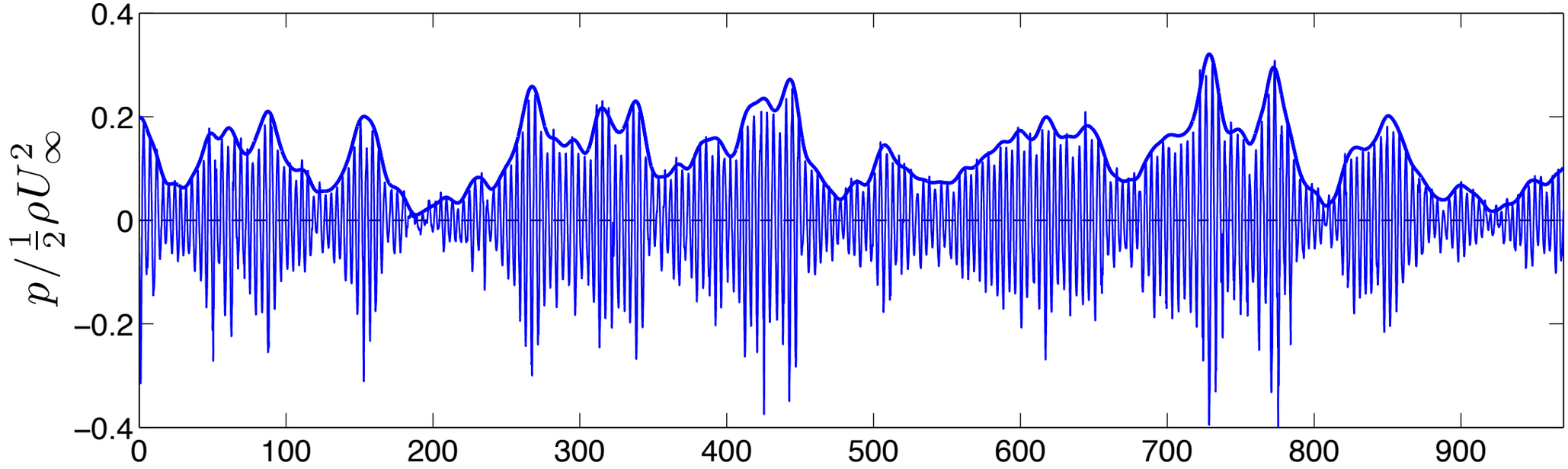

- $A_p(t)$ determined from wavelet transform, using MATLAB software by Torrence & Compo (1998)
- Szepessy (1994), Wu *et al.* (2005), Lehmkuhl *et al.* (2013): modulation at frequency one order of magnitude less than shedding
- Conditional average based on amplitude

$$U^- = \langle u \mid A_p \leq \overline{A_p} - \beta\sigma_A \rangle$$
$$U^+ = \langle u \mid A_p > \overline{A_p} + \beta\sigma_A \rangle$$

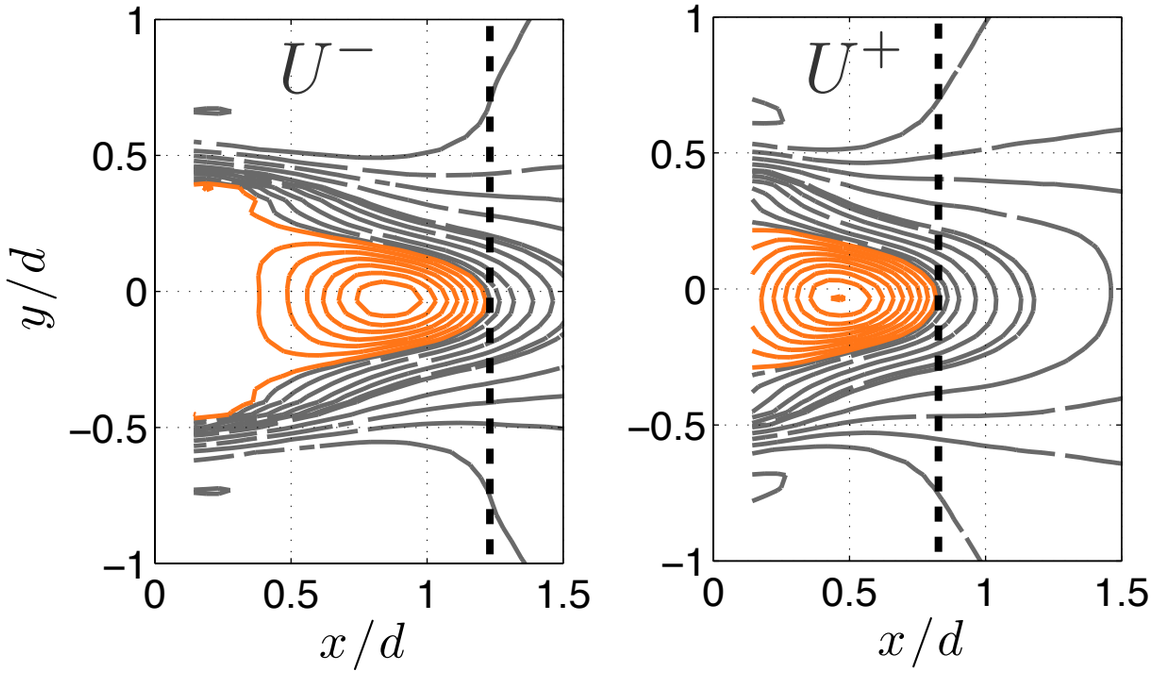

Spanwise Amplitude Correlation

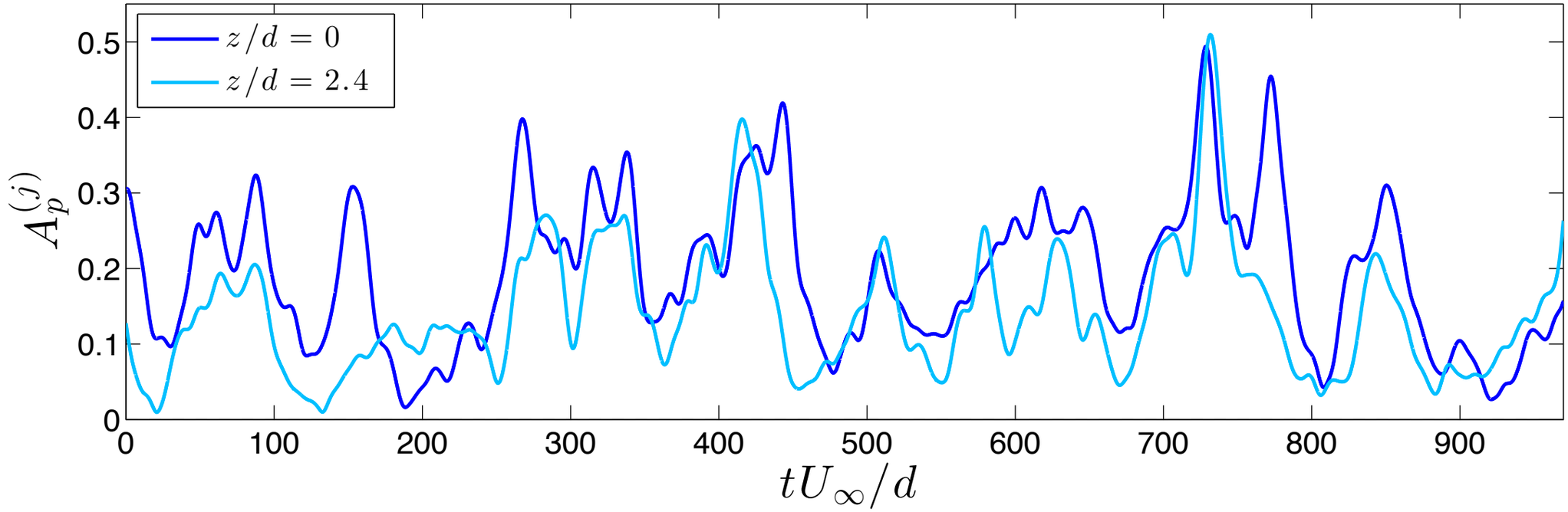

- Correlation of amplitude performed for all combinations of locations in array

$$r_{AA}(i,j,\tau) = \frac{\left\langle A_p^{(i)}(t) A_p^{(j)}(t+\tau) \right\rangle}{\sigma_p^{(i)} \sigma_p^{(j)}}$$

- Spanwise coherence of low-frequency modulation increased by forcing

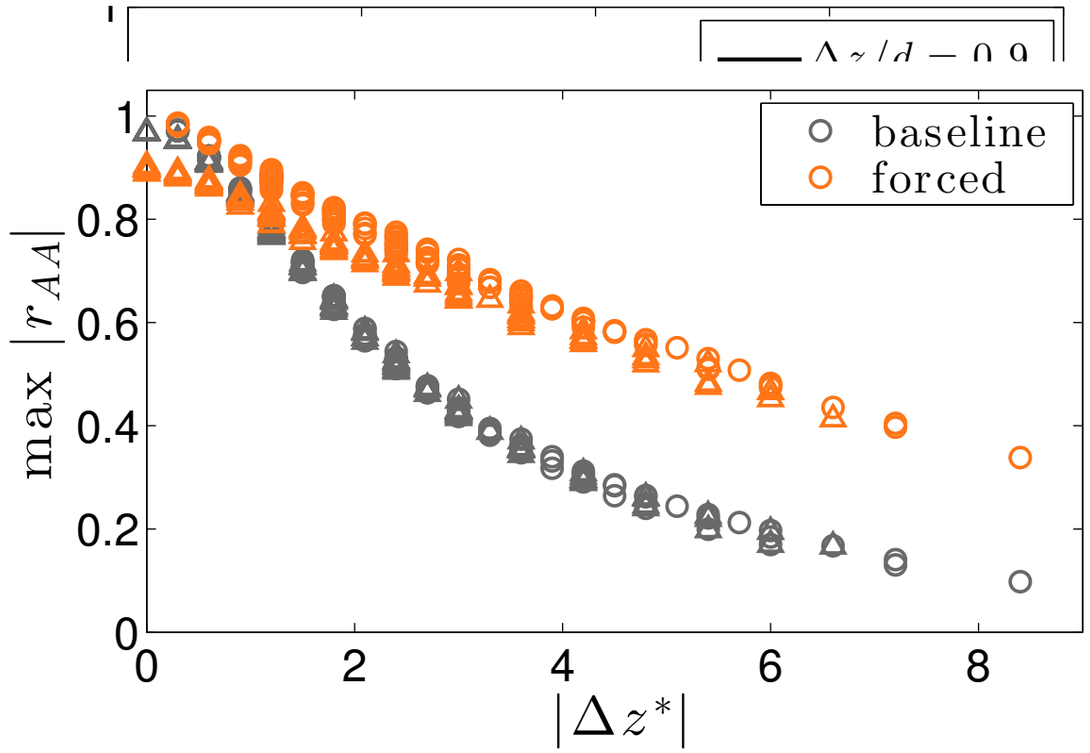

Modulation and vortex dislocations

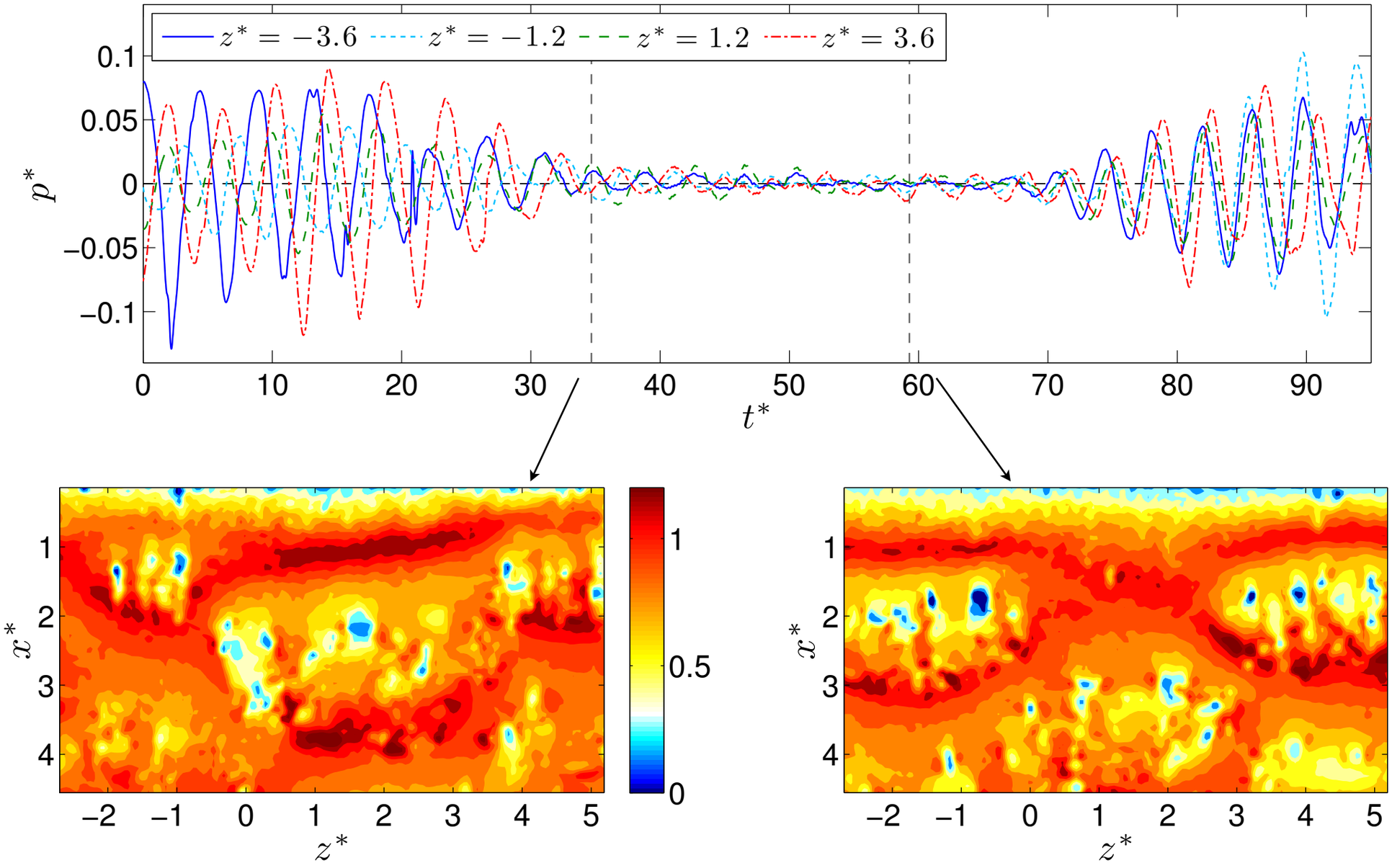

- Complex vortex distortions and interactions occur with globally reduced amplitude
- Najjar & Balachandar (1998): switching between regimes in wake of normal flat plate, primary vortices torn apart and secondary vortices disorganized in low drag state

Stochastic Estimator

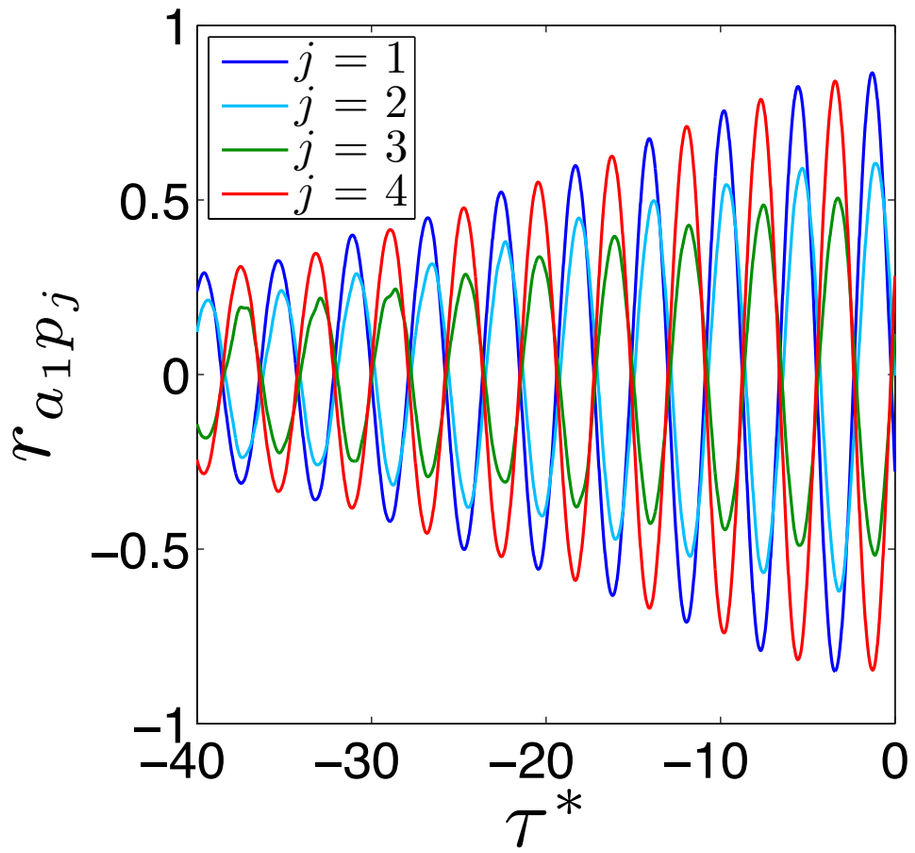

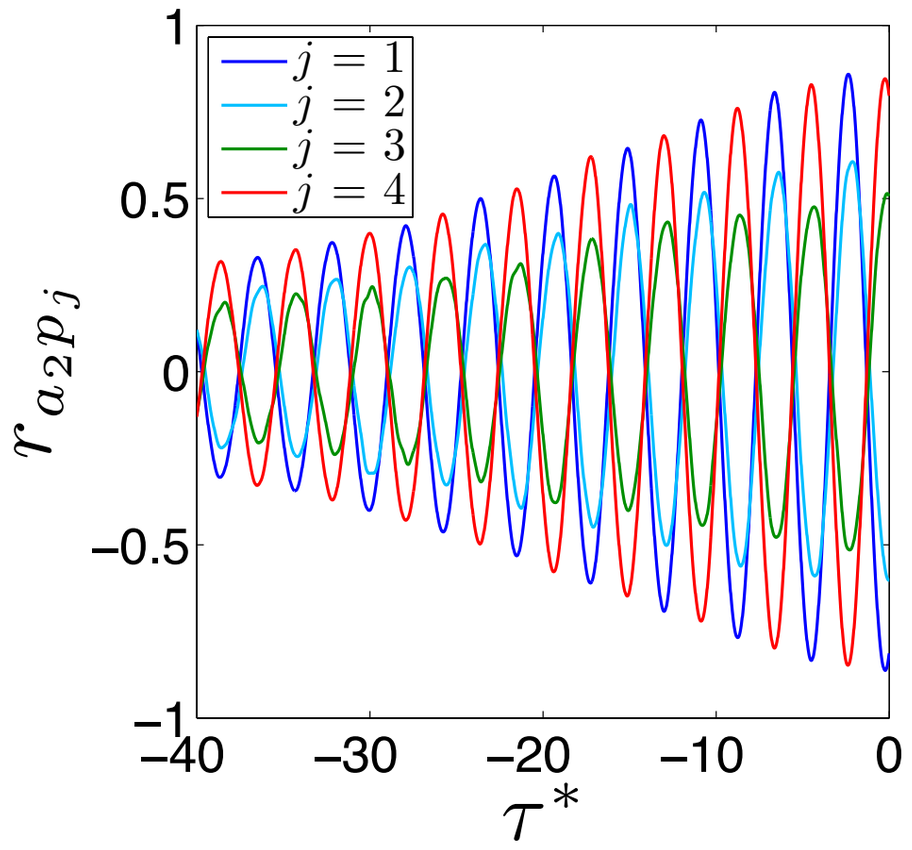

$$r_{a_i p_j}(\tau) = \frac{\langle a_i(t) p_j(t+\tau) \rangle}{\sqrt{\langle a_i^2 \rangle \langle p_j^2 \rangle}}$$

$$\tau^* = \tau U_\infty / d$$

- Maximum $r_{a_i p_j} \simeq 0.85$ for $j = 1, 4$
- $r_{a_i p_j} < 0.3$ for $i > 2$: higher modes not observable with current sensing strategy
- High linear correlation coefficient $\longrightarrow$ linear model: multi-time-delay LSE, used in similar BTE geometry by Durgesh & Naughton (2010) and Tu et al. (2013), curvilinear cavity by Lasagna et al. (2013)

Model Construction

- Model construction

$$\hat{a}_i(t) = \beta_{ijk} p_j(t + \tau_k), \quad \tau < 0$$

$i = 1, 2$ as motivated by correlation

- Varying parameters in model construction:

$m_1,\ m_2,\ \Delta\tau^*$, and number of sensors used

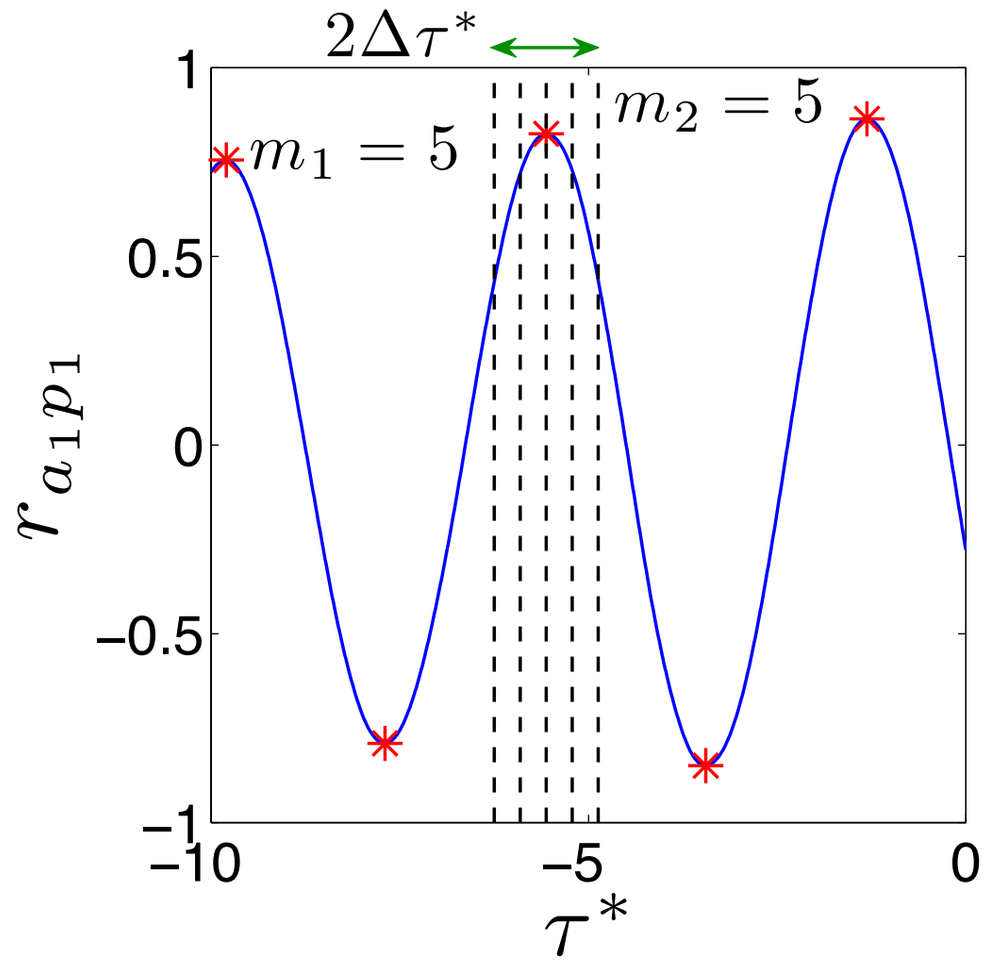

Performance Quantification

- Fraction of variance residual

$$e_v = \frac{\left\langle (\hat{a}_1 - a_1)^2 + (\hat{a}_2 - a_2)^2 \right\rangle}{\langle a_1^2 + a_2^2 \rangle}$$

- Phase $e_\theta = \left\langle \left| \hat{\theta} - \theta \right| \right\rangle / \pi,\ \theta = \tan^{-1}\left(\frac{a_2/\sqrt{2\lambda_2}}{a_1/\sqrt{2\lambda_1}} \right), \theta \in [-\pi, \pi]$

- Variance Inflation Factor (VIF) of regression coefficients quantifies collinearity of predictors: use average value $\overline{VIF} = \sum_{j=1}^{n} 1/\left(1 - R_j^2\right)$

Correlation and Variance Inflation

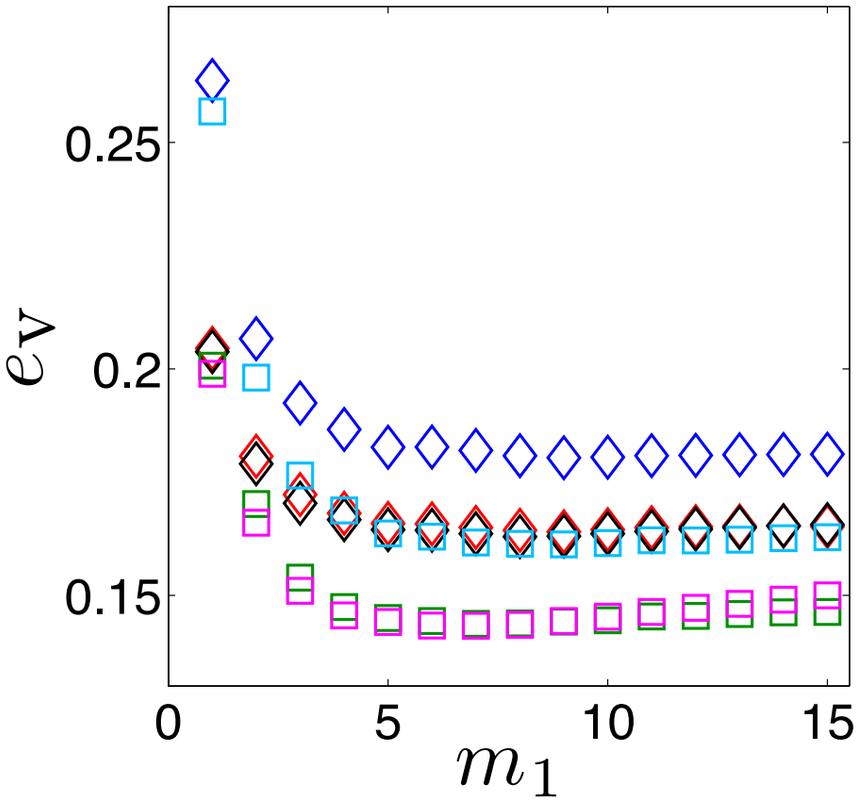

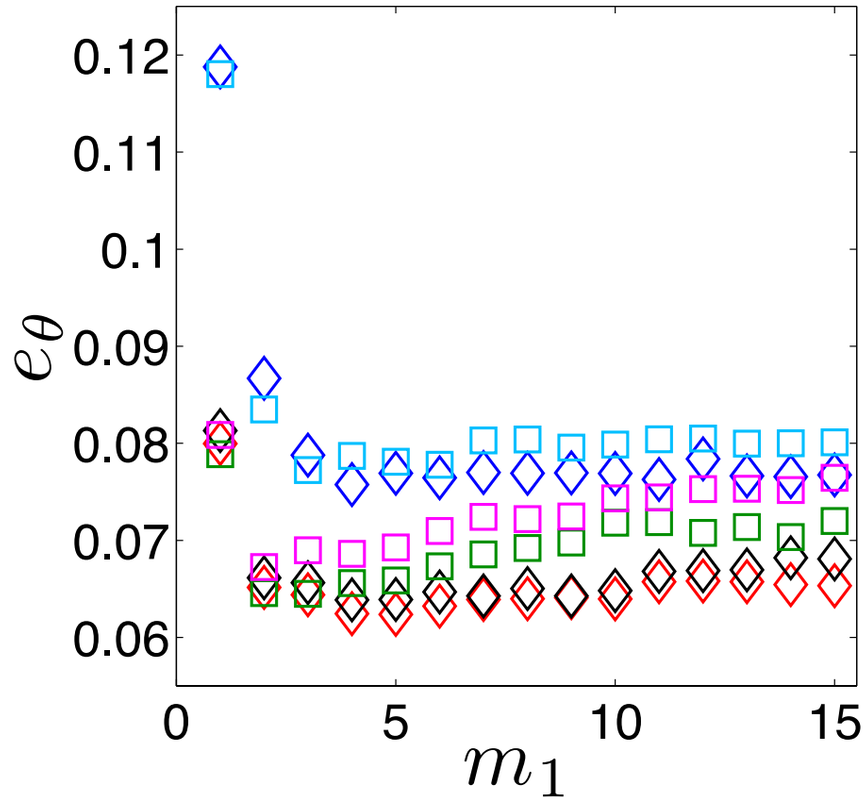

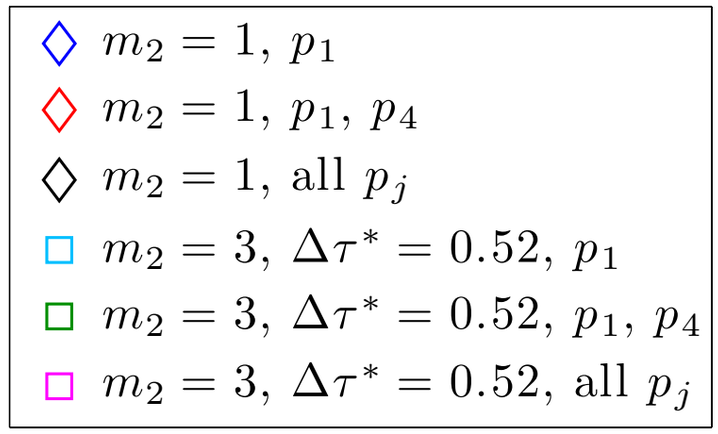

- Optimum m_1 around 5
- Significant improvements when using both p_1 and p_4
- p_2 and p_3 are not useful

Correlation and Variance Inflation

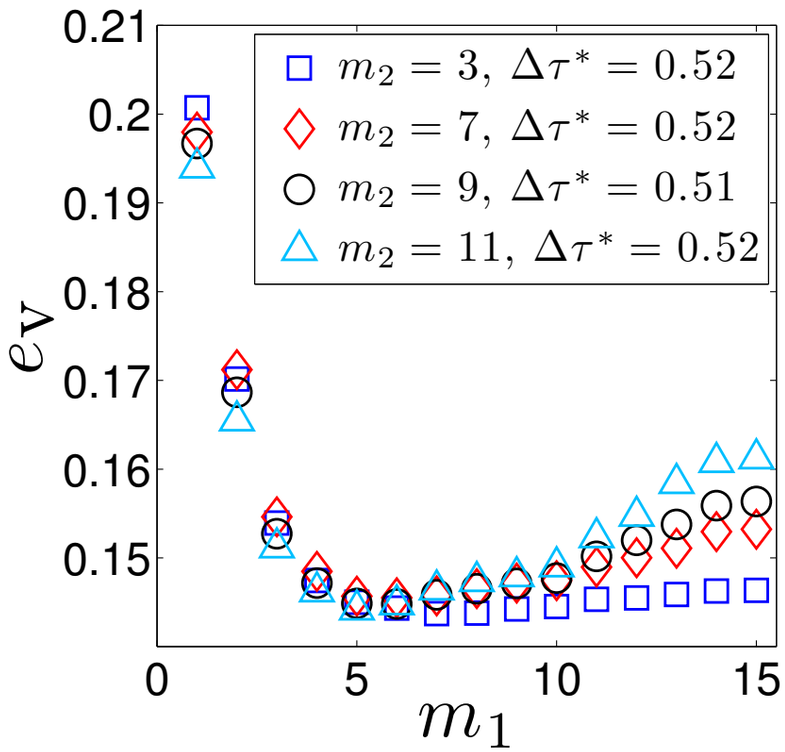

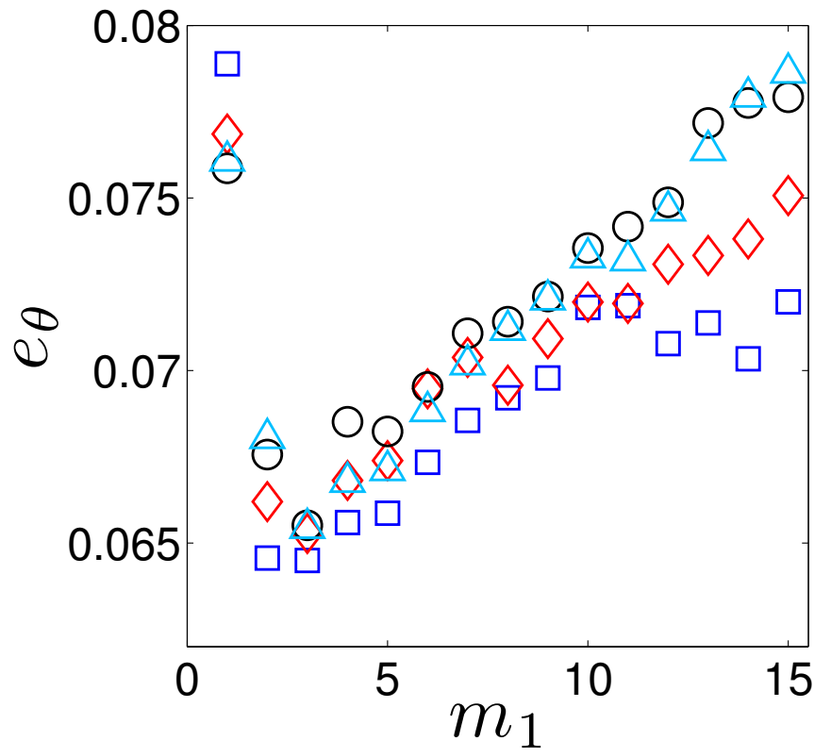

Varying m_2:

$\overline{VIF} \simeq 12$ to 10^9

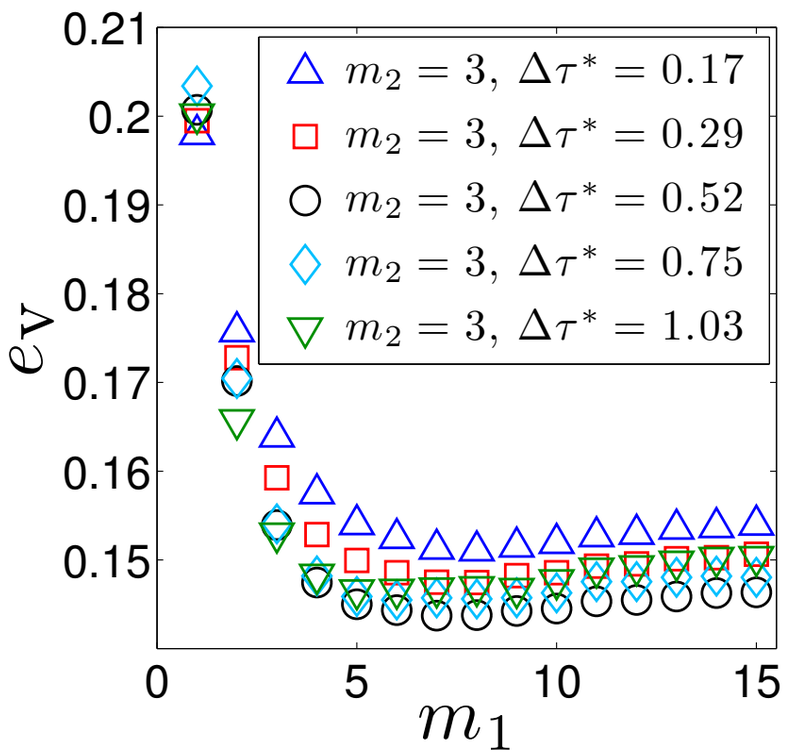

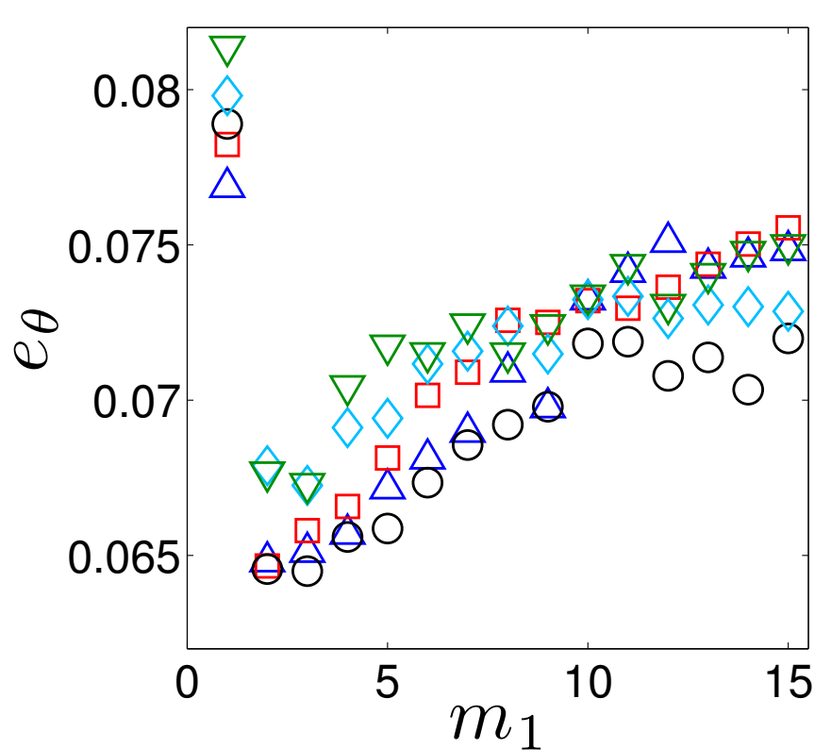

Varying $\Delta\tau^*$:

correlation of some predictors decreasing

Validation Set: All Observation

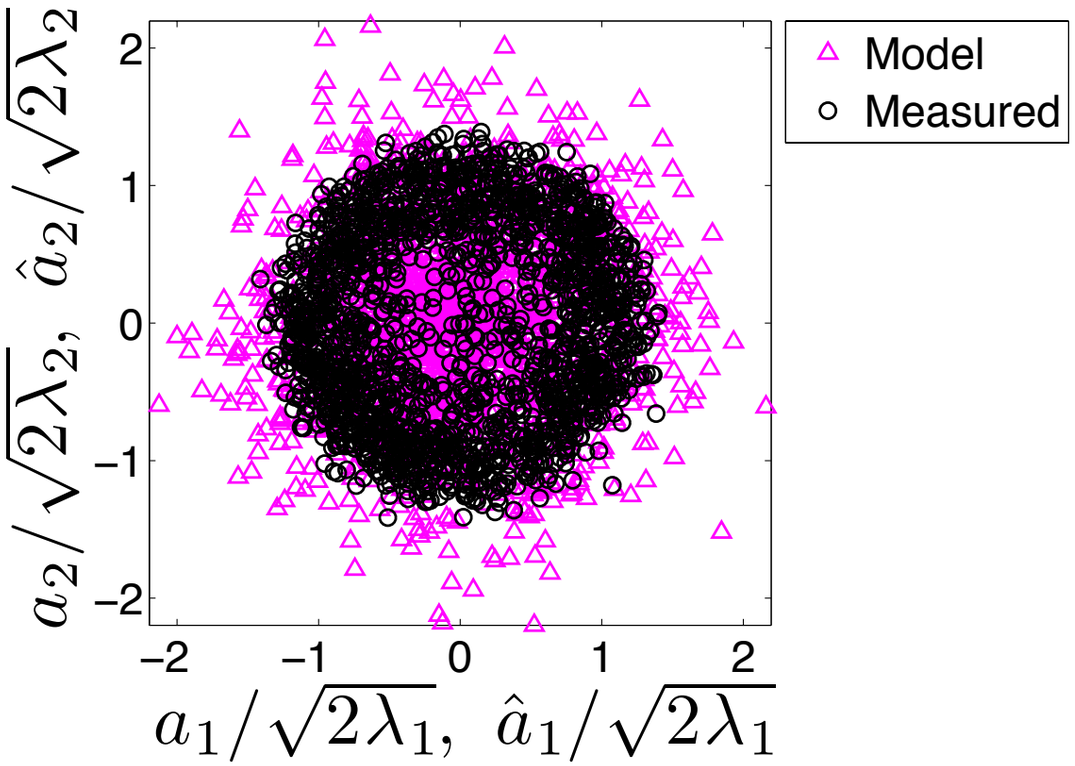

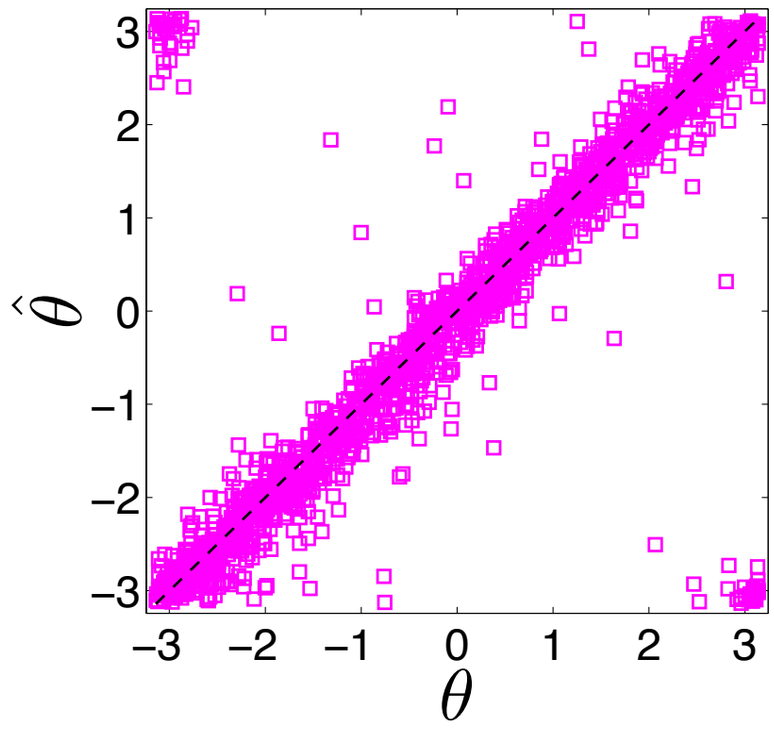

- Model parameters $m_1 = 5,\ m_2 = 3,\ \Delta\tau^* = 0.52$
- $e_v = 0.145,\ e_\theta = 0.07$
- Linear regression model uses only correlations

  e.g., $\langle p_i p_j \rangle\ ,\ \langle a_i p_j \rangle$
- Amplitude modulation of pressure results in model prediction outside of physical variation of $a_1,\ a_2$

Validation Set: Categorized Observation

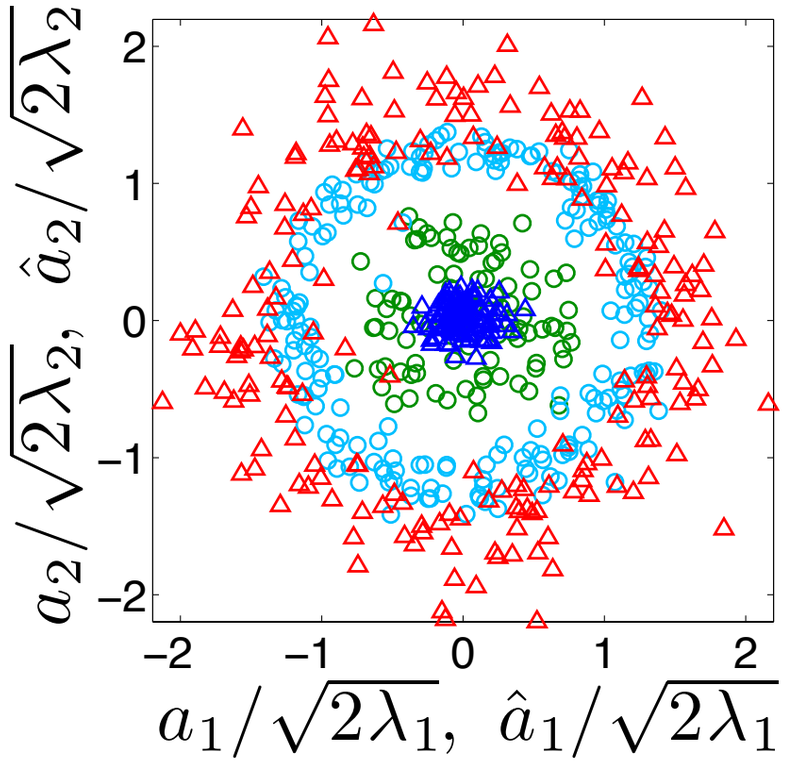

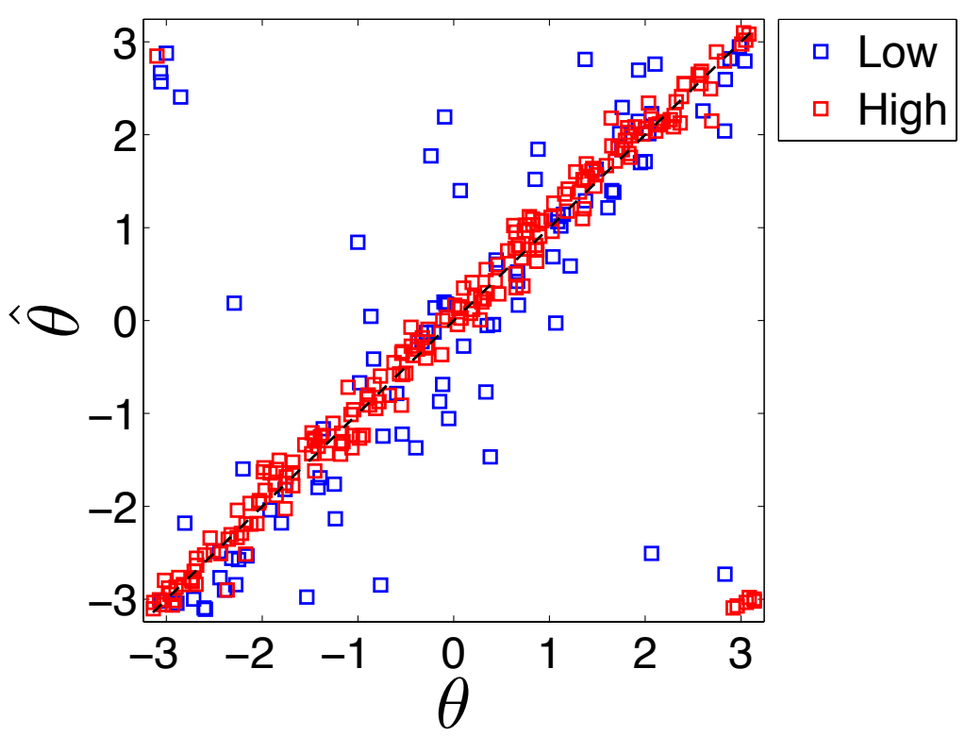

- Separated snapshots at times of low- and high-amplitudes pressure fluctuations
- Lower $a_1^2 + a_2^2$ related to low pressure, but not linearly
- Low: $e_v = 0.56,\ e_\theta = 0.18$
- High: $e_v = 0.15,\ e_\theta = 0.04$
- Degradation of phase relationship typical of low amplitude pressure state

Time-resolved Estimation

- What physical differences result from parameter changes?
- Model I: $m_1 = 5,\ m_2 = 1 \quad \rightarrow \quad e_v = 0.166$
- Model II: $m_1 = 5,\ m_2 = 5 \quad \rightarrow \quad e_v = 0.141$

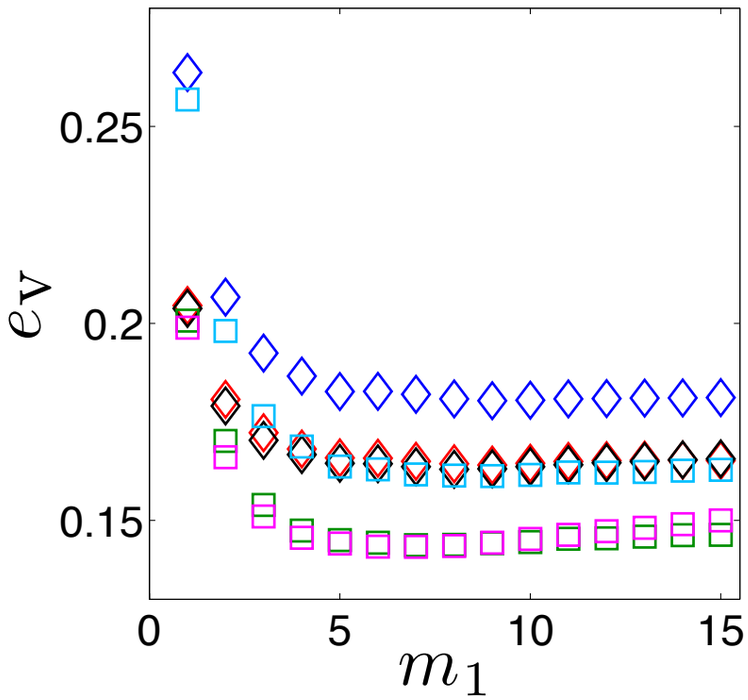

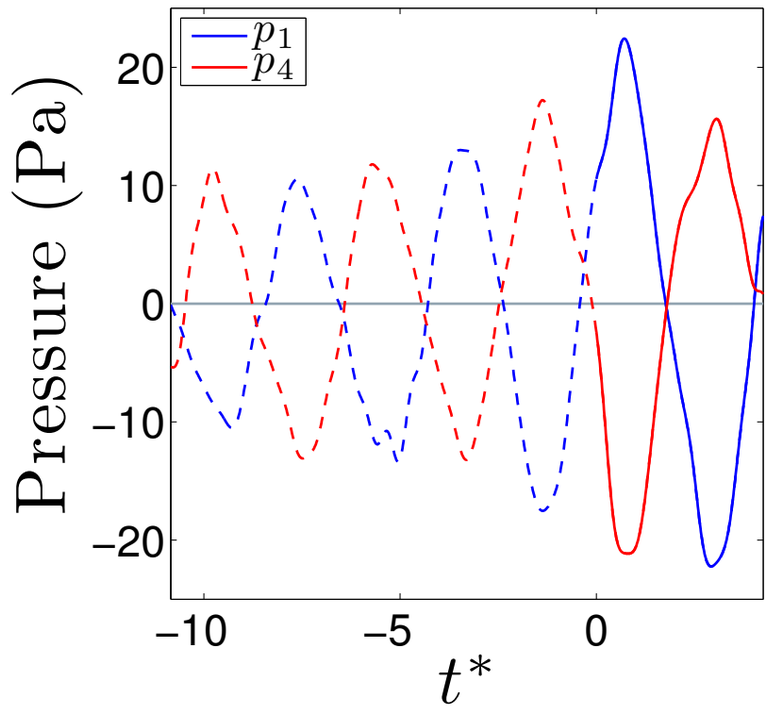

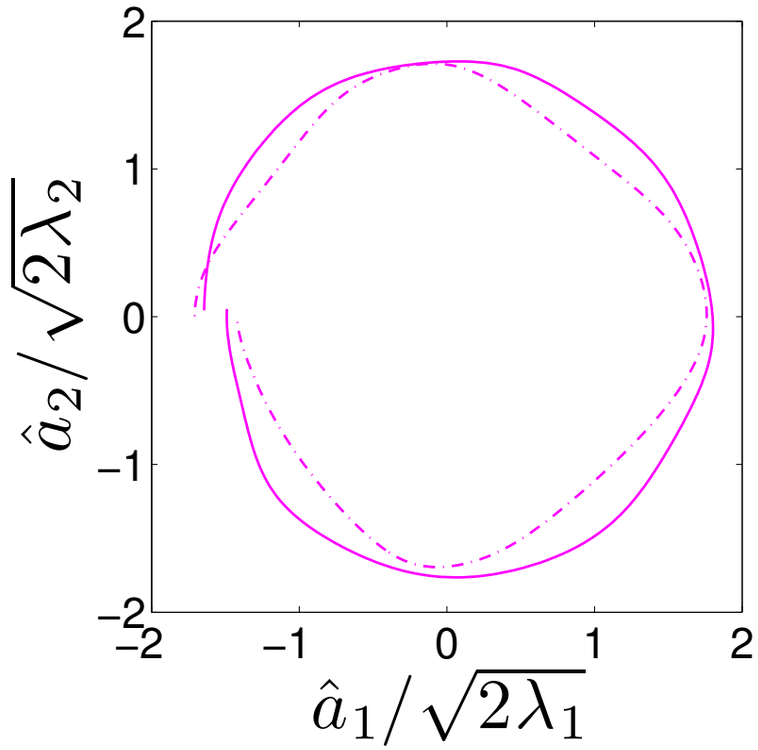

- Lower minimum e_v associated with more round trajectory in phase-space, believed to match physical evolution more closely
- $m_2 = 1$ (predictors at peak correlation only) shows that pressure fluctuations are not purely sinusoidal. Curvature modified by $m_2 > 1$

Effect of Variance Inflation

- High VIF becomes problematic if input to model is nosier than the training data
- Model I:

$$m_1 = 5,\ m_2 = 3,\ \Delta\tau^* = 0.52 \quad \rightarrow \quad \overline{VIF} \simeq 12,\ |\hat{\beta}_j| \simeq 1$$

- Model II:

$$m_1 = 5,\ m_2 = 7,\ \Delta\tau^* = 0.52 \quad \rightarrow \quad \overline{VIF} \simeq 900,\ |\hat{\beta}_j| \simeq 10$$

- Estimate from unfiltered pressure signals in test set

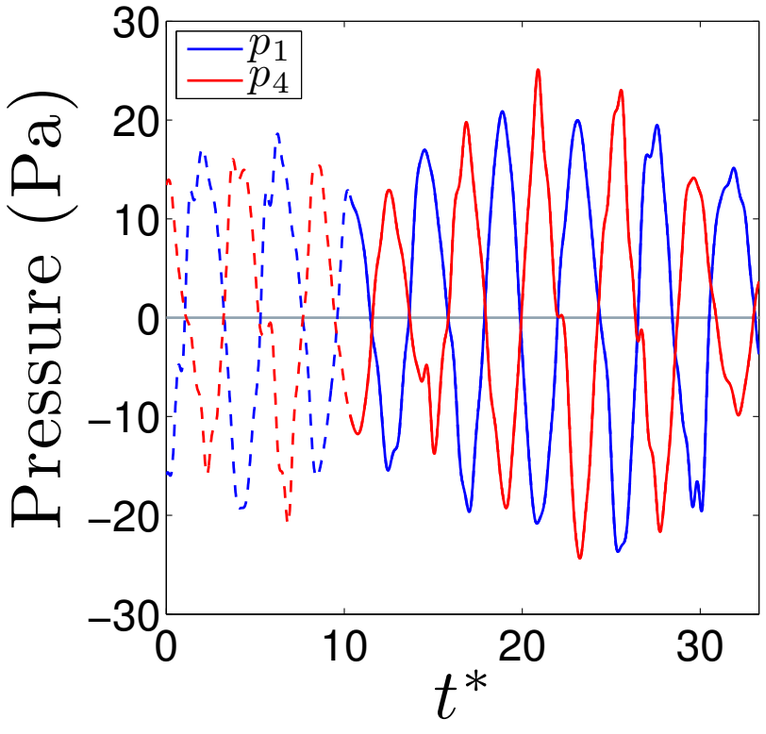

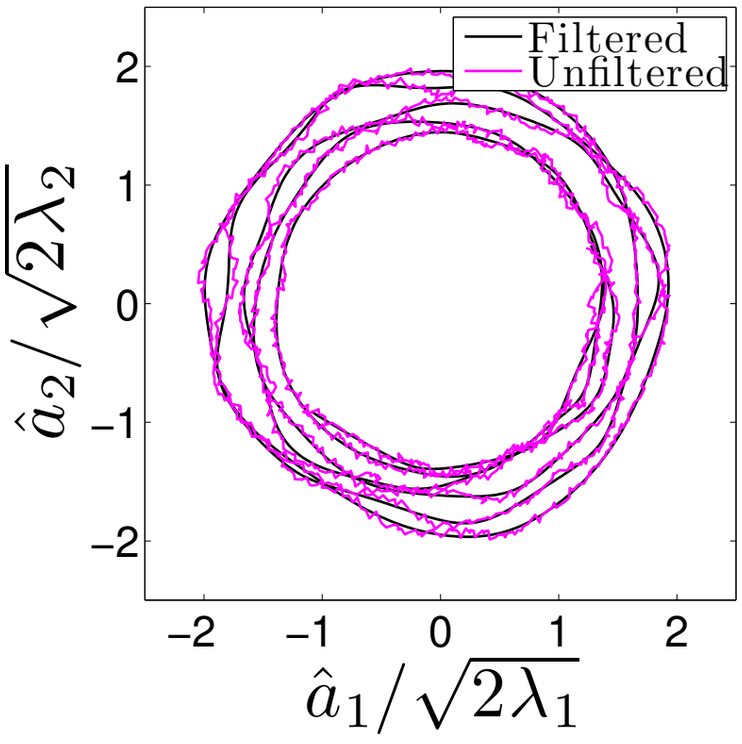

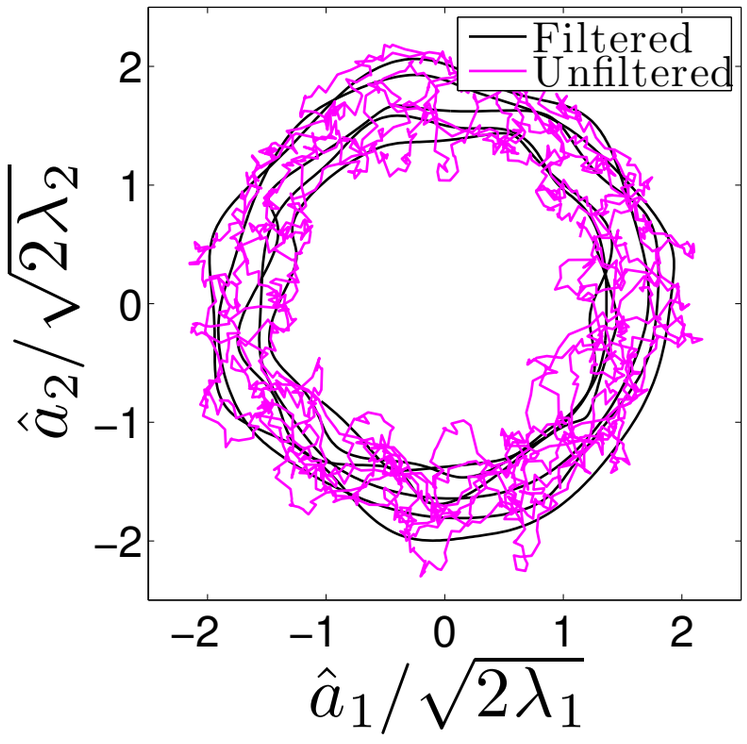

Summary and Perspective

- Active control of flow separation can have some significant benefits to improve aircraft performance.
- Commercial aviation: primarily indirect benefits to be gained.
- Approach to separation control fundamentally different for streamlined bodies (e.g., airfoil) and bluff bodies (e.g., landing gear).
- Streamlined bodies: unsteady forcing at high-frequency is promising
  - use of 3D forcing and/or closed-loop control could further improve performance and efficiency
- Bluff bodies: inhibiting movement transfer in the wake reduces unsteadiness and pressure drag
- Beginning to see application in industry - with much more potential to be reached